Universidad de Valladolid

Escuela de Doctorado Universidad de Valladolid

PROGRAMA DE DOCTORADO EN FÍSICA

DOCTORAL THESIS/*TESIS DOCTORAL*:

MOLECULAR AGGREGATION OF THIOLS AND ALCOHOLS: STUDY OF NON-COVALENT INTERACTIONS BY MICROWAVE SPECTROSCOPY

Presented by/*Presentada por*
Marcos Juanes San José
in fulfillment of the Degree of/ *para optar al Grado de*
Doctor
by the/*por la*
Universidad de Valladolid

Supervised by/ *Dirigida por*:
Dr. Alberto Lesarri Gómez
Dra. Ruth Pinacho Gómez

Preface

We /ˈwiː/ *(pronoun)*: used by a speaker to refer to himself or herself and one or more other people considered together.

Sometimes it is too difficult to take into account all the people who have been involved in a deep and personal study. Avoiding forgetting someone (and, above all, avoiding to underestimate all the support provided by everyone around me), from now on I feel the need to use the pronoun “We” in the Thesis presented below with the aim of making reference to all these people present in my life who have made this work posible, including you (maybe the most important part of these lines) as a reader.

Table of Contents

Preface

Table of Contents i

Abstract v

Resumen vii

Acknowledgements ix

Chapter I. INTRODUCTION I.1
- I. Non-covalent interactions I.3
  - I.1. Non-covalent interactions. The Hydrogen Bond I.5
    - I.1.1. Hydrogen Bonds involving Oxygen: The O-H···O bond I.8
    - I.1.2. Hydrogen Bonds involving Sulfur I.10
  - I.2. Gas-Phase Rotational Investigations of NCIs I.11
- II. Methods I.13
  - II.1.Rotational spectroscopy I.13
    - II.1.1. General aspects I.13
    - II.1.2. Theory od molecular rotation I.14
    - II.1.3. Balle-Flygare FTMW spectrometer @ UVa I.17
    - II.1.4. Chiped-Pulse FT-MW spectrometer @ UVa I.20
  - II.2. Computational Methods I.22
    - II.2.1. Density Functional Theory and Ab initio calculations I.23
    - II.2.2. Complementary computational tools I.24

Chapter II. HYDRATION OF CYCLOHEXANOL: (Cyclohexanol) and (Cyclohexanol··· H_2O) II.1
- I. Introduction II.3
- II. Cyclohexanol and Cyclohexanol ··· H_2O adduct II.5
  - II.1. Experimental set up II.5
  - II.2. Rotational spectra of CHO II.5
  - II.3. Theoretical calculations II.9
  - II.4. Molecular Struct. and Potential energy functions of the OH internal rotation II.10
  - II.5. Water dimer geometry and dynamics II.12
  - II.6. Discussion and Conclusions II.13

Chapter III. DIMERIZATION OF CYCLOHEXANOL: (Cyclohexanol)$_2$ III.1
- I. Introduction III.3
- II. Cyclohexanol homodimer III.4
  - II.1. Experimental set up III.4
  - II.2. About Chirality III.4
  - II.3. Rotational spectra of (Cyclohexanol)$_2$ III.6
  - II.4. Dispersion model III.7
  - II.5. Non-covalent interactions III.10

Chapter IV. HYDRATION OF FURFURYL COMPOUNDS: (Furfuryl Mercaptan ··· H_2O) and (Furfuryl Alcohol ··· H_2O) IV.1
- I. Introduction IV.3
- II. Furfuryl Mercaptan and Furfuryl alcohol IV.5
  - II.1. Experimental IV.5
  - II.2. Computational methods IV.5
  - II.3. Rotational spectra of FM and FA IV.6
  - II.4. Rotational spectra of the of the FM and FA monohydrates IV.7
  - II.5. Discussion IV.12

Chapter V. HYDRATION OF THENYL COMPOUNDS:
(Thenyl Mercaptan ··· H_2O) and (Thenyl Alcohol ··· H_2O) V.1
- I. Introduction V.3
- II. Thenyl Mercaptan and Thenyl alcohol V.5
  - II.1. Experimental set up V.5
  - II.2. Rotational spectra of TM and TA V.6
  - II.3. Rotational spectra of the monohydrates V.7
  - II.4. Molecular structures V.11
  - II.5. Non-covalent interactions V.13
  - II.6. Conclusion V.15

Chapter VI. DIMERIZATION OF THENYL AND FURFURYL COMPOUNDS:
(Furfuryl Alcohol)$_2$ and (Thenyl Alcohol)$_2$ VI.1
- I. Introduction VI.3
- II. Furfuryl alcohol and Thenyl alcohol homodimers VI.5
  - II.1. Experimental set up VI.5
  - II.2. Computational methods VI.5
  - II.3. Conformational landscape VI.5
  - II.4. Rotational Spectrum VI.10
  - II.5. Non-covalent interactions VI.13
  - II.6. Conclusion VI.15

Chapter VII. COMPLEMENTARY STUDIES V.1
- I. Complementary Studies VII.3
  - I.1. Equilibrium structures of fluorocyclohexane VII.5
  - I.2. Accurate equilibrium structure of the ethynylcyclohexane VII.6
  - I.3. Intramolecular hydrogen bonding in 1,2-butanedithiol VII.7
  - I.4. Intramolecular hydrogen bonding in 2,3-butanedithiol VII.8
  - I.5. Observation of trans - Matrine and cis - Matrine VII.9
  - I.5. Perspectives for Rorational Investigations of NCI VII.10

Abstract

The study and understanding of non-covalent interactions at molecular level is a field in continuous development and essential to determine the structural behavior of many molecules of chemical, technological or biological interest. In this PhD thesis, the intermolecular interactions involved in the formation of neutral molecular aggregates, both dimers and microsolvation products, have been analyzed in the gas phase. The intermolecular complexes were generated by pulsed supersonic expansions, and later characterized by rotational spectroscopy. This work has used two spectroscopic techniques, including a Balle-Flygare Fourier-Transform Microwave (FTMW) spectrometer in the 8-20 GHz frequency range, and a broadband Chirped-Pulse Fourier Transform Microwave (CP-FTMW) spectrometer covering the 2-8GHz spectral range. The intermolecular complexes studied have included molecules with alcohol and / or thiol groups, in order to analyze the differences between the intermolecular interactions involving oxygen or sulfur atoms, especially hydrogen bonds. Molecules that comprise both aliphatic (cyclohexanol) and aromatic (furfuryl alcohol, furfuryl mercaptan, thenyl alcohol, thenyl mercaptan) ring systems have been studied. The analyzed hydrogen bonds included especially O-H···O, O-H···S and S-H···S interactions. The formation of intermolecular complexes has revealed a great conformational diversity in some of them, such as the observation of six isomers of the cyclohexanol dimer. With regard to the monohydrates, tunnelling splittings associated with internal large amplitude motions have been observed in some cases, such as the rotation of the water molecule in the monohydrates of cyclohexanol, thenyl alcohol and thenyl mercaptan. In the case of chiral molecules, dimerization has made it possible to observe the relative stability of homo- or heterochiral diastereoisomers. The experimental study has been supported by different theoretical molecular orbital calculations, in particular Density Functional Theory (DFT) calculations, in order to characterize the interactions structurally, energetically and by a topological analysis of electron density. The set of experimental and theoretical data will advance the existing information on hydrogen bonds involving sulfur atoms, generally scarcely studied, and their comparison with the oxygenated analogues.

Resumen

El estudio y comprensión de las interacciones no covalentes a nivel molecular es un campo que está en continuo desarrollo y cobra vital importancia para determinar el comportamiento estructural de muchas moléculas de interés químico, tecnológico o biológico. En esta tésis doctoral se han analizado las interacciones intermoleculares implicadas en la formación de agregados moleculares neutros, tanto dímeros como productos de microsolvatación, en fase gas. Los complejos intermoleculares se han generado mediante expansiones supersónicas pulsadas, caracterizándose posteriormente mediante espectroscopía de rotación. Este trabajo ha utilizado dos técnicas espectroscópicas, incluyendo un espectrómetro de microondas con transformada de Fourier (FTMW) de tipo Balle-Flygare en el rango de frecuencias 8-20 GHz, y un espectrómetro de transformada de Fourier de banda ancha con excitación multifrecuencia (CP-FTMW) cubriendo el rango espectral de 2-8 GHz. Los complejos intermoleculares estudiados han incluido moléculas con grupos alcohol y/o tiol, con objeto de analizar las diferencias entre las interacciones intermoleculares que implican átomos de oxígeno o azufre, en especial el enlace de hidrógeno. Se han estudiado moléculas incluyendo tanto sistemas cíclicos alifáticos (ciclohexanol, ciclohexanotiol) como aromáticos (furfuril alcohol, furfuril mercaptano, tienil alcohol, tienil mercaptano). Los enlaces de hidrógeno analizados han comprendido especialmente interacciones de tipo O-H···O, O-H···S y S-H···S. La formación de los complejos intermoleculares ha revelado en algunos de ellos una gran variedad conformacional, como la observación de seis isómeros del dímero de ciclohexanol. En el caso de los monohidratos se han observado en algunos casos desdoblamientos asociados a movimientos internos de gran amplitud, como la rotación de la molécula de agua en los monohidratos de ciclohexanol y tienil mercaptano. En los casos de moléculas quirales la dimerización ha permitido observar la estabilidad relativa de los diastereoisómeros homo o heteroquirales. El estudio experimental se ha completado con diferentes cálculos teóricos de orbitales moleculares, en especial teoría del funcional de la densidad, a fin de caracterizar las interacciones estructuralmente, energéticamente y mediante análisis topológico de la densidad electrónica. El conjunto de datos experimentales y teóricos permite aumentar la información existente sobre enlaces de hidrógeno con átomos de azufre, generalmente poco estudiados, y su comparación con los análogos oxigenados.

Acknowledgements

By respect, honesty and proud, before starting I would like (and I feel it necessary) to highlight that all the time, effort and enthusiasm invested into this work is a direct response of the kindness received and felt since I was welcomed at the Alberto Lesarri's laboratory and at the electronics department of the ETSIT-UVa (more than four years ago since I decided to start this adventure). This gratitude specifically corresponds to Lourdes, José Emiliano, Martín (without their support most of the theoretical calculations carried out in the following studies presented in this thesis would nothave been possible), to Ruth Pinacho for always being ready to help (both scientifically and personally) at any time and to Alberto Lesarri for showing me that always working with a smile on your face is much more than rewarding. I also want to thank the good treatment and help I have received from all the people who have made it possible to carry out different research periods in laboratories outside my country at the *Leibniz Universität Hannover* and at the *Universität zu Köln* (both in Germany) during my PhD period.

When a human being starts a new episode in his/her/its life, it is fair to keep on mind that each lived experience would not be possible without the support of the family. The concept family, from my point of view, is one of the most difficult terms to be defined:

Following a rigorous grammar definition, there is always a blood component that genetically creates a biological link to others who are generally considered family members. Personally, going a couple of steps further, what I understand (specially, what I perceive) as family is the selected set of people who have accompanied me, who accompany me or who will accompany me in the path of my life. I would like to thank strongly the support received from my parents during these 30 years (honestly, without their help, none of the words written in this Thesis would be possible): thank you very much Juan and Sole. Thanks to my brother who have always been a reference in my life (both academically and familiarly). Thanks to Quique, Saul and Cristian who made me understand how important friendship was at the university. Thanks to the mother earth and its nature for allowing me to enjoy its mountains while climbling and hiking every weekend. Thanks to all my Friends (who I consider closer than brothers) for doing everything easier at every time and always being by my side. And, to finish, thank two human beings who (unexpectedly) have become an essential part of my life for giving me the opportunity to live this incredible experience with the feeling of always feeling supported and loved: thank you very much for everything to Alberto Lesarri and Rizalina T. Saragi.

Marcos Juanes San José

Siempre en mi recuerdo,
a mi tío Alberto Juanes

Chapter I

INTRODUCTION

I. Non-covalent interactions

This Thesis contains a molecular study of non-covalent interactions (NCIs) in neutral intermolecular complexes using rotational spectroscopy.

NCIs have profound consequences in Biology and Chemistry and affect molecular properties at multiple chemical scales, from the realm of small-molecules to aggregates and supramolecular structures (Figure 1). For this reason, NCIs have both a fundamental and practical importance extending to technological applications, crystal engineering and supramolecular Chemistry, among others.

The fist query we must clarify in the Introduction is the meaning of the commonly used concept of NCIs. Generally speaking, a non-covalent interaction differs from a covalent bond in that it is a weak chemical force and does not involve the formation of a permanent chemical bond. Quoting Scheiner from the introduction of the *Noncovalent forces* volume,[1] he approaches the issue as follows:

> *"By its very name, it is clear that these* (non-covalent) *forces exclude the strong bonds that hold atoms together within a molecule. What is usually meant is the collection of phenomena that attract molecules or ions toward one another."*

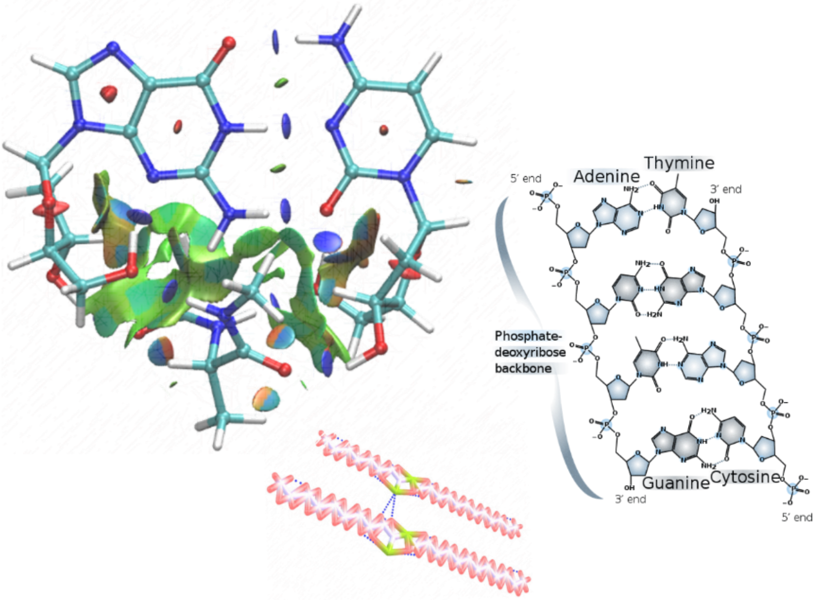

Figure 1. Illustrations of some non-covalent interactions. On the left, an NCI-Plot example of a DNA base pair complexed with alanine. On the right a scheme of the chemical structure of DNA. At the bottom a Fatty-acid complex of two different alkyl esters.

As a first step it would be convenient to try to understand what kind of phenomena come into play when NCIs are involved. Probably, when we speak of any inter/intra-molecular interaction, the main thought is centered on how "strong" is that interaction. Of course, the "strength" of any chemical-physical interaction is directly connected with how powerful and how stable are those forces, but a better understanding of these non-covalent forces is not that simple and it is also necessary to consider and evaluate the electronic effects, binding preferences, the geometry, the possible solvent or matrix effects, the probability of being formed, how this interaction occurs, and so on. In natural sciences non-covalent intermolecular interactions manifest in the properties and functions of matter under all conditions, from solid-state materials to biological systems (for instance, even at large scales, the Van der Waals dispersion inherent to NCIs has been proposed as an important force behind the formation of the rings around Saturn[2] or as the force that enables geckos to stick to walls[3]).

Non-covalent interactions play a fundamental role in layered materials, and sustain molecular aggregation in biological systems, large molecular complexes and technological processes with a strikingly diverse array of interaction energies and geometries.[1,4,5] Diversity arises not only by the multiple combinatorial possibilities of different atomic groups, but also because of the fuzzy character of NCIs, which, quite contrary to covalent bonds, admit broad and diffuse structural and energetic limits. Moreover, in the last decade our vision of non-covalent forces has expanded considerably, moving from the conventional hydrogen bond[4] (HB) to a whole new palette of previously unanticipated donor-acceptor interactions.[1,5] First, the now centenary HB was redefined by IUPAC in 2011[6,7] to accommodate weak interactions like aliphatic donors[8] (C-H···O, C-H···N, etc.), π acceptors[9] (C-H···π, N-H···π, etc.), low-electronegativity donors[10] (S-H, P-H, etc.) or H acceptors,[11] among others. Then, further developments in crystal engineering[5] catalyzed the IUPAC move to define the halogen bond[12] (XB) in 2013. In the XB the anisotropic electron distribution within halogen atoms makes terminal σ-hole[13] or lateral π-hole[14] regions new electrophilic attractors, turning common electron donors into acceptors.[15,16] The electrostatic argument was later generalized[17,18] to explain experimental observations into the new conceptual frames of chalcogen bonds (CB),[19] pnictogen bonds[20,21] (NB) or tetrel bonds[22,23] (TB), involving atoms of groups 14, 15, 16[24] or even coinage-metals[25] in R-A···B bridging interactions formally analogue to the HB or XB (R-H/X···B). Legon has noticed that rotational[26–28] and vibrational[29,30] experiments existed for the new bonds long before they had a name, occasionally being called "anti-hydrogen bond".[31] This extension of the chemical discourse makes NCI more diverse and attractive than ever.

The understanding of non-covalent interactions has been gained from decades of experimental observations supplemented by theoretical predictions.[32] To make a proper analysis of the NCIs it would be necessary more time and space than a single PhD thesis and, even so, the subject would not be concluded.[33] In order to make sense and try to easily introduce results presented in later chapters, we will focus our introduction on non-covalent forces on those produced by the hydrogen bonds, in particular those containing sulfur and/or oxygen.

1. Non-covalent interactions. The Hydrogen Bond

The HB is a donor-acceptor attractive directional bridging interaction specifically involving hydrogen atoms. Condensing the large volume of literature that the HB entails, we can start from the classical concepts proposed by Pauling in *The Nature of the Chemical Bond*[34] (1939) and established by Pimentel and McClellan[35] (1960),

> “*A hydrogen bond [A−H···B] exists between a functional group A−H and an atom or a group of atoms B in the same or a different molecule when:*
> *(a) there is evidence of bond formation (association or chelation) and (b) there is evidence that this new bond linking A−H and B specifically involves the hydrogen atom already bonded to A.*”

This description was extended by Vinogradov and Linnell (1971),[36]

> “*Hydrogen bonding occurs between a proton-donor group A−H and a proton-acceptor group B, where A is an electronegative atom, O, N, S, X (F, Cl, Br, I) or C, and the acceptor group is a lone pair of an electronegative atom or a π bond of a multiple bond (unsaturated) system. Generally, a H-bond can be characterized as a proton shared by two lone electron pairs.*”

and was summarized in the IUPAC definition of 1997:

> “*form of association between an electronegative atom and a hydrogen atom attached to a second, relatively electronegative atom. It is best considered as an electrostatic interaction, heightened by the small size of hydrogen, which permits proximity of the interacting dipoles or charges...*”, where “associated energies are less than 21–25 kJ mol^{-1}”.

By 2010 new experimental and theoretical advances required an extension of these concepts to much weaker, broader and diverse (2-170 kJ mol^{-1}) interactions, including atoms different from the first-row, as exposed in the most recent IUPAC’s definition of 2011,[7]

> “*The hydrogen bond is an attractive interaction between a hydrogen atom from a molecule or a molecular fragment X–H in which X is more electronegative than H, and an atom or a group of atoms in the same or a different molecule, in which there is evidence of bond formation.*”

As seen from the above definitions, to simplify a complex phenomenon like the concept of HB is complicated. We can essentially state that the main feature that characterizes the HB and differs from another donor-acceptor interactions is the sharing of the hydrogen atom between the hydrogen bond donor and acceptor and some form of electron sharing with dominant electrostatic character. That is, we can see this non-covalent force as *a shared-proton interaction* (on the other hand, the inverse argument may not be true and not all shared-proton interactions necessarily conform a HB). These types of interactions can occur intramolecularly (if the donor and acceptor groups are on the same molecule) and/or intermolecularly (when they are on different molecules).

Table 1. Pauling’s dimensionless electronegativities (χ) for the elements of the upper-right corner of the Periodic Table.

								H	2.20
B	2.04	**C**	2.55	**N**	3.04	**O**	3.44	**F**	3.98
		Si	1.90	**P**	2.19	**S**	2.58	**Cl**	3.16
		Ge	2.01	**As**	2.18	**Se**	2.55	**Br**	2.96
				Sb	2.05	**Te**	2.1	**I**	2.66

From the earliest studies, the donor/acceptor electronegativities are one of the main determinants of the hydrogen bond strength. The studies on hydrogen bonding initiated by Pauling and the first definitions involved only proton donors with atoms of large electronegativity, like those of the first row[34] in Table 1. The palette of atoms that can be considered part of the hydrogen bonding phenomenon has been increasing with time, now achieving a much wider range of possible donors and atoms of low electronegativity (Figures 2 and 3). In parallel, the number of proton acceptor groups has increased. Several reports discussing the donor-acceptor pairs involved in the hydrogen bond interaction can be found in the literature.[1,4,5,37,38]

A chemical classification of the HB according to *The Nature of the Hydrogen Bond* of Gilli and Gilli[4] can be seen in Figures 2 and 3. The HBs which include in donor/acceptor roles the most electronegative atoms ($\chi > 3.0$) like those of the first row (N, O, F) and some halogens (Cl, Br), are classified as "conventional" HBs and, due to their large electronegativities, they are also the ones that can form the stronger hydrogen bonds in neutral molecules. Conventional HBs include most of the interactions analyzed since the beginning of HB studies, comprise a large volume of experimental and theoretical information and often play a determining role in Chemistry, Biology and Biochemistry. In this Thesis we have analyzed in particular several conventional HBs including the oxygen atom, like those involving water, alcohols or heterocyclic aromatic rings. For this reason, section **1.1** will be dedicated to this kind of HBs.

HBs including atoms of lower electronegativity like C or the second-row atoms P and S are generally classified as weak donors or acceptors, and the information available is scarce compared to the conventional HBs. In particular, the HBs involving sulfur as part of the proton donor group or as acceptor has been much less studied that the conventional ones, despite the fact that they display the full spectrum of HBs energies and geometries, from strong, short-linear and proton-centered bonds of covalent nature to weak, long, bent and proton out-centered electrostatic ones. This problem called our attention since the beginning of the Thesis and motivated a series of comparative studies of HBs involving the sulfur atom, mostly in thiol, sulfide, disulfide and aromatic ring molecules.

For this reason, some characteristics and peculiarities of HBs including sulfur-centered atoms will be presented in Section **1.2**.

There are other structural and energetic factors to consider when making a consistent HB classification. Concerning energetics, the hydrogen bonds can be categorized as strong bonds (60-160 kJ mol^{-1}), moderate bonds (16-60 kJ mol^{-1}) or weak bonds (2-16 kJ mol^{-1}) attending to their binding energy.[a] The main difference between the first two categories is that the strong HBs are groups in which there are permanent electric charges or an important deficiency or excess of electron density in the donor or acceptor groups, while the moderate HBs are formed by neutral donor and acceptor groups, typically with electronegative atoms and lone-pair unshared electrons in the acceptor. As mentioned before, this last category includes the most common or *normal* HBs in Chemistry and nature because they are essential components of biological molecules. The concept of weak hydrogen bonds includes many other groups with small binding energies, characteristically close to the van der Waals interactions.

---

[a] Binding energy refers to the complexation energy relative to the conformations of the monomers in the lowest energy configuration. Complexation energy refers to the monomers in the geometry of the complex.

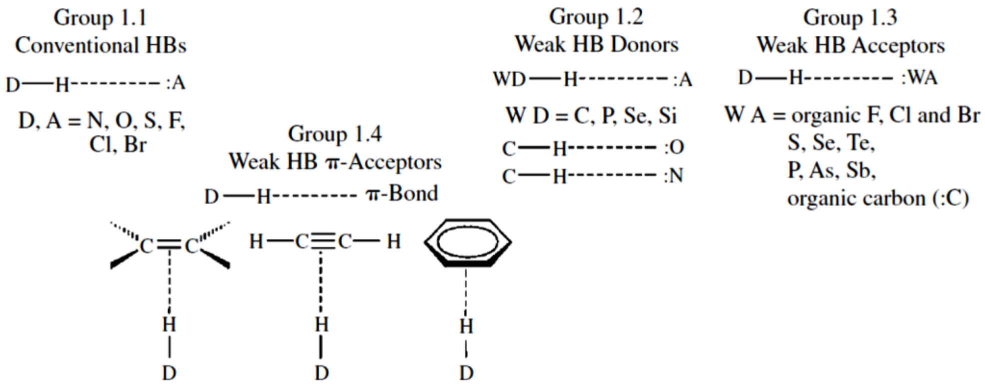
Group 1.1
Conventional HBs
D—H---------:A
D, A = N, O, S, F, Cl, Br
Group 1.2
Weak HB Donors
WD—H---------:A
W D = C, P, Se, Si
C—H---------:O
C—H---------:N
Group 1.3
Weak HB Acceptors
D—H--------- :WA
W A = organic F, Cl and Br
S, Se, Te,
P, As, Sb,
organic carbon (:C)
Group 1.4
Weak HB π-Acceptors
D—H--------- π-Bond
H—C≡C—H
H
D

Figure 2. Hydrogen bonds involving main-group elements classification given by Gilli and Gilli.[4]

Furthermore, there are other typical characteristics of the HBs that should be listed in this section to arrange properly the different features that make the hydrogen bond unique and distinguishable from all other types of chemical bond. These specific characteristics include structural aspects, like linearity or directionality, together with energetic and electronic aspects related to the origin of the HB, like co-operativity, electronic density distribution, charge and proton transfer effects. All these aspects permit globally the categorization and comparative analysis of hydrogen bonding.

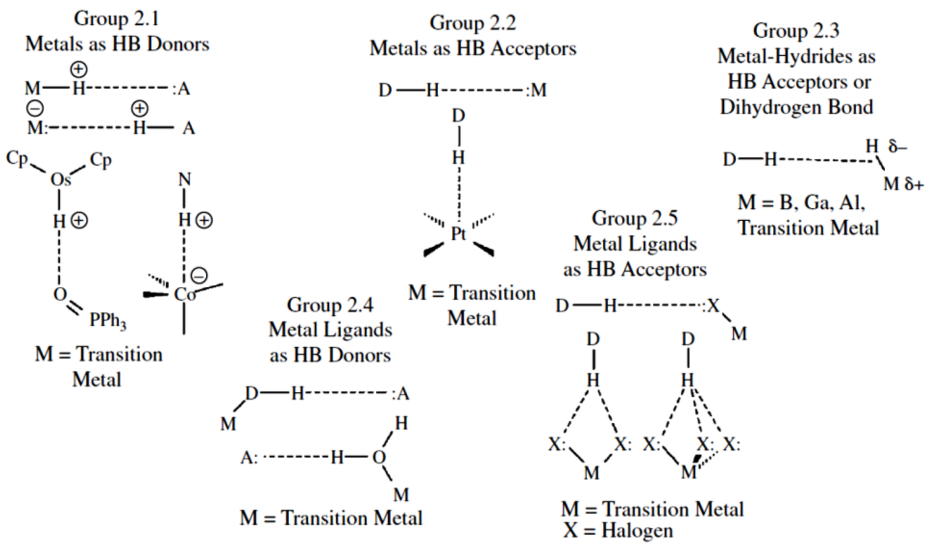
Group 2.1
Metals as HB Donors
M—H---------:A
M:---------H— A
Cp
Os
Cp
H
O
PPh3
N
H
Co
M = Transition Metal
Group 2.2
Metals as HB Acceptors
D—H---------:M
D
H
Pt
M = Transition Metal
Group 2.3
Metal-Hydrides as HB Acceptors or Dihydrogen Bond
D—H-----------H δ–
M δ+
M = B, Ga, Al, Transition Metal
Group 2.4
Metal Ligands as HB Donors
D—H---------:A
M
A:--------H—O
H
M
M = Transition Metal
Group 2.5
Metal Ligands as HB Acceptors
D—H---------:X
M
D
H
X:
X:
M
M = Transition Metal
X = Halogen

Figure 3. Hydrogen bonds involving metal-centers classification given by Gilli and Gilli.[4]

In order to simplify the categorization of the HB as a global chemical phenomenon, Gilli and Gilli[4] proposed a classification of HBs into three classes representing the three basic mechanisms by which the HB is formed, shown in Table 2:

Class 1, or proton-transfer hydrogen bonds, includes all HBs formed by main-group elements that are associations of an acid (as donor) with a base (acceptor).

Class 2, or proton sharing HBs. These are charged acid-acid or base-base HBs associated with positive and negative charged-assisted hydrogen bonds.

Class 3, or resonance-assisted HBs. These are the proton-sharing interactions in where it is not clear which partners share the proton because of the π-delocalization.

Table 2. Hydrogen bonds categories by Gilli and Gilli in *The Nature of the Hydrogen Bond*[4]

	Class 1			Class 2		Class 3
HB Notation	Ordinary	Double charge-assisted	σ-bond cooperative	Negative charge-assisted	Positive charge-assisted	π-bond cooperative
Maximum HB strength	Weak	Very strong	Moderate	Very strong	Very strong	Strong
D···A proton exchange	Proton-transfer	Proton-transfer	Proton-transfer	Proton-sharing	Proton-sharing	Proton-sharing
D···A acid-base exchange	Acid-base	Acid-base	Acid-base	Acid-acid	Base-base	None

1.1. *Hydrogen Bonds involving Oxygen: The O-H···O bond*

The hydrogen bonds involving an oxygen center, like O-H···O, O-H···N or N-H···O, are among the best-known conventional hydrogen bonds. In particular, the O-H···O hydrogen bond is crucial in nature because of its influence on molecular packing and solvation in small biological compounds and macromolecules, like carbohydrates, amino acids or nucleosides, among others. This HB is also relevant in the structure of many compounds daily used by humans such as cellulose and derived polymers in its many different forms in nature[39] (both involving inter- and intra-molecular hydrogen bonding). Due to its abundance in most of the compounds that surround us and due to its diversity in different classes of compounds, these HBs are the most studied, both in solutions, crystals (obtained by X-ray or neutron diffraction and documented in the CCDC Cambridge structural database[40]) and, in less extent, in the gas-phase (mostly spectroscopically). For this reason, they are indeed the hydrogen bonds for which more structural and spectroscopic data is available.

The structural characteristics of the O-H···O HB can be obtained from the statistical surveys of experimental data and theoretical calculations, as illustrated in Table 3. These investigations point to a soft interaction with wide interval ranges for the hydrogen bond distances and linearity of 0.2-0.6 Å and 140-180°, respectively.[4,41] The hydrates of carboxylic acids are close to the properties of the strong hydrogen bonds, with a lengthening of the covalent bond and high linearity.[41] In carbohydrates, where the donor and acceptors are alcohol or ether groups, the hydrogen bond distances maintain a shorter interval of r =1.74-1.96 Å. The O-H···O_w and O_w-H···O_w hydrogen bonds are, respectively, shorter and longer than the O-H···O and O_w-H···O, reflecting the weak donor and stronger acceptor characteristics of water.

Table 3. O-H···O Bond Lengths (Å) from different classes of small molecules.

	Carboxylic acids	Amino acids	Carbohydrates	Inorganic salt hydrates	Purines and pyrimidines	Organic hydrates	Nucleosides and nucleotides
Number of data[a]	26	26	255	296	66	46	322
min	1.40	1.44	1.74	1.74	1.60	1.60	1.55
max	2.01	2.06	1.96	2.26	2.46	2.25	2.18
mean	1.71	1.74	1.82	1.82	1.83	1.90	1.92

[a]Data based on neutron diffraction analyses (pag. 61 '*An introduction to Hydrogen Bonding*', *1997*, Jeffrey)[41].

Steiner[42] has produced a scatter plot of O-H···O HB angles versus the HB lengths, reproduced in Figure 4, identifiying several interaction regions. The most interesting region for the gas-phase studies of the present Thesis is the region of bidirectional two-center bonds (or region 1), where hydrogen bond distances group around distances of 1.8-1.9 Å and angles of 160-180°. Previous gas-phase studies of this hydrogen bond are reviewed elsewhere.[43]

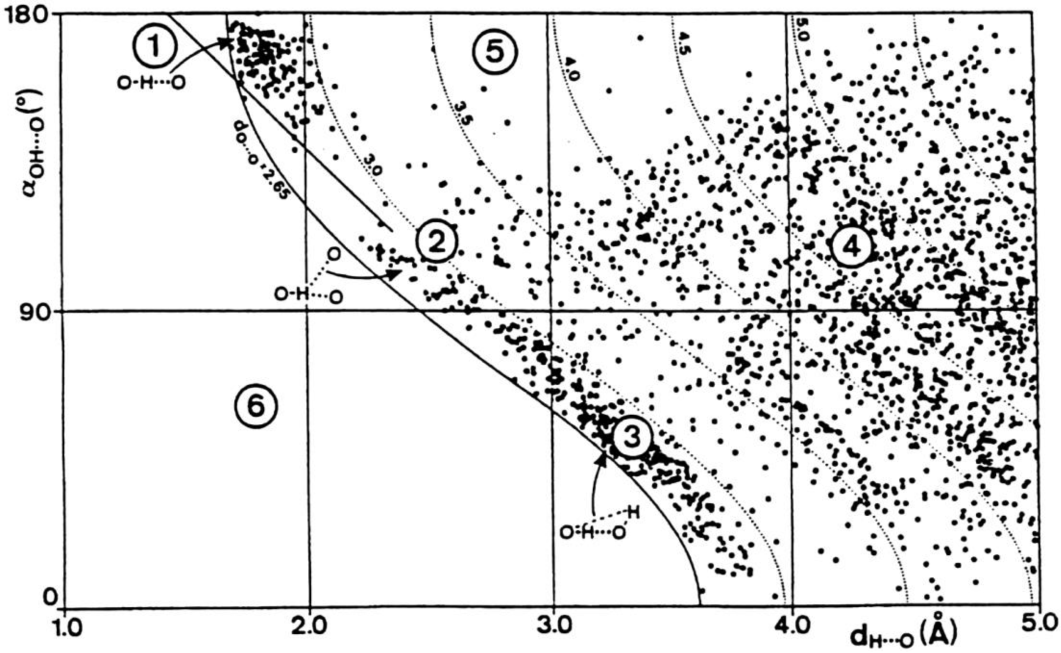

Figure 4. Scatter plot of O–H···O angles versus *r*(H···O) HB bond lengths for hydroxyl and water donors in carbohydrate crystal crystal structures from *Steiner*.[42] (1) two-center and major component of three-center bonds. (2) minor components of three- (and four-) center bonds. (3) non-bonding next neighbours. (4) non-bonding second-next neighbours. (5) near-linear stretched bonds. (6) excluded region due to repulsive forces

Recent computational predictions have also contributed to the understanding of the physical characteristics of the HB, in particular, the magnitude of the electrostatic contributions.[44–47] This characteristic has been useful in several studies[48–50] to describe the proton affinity as a hydrogen bond descriptor for the O-H···O hydrogen bonded systems while, on the other hand, there are some cases where the dispersive energy contribution increases notably (together with the increase of the alkyl chain length of the HB acceptors) as in the case of tyrosine and methionine intermolecular complexes with *para*-Cresol (see Biswal *et al*. review)[51].

Concerning the data presented in this Thesis, the structural influence of the moderately strong O−H···O hydrogen bond has been observed both in the monomers, monohydrates and homodimers of several molecular systems including aromatic and saturated five- and six-membered rings like cyclohexanol, furfuryl alcohol and thenyl alcohol. More specifically, cyclohexanol ··· H_2O and the homodimer (cyclohexanol)$_2$ in *Chapters II and III*, furfuryl alcohol ··· H_2O in *Chapter IV*, thenyl alcohol ··· H_2O in *Chapter V*, and the homodimers of (furfuryl alcohol)$_2$ and (thenyl alcohol)$_2$ in *Chapter VI*.

1.2. *Hydrogen Bond involving Sulfur.*

In his book *The Hydrogen Bond*,[35] Pimentel mentioned the thiol group as a possible HB donor, with the S−H stretching mode broadening, shifting to lower vibrational frequency and becoming much more intense. However, HBs to sulfur centers have been conventionally dismissed as weak interactions of dispersive character, with reduced structural influence compared to conventional first-row HBs like O-H···O, O-H···N or N-H···O.[35,37,52] More recently, Biswal[51] and Wategaonkar[44] have reviewed sulfur HBs, concluding that they are multifaceted interactions with several points of interest: 1) Sulfur forms σ and π HBs as donor (S-H···O, S-H···S, S-H···π, etc) and acceptor (O-H···S, N-H···S, etc), 2) Sulfur HBs can be as strong as conventional HBs, 3) Sulfur HBs may display considerable electrostatic character and 4) Sulfur HBs influence structure and function of many proteins and organic crystals.

Despite these posibilities for sulfur-centered interactions the number of studies on HBs involving sulfur is still much lower than others involving more electronegative atoms. For this reason and with the aim of better understanding the properties of the diverse HBs interactions, the interest in sulfur (and other atoms in groups 14–16) has grown quantitatively in recent years. As a consequence, molecular studies are justified to contribute information on the structure, physical nature and balance of electrostatic and dispersive forces in NCIs involving sulfur centers. In particular, the observation of weakly-bound intermolecular clusters in the gas phase simultaneously provides empirical data unbiased by crystal or matrix effects and validation of theoretical models. Vibrational evidence of sulfur hydrogen bonding generally originates from IR,[53,54] and double-resonance (UV–UV or UV–IR) laser spectroscopy, [45,51,55–64] but is mostly of low resolution and not always structurally univocal. High-resolution rotationally-resolved[65,66] studies are still scarce, as illustrated by the fact that the hydrogen sulfide dimer was reported only in 2018.[56] To date, rotational spectroscopy has addressed several intra-[67–69] and intermolecular interactions in hydrogen sulfide dimers or sulfur-containing complexes.

Molecular studies on sulfur hydrogen bonding have mostly observed thiols as proton acceptors, especially in O-H···S,[58,59,62,70] N-H···S,[57] F-H···S[71] and C-H···S[72] hydrogen bonds. The description of thiol as proton donors in S-H···S[56,61] and other weak sulfur interactions like S-

H···O,[63] S-H···N[73] and S-H···π[74] has been far less investigated. Structurally, sulfur HBs are much longer than the equivalent oxygen HB (r(S-H···S)= 2.778(9) in the H_2S dimer).[56,64] The structures also reflect reflect the larger size and polarizability of the sulfur atom and a change in acceptor directionality associated to the larger inter *n*-pair angle at S than O in thiols and thioethers (close to 90°), i.e., 85(3)° in tetrahydrothiophene···water.[58]

Concerning the physical origin of the sulfur-centered interactions it is convenient to use energy decomposition to express the energy of the HB as a result of contributions from electrostatics, polarization, exchange repulsion, charge transfer and dispersion. The information collected so far corroborates that hydrogen-bonding interactions involving sulfur as acceptor are primarily dominated by dispersive forces, in some cases accounting for more than 50% of the total binding energy.[45,55,64] At the same time it is observed that they are not much weaker than the interactions involving oxygen, which have a stronger electrostatic component.[51,62]

For all these reasons, the gas-phase investigations are thus clearly oriented to complement previous molecular descriptions relying solely on crystal data and theoretical calculations.[75–82]

2. Gas-Phase Rotational Investigations of NCIs

The HB and other non-covalent interactions have been mostly investigated in condensed phases, either in crystal structures or liquids. The gas-phase investigations, in particular those of high-resolution rotational or vibrational studies, are much less developed.[43,66]

The advantage of the gas-phase studies is that they provide disaggregation, i.e., they permit to study isolated molecules without the influence of matrix effects like the solvent or the crystal structure. In particular, the introduction on supersonic jet techniques in the 1980s made possible the generation of weakly-bound intermolecular complexes with specific sizes and functional groups.[83–86] In this way it is possible to select specific interactions for study, permitting a systematic and mass-selected analysis of different families of NCIs.

A second difference between solid-state and gas-phase studies is the direct comparison of the isolated complexes with powerful molecular orbital theoretical calculations (either DFT or ab initio). In relation with the investigations in gas-phase, the objective of the research carried out in this Thesis is to contribute to the understanding of hydrogen bonding through MW spectroscopy studies, supplemented by computational studies. The generation of intermolecular complexes in supersonic jets combined with rotational investigations may thus contribute to enlarge the empirical data on HBs, offering benchmark comparisons with the condensed phase and theoretical calculations.

Among the gas-phase techniques totational spectra offer very detailed structural data by obtaining molecular geometries, bond energies, force constants, electric dipole moments, electric charge distribution, etc., easily discriminating the isomeric or isotopic composition. Moreover, the introduction in the last decade of chirped-pulse microwave fast-passage techniques has revolutionized the field of rotational spectroscopy offering broadband capabilities for high-resolution studies in the gas phase. The direct comparison with quantum mechanical predictions provides insight into the origin of the inter- and intramolecular interactions with much greater precision than any other spectroscopic technique, simultaneously serving as testbed for fine-tuning of theoretical methods. Rotational spectroscopy appears particularly useful for complex multiconformational biochemical systems, where conventional techniques in condensed phases such as IR and VCD may show deficiencies for structural identification. In these cases, the broadband and high-resolution advantage of rotational spectroscopy may contribute significantly to the advancement of the techniques of chemical analysis used in academia and industry.

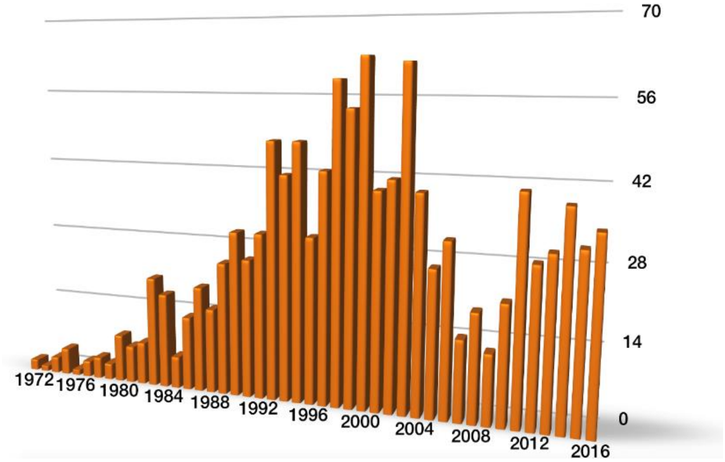

Figure 5. Rotational studies of intermolecular clusters, as collected in the database MOGADOC.

II. Methods

The results presented in this PhD thesis are based on the analysis of microwave rotational spectra with the support of molecular orbital calculations. Rotational spectroscopy is a highly sensitive and suitable technique for the study of the gas-phase molecular structure, as the rotational spectrum of a polyatomic molecule is directly related to the geometric distribution and atomic masses through the moments of inertia. Depending on the molecular size and temperature, pure rotational spectra are observed predominantly in the frequency range from the cm- to the mmw- and submmw-wave ranges (1 GHz to 1 THz). In particular, the studies presented in this Thesis have been conducted in the cm-wave region of 2-18GHz. In this section we will summarize some fundamentals of rotational spectroscopy from its historical evolution to the techniques used and the theoretical approaches.

More specific details can be found in the bibliography, including experimental techniques,[87,88] theory of rotational spectroscopy,[89–91] supersonic jets expansions[83–86] or the theoretical computational methods.[92]

1. Rotational spectroscopy

1.1. *General aspects*

Rotational spectroscopy has evolved considerably from the first studies in 1934[93] to the present, developing different complementary techniques. Nowadays, the spectral analysis is considerably improved as a result of the introduction of time-domain and supersonic jet techniques, permitting a great improvement of the spectral resolution, bandwidth, and sensitivity. Rotational spectroscopy uses microwave (MW) radiation to probe the transitions between quantized molecular rotation energy levels in the gas-phase. The MW experiments[93] expanded from 1945 thanks to the development of radar during World War II, in particular with the introduction of Wilson's Stark modulation direct-absorption techniques in the cm-wave range and the development of radiation sources in the mm-wave region. These experiments were done in a static gas cell using frequency scanning techniques, where monochromatic radiation passes through a sample cell and the transmitted intensity is registered versus the frequency. A noticeable step forward came in 1975 with the introduction by Flygare of time-domain rotational spectroscopy[94–96] or Fourier-transform microwave spectroscopy (FTMW), following conceptual developments similar to FTNMR. The FTMW technique uses a short (μs) MW pulse to produce a transient excitation polarizing the sample, recording in the time-domain the molecular relaxation signal or free-induction-decay. In 1981 Flygare combined the time-domain spectroscopic techniques with a supersonic jet expansion,[97] using a tunable high-quality Fabry-Pérot resonator[98,99] to couple the radiation to the sample. This spectrometer is known as Balle-Flygare or molecular beam (MB-FTMW) cavity spectrometer.

The Balle-Flygare FTMW spectrometer has been heavily used (even today it is the main technique in many research groups). Because of many modifications and improvements, in particular the coaxial orientation of the beam and the resonator (COBRA setup) implemented by Grabow[100] in 1996, the spectrometer produces sub-Doppler resolution (FWHM linewidths of 10 kHz) and very high sensibility, but the operation has limited bandwidth (1 MHz) and requires slow scanning. In 2006, Pate brought up the revolutionary chirped-pulse spectroscopy,[101] a broadband FTMW spectrometer which has a bandwidth limit that is only imposed by the technical limitations of microwave power amplifiers and high-speed digitizers.[102] This instrument uses a fast-passage technique based on a frequency modulated (chirped) excitation pulse, simultaneously exciting the full operating bandwidth. The CP-FTMW technique allowed to exponentially reduce the spectral acquisition time and the amount of sample while increasing the frequency operation bandwidth four orders of magnitude.[87] Other designs for broadband spectroscopy have been contributed by Grabow, considerably improving the spectral linewidth (In-phase/quadrature-phase-modulation passage-acquired-coherence technique, IMPACT, by Grabow's group)[103]. In 2013 Patterson introduced the detection of molecular chirality by use of a triple resonance or three-wave-mixing. The techniques on chirality detection are presently progressing in several laboratories.

In the experimental work done in this Thesis we have used both a Balle-Flygare FTMW spectrometer (covering the 8-18 GHz frequency range) and a commercial CP-FTMW spectrometer (2-8 GHz) provided by BrightSpec and following Pate's design.[104] Both spectrometers are settled in the *Group of Supersonic Jet and Plasma Spectroscopy* laboratory at the Department of Physical Chemistry of the University of Valladolid and Institute CINQUIMA.

1.2. *Theory of molecular rotation*

In order to achieve a quantitative fit of the experimental data to obtain molecular information, it is necessary to set up a quantum mechanical rotational Hamiltonian. Assuming that large-amplitude motions are not present and a complete separation of the vibrational and rotational motions, the rotational Hamiltonian can be treated independently and is based in the model of the rigid rotor. The rigid rotor deals with the mechanics of the general rotation of a rigid molecular set, taking into account the quantization of the angular momentum. Semirigid corrections and electric and magnetic effects can be added at a later stage.

The theory of molecular rotation is described in several references,[89–91] so it is only briefly summarized here. A rigid rotor can be defined by its inertia tensor (a symmetric 3x3 matrix). Diagonalization of the inertia tensor leads to a molecular coordinate system referred as principal axes of inertia, with origin at the center of mass and characterized by the three principal moments of inertia (conventionally $I_a \leq I_b \leq I_c$). The classical rotational energy in the principal axes is given by

$$E_{rot} = \frac{1}{2}\left(\frac{J_a^2}{I_a} + \frac{J_b^2}{I_b} + \frac{J_c^2}{I_c}\right) \qquad (1)$$

where J_i represents the angular momentum. The classical Hamiltonian may be converted into the quantum mechanical Hamiltonian using the standard procedures, obtaining

$$\boldsymbol{H_{rot}} = A\,\boldsymbol{J_a}^2 + B\,\boldsymbol{J_b}^2 + C\,\boldsymbol{J_c}^2 \qquad (2)$$

where the angular momentum operators are represented by $\boldsymbol{J_i}$ $(i = a, b, c)$ and A, B, C are the rotational constants (inversely proportional to their moment of inertia: $A = \left(\frac{h^2}{8\pi^2 I_a}\right)$, $B =$

$\left(\frac{h^2}{8\pi^2 I_b}\right)$ and $C = \left(\frac{h^2}{8\pi^2 I_c}\right)$, usually expressed in MHz). The expressions and solutions of the rotational Hamiltonian depend on the type of molecular rotor. A symmetric top has an internal C_n $(n \geq 3)$ rotation symmetry axes so two moments of inertia are equal (*oblate* top: $I_a = I_b < I_c$; prolate top: $I_a < I_b = I_c$). The asymmetric tops, like all molecules considered in this Thesis, have all moments of inertia different. Linear and top-symmetric rotors have analytical solutions, but the asymmetric rotors are solved numerically. For a symmetric top the square of the angular momentum $\boldsymbol{J}^2$ commutes with one of its components ($\boldsymbol{J_z}$ or $\boldsymbol{J_Z}$), so they can be defined simultaneously. In consequence, three quantum numbers are necessary: the total angular momentum J (associated with the operator $\boldsymbol{J}^2$), the projection of the angular momentum along the internal symmetry axes K $(= 0, \pm 1, \pm 2, \ldots \pm J$, associated with the operator $\boldsymbol{J_z}$) and the projection associated with the space-fixed (z) axis, or M $(= 0, \pm 1, \pm 2, \ldots \pm J$, associated with the operator $\boldsymbol{J_Z}$). Concerning the wavefunctions and eigenvalues of the Schrödinger equation, it is convenient to assimilate the problem to a complete and diagonalizable Hamiltonian matrix by an orthonormal basis $|J, K, M\rangle$. For an asymmetric top the Schrödinger the situation becomes more complicated, where the Schrödinger wave equation cannot be solved directly but its wave functions may be represented by a linear combination of symmetric rotor. None of the angular momentum components is a constant of motion, so the $\boldsymbol{J_i}$ angular momentum operators do not commute with the rotational Hamiltonian. In consequence, the quantum number K is not a good quantum number. Instead, each eigenvalue of the asymmetric Hamiltonian is approached by extrapolating to the oblate and the prolate symmetric top and is assigned pseudo-quantum numbers K_{-1} (K value in the prolate symmetric top basis) and K_{+1} (K value in the oblate symmetric top basis). In this way, each asymmetric top eigenvalue is defined by J, K_{-1} and K_{+1} and the rotational transitions are indicated as $J'_{K_{-1}',K_{+1}'} \leftarrow J''_{K_{-1}'',K_{+1}''}$ (with $\tau = K_{-1} - K_{+1}$). The general procedure for obtaining the asymmetric wavefunctions consists in expanding the functions in terms of the orthogonal symmetric-rotor wavefunctions:

$$\Psi_{J\tau M} = \sum_{J,K,M} a_{JKM} \Psi_{JKM} \tag{3}$$

The secular determinant is then set-up for each J level and solved numerically by matrix diagonalization. Only for the low J values it is possible to obtain explicit solutions for the rotational energies.

In order to observe a rotational transition, it is necessary to consider the selection rules for electric dipole transitions, requiring a non-zero value for the integral moment of transition in the space-fixed axes: $\langle J', \tau', M' | \boldsymbol{\mu} | J'', \tau'', M'' \rangle \neq 0$. The first requirement is thus that the molecular system has non-zero permanent dipole moment $\boldsymbol{\mu}$. In the case of an asymmetric top, is convenient to take into account the components along the principal axes $\{\boldsymbol{\mu_a}, \boldsymbol{\mu_b}, \boldsymbol{\mu_c}\}$ to know which transitions are possible. Since the wavefunctions were expressed as linear combinations of the symmetric rotor the selection rules for J are the same as in a symmetric rotor:

$$\Delta J = 0, \pm 1 \tag{4}$$

(transitions with $\Delta J = -1$, $\Delta J = 0$ and $\Delta J = +1$ are designated P, Q or R). The selection rules for the pseudo quantum numbers K_{-1}, K_{+1} may be obtained from the symmetry of the ellipsoid of inertia and are collected in Table 4.

Table 4. Selection rules for the pseudo quantum numbers of the asymmetric rotor.

μ-type transition	ΔK_{-1}	ΔK_{+1}
a ($\mu_a \neq 0$)	0, ± even number	± odd number
b ($\mu_b \neq 0$)	± odd number	± odd number
c ($\mu_c \neq 0$)	± odd number	0, ± even number

For low values of J the rigid rotor model is approximately valid for asymmetric tops, and it can be used to predict the molecular levels. Alternatively, a set of pure rotational transitions can be fitted to obtain the three ground-state rotational constants. However, perturbative corrections to the rigid rotor are often required for larger quantum numbers. These corrections are classically interpreted as vibrational distortions of the molecular rotating structure and are known as centrifugal distortion. The centrifugal distortion corrections are several orders of magnitude less significant than those related with the rotational constants. The most widely used semirigid-rotor model is the Watson's reduced Hamiltonian,[105,106] either with symmetric (S) or asymmetric reductions (A), which is precise enough for quantitative assignment of pure rotational spectra into the millimeter-wave range. The semirigid Hamiltonian is

$$\boldsymbol{H}_{\boldsymbol{rot}} = \boldsymbol{H}_{rigid\ rotor} + \boldsymbol{H}_{centrifugal\ distortion} \tag{5}$$

This Thesis has mostly used the Watson's S-reduction of quartic order, which uses five centrifugal distortion constants ($D_J, D_{JK}, D_K, d_1, d_2$) and has numerical advantages over the A-reduction:

$$\boldsymbol{H}_{\boldsymbol{rot}} = \underbrace{A\boldsymbol{J}_{\boldsymbol{a}}{}^2 + B\boldsymbol{J}_{\boldsymbol{b}}{}^2 + C\boldsymbol{J}_{\boldsymbol{c}}{}^2}_{rigid\ rotor} \underbrace{-D_J\boldsymbol{J}^4 - D_{JK}\boldsymbol{J}^2\boldsymbol{J}_{\boldsymbol{c}}^2 - D_K\boldsymbol{J}_{\boldsymbol{c}}^4 + d_1\boldsymbol{J}^2\left(\boldsymbol{J}_+^2 + \boldsymbol{J}_-^2\right) + d_2\boldsymbol{J}^2(\boldsymbol{J}_+^4 + \boldsymbol{J}_-^4)}_{quartic\ centrifugal\ distortion\ terms} \tag{6}$$

with $\boldsymbol{J}_+$ and $\boldsymbol{J}_- = (\boldsymbol{J}_a \pm i\,\boldsymbol{J}_b)$.

Occasionally the molecular systems may present additional complications like the presence of large-amplitude-motions or electric or magnetic effects, which require more complicated Hamiltonians. During this Thesis we have encountered two particular cases: 1) fine effects due to large-amplitude tunnelling motions, and 2) hyperfine effects due to nuclear quadrupole coupling. Tunnelling effects are produced when the molecule experiments a large-amplitude-motion interconverting between two symmetry-equivalent configurations, like an internal torsion or inversion. In this case the double-minimum potential function splits the ground vibrational state in two distinct torsional substates for moderately low barriers. As a result, there are two manifolds of spectral rotational levels associated to each of the torsional levels (see Chapters II and III).[89,107] The nuclear quadrupole coupling effects result of the electric interaction between a nuclear quadrupolar moment (present in nuclei with spin $I \geq 1$, like ^{14}N) and the molecular electric field gradient at the quadrupolar nucleus.[89]

1.3. *Balle-Flygare FTMW spectrometer @ UVa*

The experimental data presented in this Thesis have been obtained essentially by using two different but complementary spectrometers at the UVa (the spectrometers used in the research visits done during the Thesis are not included here but are referred in the publications). The UVa spectrometers have in common the use of supersonic jet expansions and include:

- A Balle-Flygare FTMW cavity spectrometer (8-18GHz)
- A chiped-pulse FTMW spectrometer (2-8 GHz)

The benefits and characteristics of jet expansions for spectroscopic research are discussed elsewhere.[108] Briefly, supersonic jet experiments are based on a near-adiabatic gas expansion through a pin-hole nozzle into an evacuated chamber. The pressurized region and the expansion chamber maintain a huge difference of pressure, so the expanding molecules pass from a situation of high-pressure (1-10 bar) random thermal motion to a directed motion in the low-pressure region (10^{-5}-10^{-7} mbar). The sudden change in the kinetic conditions turns the broad velocity distribution into a narrow distribution centered around the terminal speed. This process converts the internal molecular energies into kinetic energy, producing a considerable molecular freezing. However, since the different internal motions cannot equilibrate, the translational, rotational and vibrational temperatures are different. The effective rotational temperatures are of 2-3 K, while vibrational temperatures reach 100-150 K, moving the molecular population to the lower rotational levels of the vibronic ground-state and simplifying the spectrum. Another important benefit of the supersonic jet is the reduction of intermolecular collisions, avoiding any mechanism of chemical reaction or decomposition. For this reason, the supersonic jets are used as a source of intermolecular clusters. The clusters are generated by many-body collisions in the first moments of the expansion and are later stabilized in the later expansion by the absence of collisions. For this reason the jet expansions are the most effective way to study weak intermolecular complexes.[97] The reduction of intermolecular collisions additionally contributes to the reduction in the spectral linewidth, which may reach sub-Doppler (kHz) levels. These features make this type of expansion a useful tool for spectroscopy investigations characterizing molecular structures in the gas phase (in particular, rotational, vibrational and electronic spectroscopy) and constitute the fundamental principle on which our experimental experiments are conducted.[83–86]

The **Balle-Flygare FTMW spectrometer** in the *Group of Supersonic Jets and Plasma Spectroscopy* laboratory is a non-commercial instrument based on the Balle-Flygare[99] design, and includes a Fabry-Perot cavity made of two spherical mirrors. Figures 5 and 6 shown the general design of the spectrometer and a functional diagram. The sample can be prepared as a gaseous mixture (typically 0.1-0.5%) in a carrier gas or located in a reservoir nozzle if it is liquid or solid for vaporization. The spectrometer uses several nozzles (diameters ϕ=0.8-1.2 mm) and may be heated to ca. 373 K (depending on the macroscopical properties such as melting and boiling point, vapor pressure, etc.). The sample is entrained in a carrier gas (He, Ne or Ar) at stagnation pressures of 1-5 bar and expanded through a solenoid valve, creating a pulsed supersonic jet probed within the Fabry-Perot MW resonator. The resonator is mounted

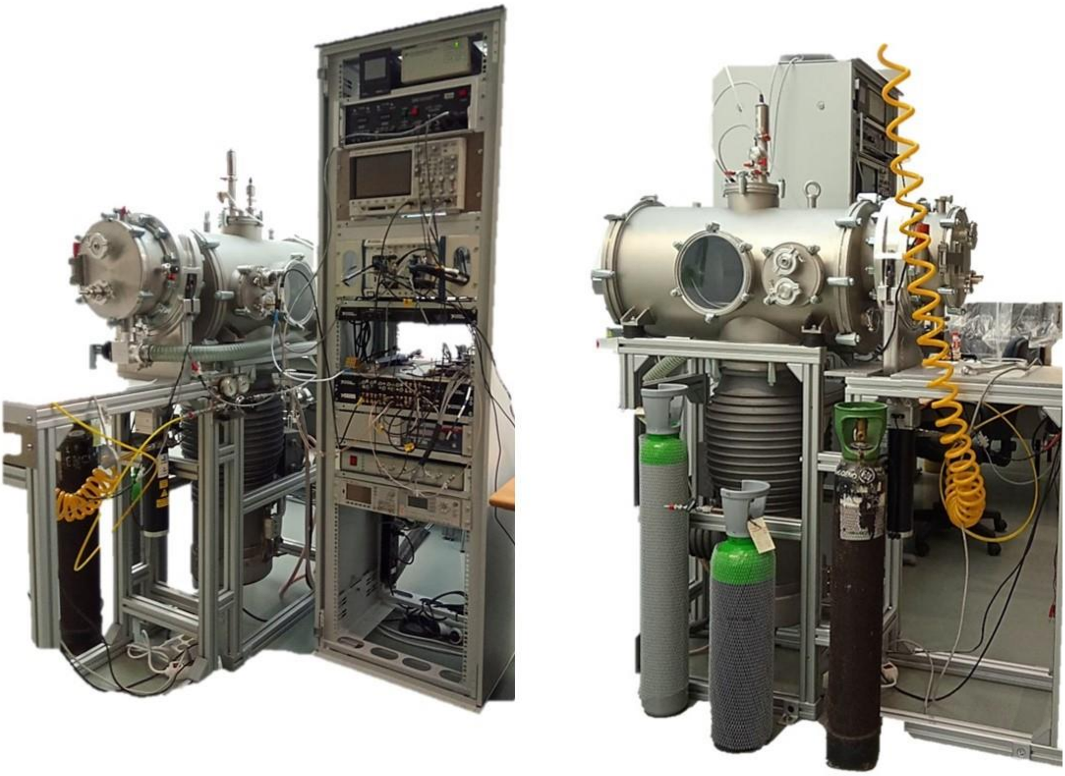

Figure 6. Two different views of the Balle-Flygare FTMW spectrometer in the *Group of Supersonic Jets and Plasma Spectroscopy* of the University of Valladolid (UVa), showing the expansion chamber, diffusion pump and electronics rack.

inside the vacuum chamber and is formed by two spherical mirrors in near confocal position (ϕ=33 cm). Two dipole antennas are located at the center of the mirrors, while the injection valve is positioned off-axis near the center of one of the mirrors. The collinear arrangement of the jet and resonator axis[100,109] doubles each transition into two Doppler components. The gas pulses extend for 500-1000 μs and are followed by short microwave impulses (~1 μs, < 100 mW) at a fixed frequency, which allow the molecules to be polarized. Typically, up to 4 microwave pulses may be used per gas pulse. The emitted free-induction-decay, recorded in the time-domain (400-900 μs), is amplified and recorded with a heterodyne receiver centered at 30 MHz. The resulting signal is processed with the FTMW++ software implemented at the University of Hannover by Grabow[110] getting a real-time Fourier transformation and accumulation of successive experiments. All frequency oscillators in the system are locked to a rubidium standard, providing frequency accuracies of the rotational transitions below 5 kHz.

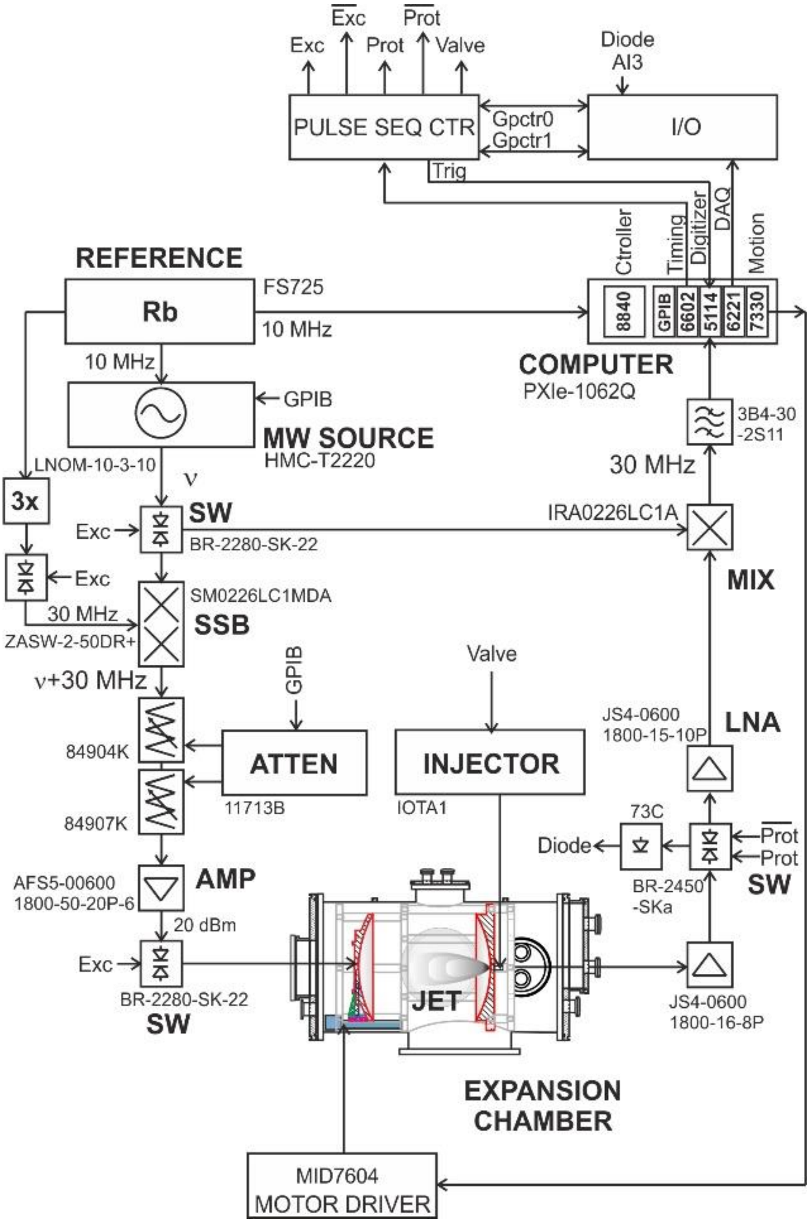
$\overline{\text{Exc}}$
$\overline{\text{Prot}}$
Exc
Prot
Valve
Diode
AI3
PULSE SEQ CTR
Gpctr0
Gpctr1
I/O
Trig
Ctroller
Timing
Digitizer
DAQ
Motion
REFERENCE
Rb
FS725
10 MHz
8840
GPIB
6602
5114
6221
7330
COMPUTER
PXIe-1062Q
10 MHz
GPIB
MW SOURCE
HMC-T2220
3B4-30
-2S11
30 MHz
LNOM-10-3-10
ν
3x
SW
Exc
BR-2280-SK-22
IRA0226LC1A
Exc
MIX
30 MHz
SM0226LC1MDA
SSB
ZASW-2-50DR+
GPIB
Valve
ν+30 MHz
JS4-0600
1800-15-10P
LNA
84904K
ATTEN
INJECTOR
84907K
11713B
IOTA1
73C
Diode
$\overline{\text{Prot}}$
Prot
AFS5-00600
1800-50-20P-6
AMP
BR-2450
-SKa
SW
20 dBm
Exc
JET
BR-2280-SK-22
SW
JS4-0600
1800-16-8P
EXPANSION
CHAMBER
MID7604
MOTOR DRIVER

Figure 7. Functional diagram of the Balle-Flygar FTMW cavity spectrometer used in the Thesis.

Despite the narrow bandwidth (1MHz), the spectral resolution (~5 kHz) that can be achieved with this apparatus cannot be obtained with other spectroscopic techniques or setups. Compared with the CP-FTMW spectrometer, it allows us to work at higher frequencies and provides a better spectral resolution necessary to determine rotational transitions split into different component lines in case of hyperfine and tunneling effects.

1.4. *Chirped-Pulse FT-MW spectrometer @ UVa*

Some years after the first experiments on FTMW spectroscopy, Flygare proposed a new technique known as fast-passage, introducing a distinction with the processes of transient excitation.[111,112] A fast-passage is achieved when a frequency is swept through a two-level resonance in a time much shorter than the relaxation period. Fast-passage was conducted initially with a fast modulating Stark electric field, switching the resonance frequencies. In 2005 Pate implemented fast-passage techniques using a digital frequency sweep carried out with an arbitrary waveform generator (AWG), sweeping at a rate much faster than the dephasing time of the molecular coherence.[113] In the present designs the sample is excited with a short microwave pulse implementing a very fast linear frequency sweep (6 GHz/μs) or "chirped" pulse, so this technique is known as chirped-pulse Fourier Transform Microwave (CP-FTMW) spectroscopy. The chirped pulse covers all molecular transitions within the frequency range of the sweep, allowing to coherently excite a large swath of molecular transitions simultaneously. This advance was only possible thanks to the progress in the available digital technology.

These spectrometers combine the AWG radiation source with broadband detection with a high-sampling-rate high-speed digital oscilloscope, simultaneously detecting all molecular emissions. The excitation capabilities of the CP-FTMW spectrometer are limited by the amplification stage, which typically requires a minimum of 20-400 W to cover the region 2-8 GHz. The CP-FTMW technique has revolutionized the field of rotational spectroscopy making its design one of the most followed and influential in MW spectroscopy research.

In 2015 the UVa bought a pulsed-jet **chiped-pulse FTMW spectrometer** from the company BrightSpec, that was installed in the laboratory of the *Group of Supersonic Jets and Plasma Spectroscopy*. This instrument follows Pate's direct-digital design covering the 2-8 GHz frequency region,[104] and has been used extensively during this Thesis. The CP-FTMW spectrometer is depicted in Fig. 7, with a functional diagram in Fig. 8. The spectrometer uses a single injection system to create a supersonic expansion in the expansion chamber. The sample injection is similar to the FTMW spectrometer, using a solenoid valve attached to a pinhole nozzle. In the case of solid or liquids of low volatility a heating nozzle with an internal reservoir can be used. This instrument has no resonator and the interaction between the radiation and the jet is produced with two (emitting and receiving) horn antennas. For this reason, the jet cannot be installed collinear to the radiation and instead it uses a perpendicular arrangement between the horn antennas and the injection valve. This orientation increases the jet volume probed with the radiation, observing molecules with a larger velocity distribution. As a result, the linewidth increases about an order of magnitude compared with the cavity spectrometer (about 150 kHz). In the present set-up the chirped pulse (1-4 μs) created by the AWG (25 GS/s in two- channel) is amplified with a solid-state power amplifier (20 W) and broadcasted into the excitation region. The detection uses a receiving antenna, a diode limiter, a PIN-diode switch (closed during excitation) and a low-noise amplifier. Finally, the time-domain signal (considerably shorter than in the cavity spectrometer) is acquired for about 40 μs with a high-speed digital oscilloscope (25 GS/s). The typical operation requires signal averaging and uses a repetition rate of 5 Hz. All frequencies are referenced to a 10 MHz Rb standard.

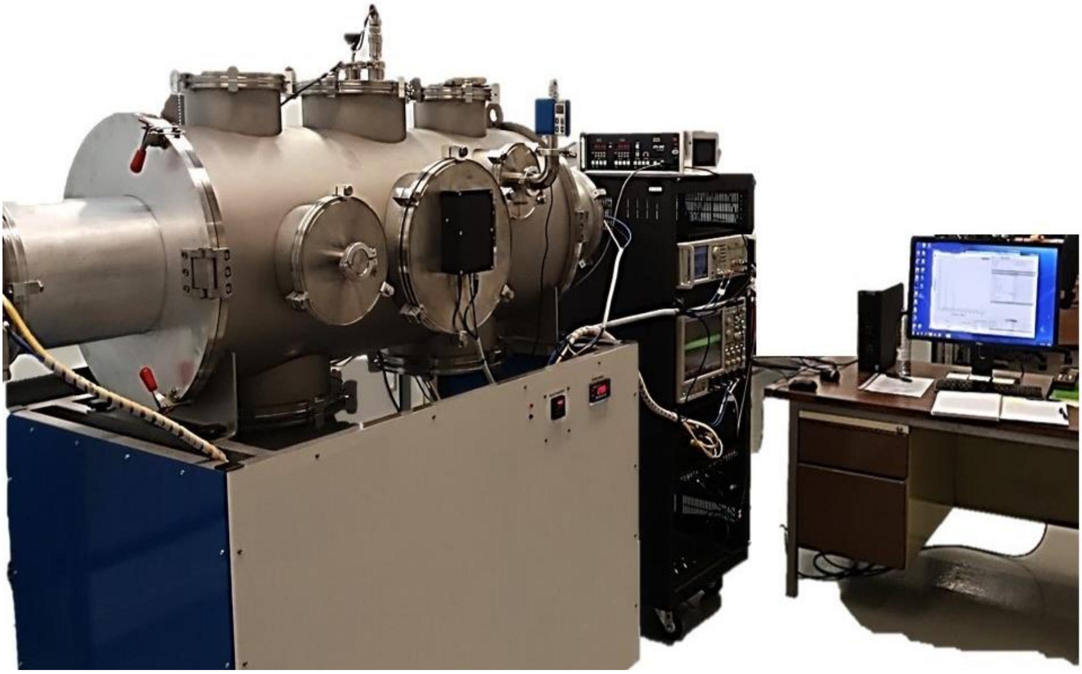

Figure 8. View of the broadband CP-FTMW spectrometer in the laboratory of the *Group of Supersonic Jets and Plasma Spectroscopy* at UVa, used in the studies of this Thesis.

A typical experiment includes the following time sequence:

a) Sample injection (either a gas mixture or vaporized in situ) to form a supersonic expansion. The expansion times depend on the carrier gas (normally 900 μs for neon).
b) Chirped pulse generation (1-5 μs). The AWG excitation bandwidth is selectable till a maximum of 6 GHz, and follows the gas injection with a delay of ~200 μs. Typically several excitation pulses (5-8) can be programmed for each injection pulse.
c) Pre-amplification and power amplification with a 20 W pulsed solid-state unit.
d) Molecular polarization of the jet sample by the chirped pulse.
e) Molecular emission signal (FID) produced by the interaction radiation-matter.
f) Amplification and detection of the molecular emission (~40 μs).
g) Digitalization in the time-domain, followed by a Fourier transformation into the frequency domain. A Kaiser-Bessel window is normally applied before the Fourier transformation.
h) Presentation and analysis.

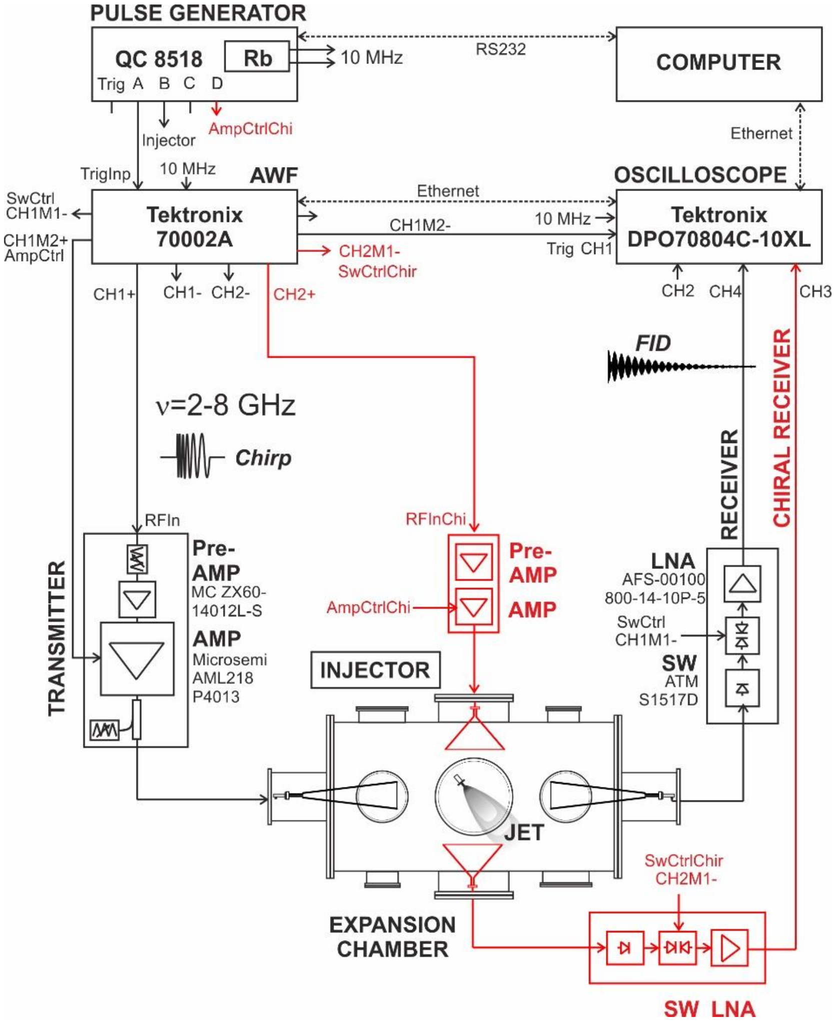
PULSE GENERATOR
QC 8518
Rb
Trig A B C D
10 MHz
RS232
COMPUTER
Injector
AmpCtrlChi
Ethernet
TrigInp
10 MHz
AWF
OSCILLOSCOPE
SwCtrl CH1M1-
CH1M2+ AmpCtrl
Tektronix 70002A
Ethernet
CH1M2-
10 MHz
Trig CH1
Tektronix DPO70804C-10XL
CH2M1- SwCtrlChir
CH1+
CH1- CH2-
CH2+
CH2 CH4
CH3
FID
ν=2-8 GHz
Chirp
RECEIVER
CHIRAL RECEIVER
RFIn
RFInChi
Pre-AMP
MC ZX60-14012L-S
AMP
Microsemi AML218 P4013
TRANSMITTER
Pre-AMP
AmpCtrlChi
AMP
INJECTOR
LNA
AFS-00100 800-14-10P-5
SwCtrl CH1M1-
SW
ATM S1517D
JET
SwCtrlChir CH2M1-
EXPANSION CHAMBER
SW LNA

Figure 9. Functional diagram of the CP-FTMW spectrometer of the *Supersonic Jets and Plasma Spectroscopy Group* at UVa.

2. Computational Methods

Theoretical calculations are powerful and necessary tools in rotational spectroscopy and other spectroscopic fields. They are fundamental in the conformational and structural analysis of gas-phase experiments and, similarly to the developments in instrumentation, they have improved considerably over time. A notable difference between early and current microwave spectroscopy molecular studies is reflected in the different theoretical approaches adopted in their analysis. In the beginning, the spectroscopic studies were based on the analysis of small molecular systems made up of a few heavy atoms (less than 10).[43] Today it is common to find analyses carried out on much larger molecules and their complexes (easily we can find studies of homodimers, trimers or even tetramers in the literature).[43] This advance has been possible not only by the experimental developments, but also thanks to continuous advances in density-functional-theory (DFT) and ab initio molecular orbital calculations, permitting the rationalization and interpretation of the experimental results with a reasonable investment of time and cost in the calculation process.

In this Thesis we have used different computational methods. An initial approach to the structural properties might be a simple molecular mechanics (MM)[92] calculation. Despite this calculation uses classical mechanics and ignores electrons, the low computational cost permits a fast scan of the potential energy surface (PES). This kind of calculation, choosing a proper force field, is tipically used to get an initial conformational search of the posible molecular isomers. In the Thesis we performed MM conformational searches with the commonly used Merck force field (MMFF)[114] and dedicated Monte Carlo[115]/low-mode[116] search algorithms. These initial calculations are not precise and a bit ambiguous, always requiring further calculations with methods based on quantum mechanics.

2.1. *Density Functional Theory and Ab initio calculations*

The computational work included in the Thesis has been mostly directed to perform conformational searches, geometry optimizations and vibrational frequency calculations (estimating the ground-state zero-point energy and centrifugal distorsion terms). Additinally, the calculation of intermolecular complexes presents the problem of the basis-set superposition error (BSSE), which has been taking into account with the counterpoise approximation of Boyds and Bernardi. There are two main tipes of quantum mechanical molecular orbital calculations used in the Thesis: those based on DFT methods and the wavefunction methods based on Hartree-Fock theory[117] and perturbative corrections, such as Møller-Plesset[118] pure ab initio calculations. More advanced calculations, like coupled-clusters methods, have not been used here. Computational methods are widely discussed in the bibliography.[92]

In rotational spectroscopy investigations the DFT and MP2 ab initio methods generally provide a satisfactory description of the experiment. The pure ab initio calculations (computations of electronic orbitals with no other hypotheses than Coulomb interactions) are those based on the Hartree-Fock theory of perturbation corrections to deal with the correlation of electrons and they are called nth order Møller–Plesset perturbation theory. The second order MP2 method corrects Hartree-Fock by calculating the sum of the amplitudes between all double combinations of occupied and virtual orbitals (it does not differ too much for other higher orders much more "expensive" terms)[119]. The MP2 method has been used as a theoretical reference in many MW studies, but as the molecular size increases it may not longer be the most appropriate method, both because of the computational cost and calculation accuracy.

In recent works, DFT calculations is increasingly used,[120] shaping modern molecular quantum chemistry like no other methodology in recent times. Nowadays, it is by far most frequently applied approach used by computational chemists. As a consequence, hundreds of density functional aproximations have been developed, each with their own advantages and disadvantages, which means that despite DFT calculations are technically easy to perform, it is no trivial task to choose the right functional.[121] In this work several DFT computational approximations have been tested to complete our experimental studies, including Minnesota dispersion-corrected MN15-L[122] and M06-2X[123] methods developed by Truhlar, and the hybrid or double-hybrid B3LYP,[124] B2PLYP[125] and ωB97XD[126] methods, supplemented by Grimme's D3[127] dispersion corrections and Becke–Johnson damping functions.[128]

The atomic basis sets used during the computational work have mostly included triple-zeta quality with polarization and difuse functions, most often the Ahlrich's polarized basis def2-TZVP,[129] Dunning's augmented correlation-consistent aug-cc-pVTZ and Pople's 6-311++G(d,p) basis set.[130] The computational calculations were implemented mostly in Gaussian16[131]. All these theoretical methods will be further presented in the following chapters.

2.2. *Complementary computational tools*

In order to reinforce the understanding of the intermolecular clusters, it is worth to complement the DFT and/or ab initio calculations with other computational analysis tools exploring the properties of the molecular electronic density. In this thesis we have used in particular the topological analyses of the reduced electronic density function known as NCIPlots[132] and a method for binding energy decomposition, in particular symmetry-adapted perturbation theory (SAPT).[133]

Symmetry-adapted perturbation theory computes the noncovalent interaction between two molecules, providing a decomposition of the interaction energy into physically meaningful components: i.e., electrostatic, exchange, induction, and dispersion terms.[134] In SAPT, the Hamiltonian of the dimer is partitioned into contributions from each monomer and the interaction. Several truncations of the closed-shell SAPT expansion are available for both the monomers and the cluster, from the simplest zero-order SAPT(0) to SAPT2+(3), with second-order intramonomer correlation corrections and third-order intermonomer dispersion corrections. The calculations may use different basis sets and was used as implemented in PSI4.

The NCIPlot method[135] is based in the analysis of the bond critical points associated to the reduced electronic density matrix, permitting a 3D mapping of the regions with attractive or non-attractive interactions and the comparison between different intermolecular clusters. The NCIPlots have been used in chapters Chapter III, Chapter IV, Chapter V and Chapter VI.

Chapter I. References:

1. Ed.: S. Scheiner. *Noncovalent Forces. Springer, Heidelberg* (2015).

2. Scheeres, D. J., Hartzell, C. M., Sánchez, P. & Swift, M. Scaling forces to asteroid surfaces: The role of cohesion. *Icarus* **210**, 968–984 (2010).

3. Autumn, K. *et al.* Evidence for van der Waals adhesion in gecko setae. *Proc. Natl. Acad. Sci.* **99**, 12252–12256 (2002).

4. Gilli, G. & Gilli, P. *The Nature of the Hydrogen Bond*. (2009).

5. Novoa, J. J. *Intermolecular Interactions in Crystals: Fundamentals of Crystal Engineering*. (RSC, 2018).

6. Arunan, E. *et al.* Defining the hydrogen bond: An account (IUPAC Technical Report). *Pure Appl. Chem.* **83**, 1619–1636 (2011).

7. Arunan, E. *et al.* Definition of the hydrogen bond (IUPAC Recommendations 2011). *Pure Appl. Chem.* **83**, 1637–1641 (2011).

8. Desiraju, G. R. The C− H···O Hydrogen Bond: Structural Implications and Supramolecular Design. *Acc. Chem. Res.* **29**, 441–449 (1996).

9. Nishio, M., Hirota, M. & Umezawa, Y. *The CH···p Interaction*. (Wiley, 1998).

10. Takahashi, O., Kohno, Y. & Nishio, M. Relevance of Weak Hydrogen Bonds in the Conformation of Organic Compounds and Bioconjugates: Evidence from Recent Experimental Data and High-Level ab Initio MO Calculations. *Chem. Rev.* **110**, 6049–6076 (2010).

11. Bakhmutov, V. I. *Dihydrogen Bonds: Principles, Experiments, and Applications*. (Wiley, 2008).

12. Desiraju, G. R. *et al.* Definition of the halogen bond (IUPAC Recommendations 2013). *Pure Appl. Chem.* **85**, 1711–1713 (2013).

13. Clark, T., Hennemann, M., Murray, J. S. & Politzer, P. Halogen bonding: the σ -hole. *J. Mol. Model.* **13**, 291–296 (2007).

14. Murray, J. S., Lane, P., Clark, T., Riley, K. E. & Politzer, P. σ -Holes, π-holes and electrostatically-driven interactions. *J. Mol. Model.* **18**, 541–548 (2012).

15. Cavallo, G. *et al.* The Halogen Bond. *Chem. Rev.* **116**, 2478–2601 (2016).

16. Metrangolo, P. & Resnati, G. *Halogen Bonding I*. (Springer, 2015).

17. Murray, J. S., Lane, P., Clark, T. & Politzer, P. σ -hole bonding: molecules containing group VI atoms. *J. Mol. Model.* **13**, 1033–1038 (2007).

18. Murray, J. S., Lane, P. & Politzer, P. Expansion of the σ -hole concept. *J. Mol. Model.* **15**, 723–729 (2009).

19. Minyaev, R. M. & Minkin, V. I. Theoretical study of O-> X (S, Se, Te) coordination in organic compounds. *Can. J. Chem.* **76**, 776–788 (1998).

20. Zahn, S., Frank, R., Hey- Hawkins, E. & Kirchner, B. Pnicogen Bonds: A New Molecular Linker? *Chem. – A Eur. J.* **17**, 6034–6038 (2011).

21. Scheiner, S. A new noncovalent force: Comparison of P···N interaction with hydrogen and halogen bonds. *J. Chem. Phys.* **134**, 094315 (2011).

22. Bauzá, A., Mooibroek, T. J. & Frontera, A. Tetrel-Bonding Interaction: Rediscovered Supramolecular

Force? *Angew. Chemie Int. Ed.* **52**, 12317–12321 (2013).

23. Mani, D. & Arunan, E. The X–C··· Y (X = O/F, Y = O/S/F/Cl/Br/N/P) 'carbon bond' and hydrophobic interactions. *Phys. Chem. Chem. Phys.* **15**, 14377 (2013).
24. Cavallo, G., Metrangolo, P., Pilati, T., Resnati, G. & Terraneo, G. Naming Interactions from the Electrophilic Site. *Cryst. Growth Des.* **14**, 2697–2702 (2014).
25. Legon, A. C. & Walker, N. R. What's in a name? 'Coinage-metal' non-covalent bonds and their definition. *Phys. Chem. Chem. Phys.* **20**, 19332–19338 (2018).
26. Goodwin, E. J. & Legon, A. C. The rotational spectrum and molecular geometry of an antihydrogen-bonded dimer of sulfur dioxide and hydrogen cyanide. *J. Chem. Phys.* **85**, 6828–6836 (1986).
27. Leopold, K. R., Fraser, G. T. & Klemperer, W. Rotational spectrum and structure of the complex HCNCO 2. *J. Chem. Phys.* **80**, 1039–1046 (1984).
28. Ngari, M. S., Xu, Y. & Jäger, W. Rotational Spectroscopic Investigation of the Weak Interaction between CO and N2O. *J. Mol. Spectrosc.* **197**, 244–253 (1999).
29. Zeng, Y. P., Sharpe, S. W., Shin, S. K., Wittig, C. & Beaudet, R. A. Infrared spectroscopy of CO 2 – D(H)Br: Molecular structure and its reliability. *J. Chem. Phys.* **97**, 5392–5402 (1992).
30. Legon, A. C. & Suckley, A. P. Pulsed-jet, diode-laser IR spectroscopy of the $v=1\rightarrow0$ transition in the CO2 asymmetric stretching mode of (CO2, HCN). *Chem. Phys. Lett.* **157**, 5–10 (1989).
31. Legon, A. C. Tetrel, pnictogen and chalcogen bonds identified in the gas phase before they had names: a systematic look at non-covalent interactions. *Phys. Chem. Chem. Phys.* **19**, 14884–14896 (2017).
32. Al-Hamdani, Y. S. & Tkatchenko, A. Understanding non-covalent interactions in larger molecular complexes from first principles. *J. Chem. Phys.* **150**, (2019).
33. Alkorta, I., Elguero, J. & Frontera, A. Not only hydrogen bonds: Other noncovalent interactions. *Crystals* **10**, (2020).
34. Pauling, L. *The nature of the chemical bond.* (CorneUUniv. Press, Ithsea, 1939).
35. Pimentel, G. C. & McClellan, M. A. *The Hydrogen Bond.* (1960).
36. Vinogradov, S. N. & Linnell, R. H. *Hydrogen Bonding.* (Van Nostrand-Reinhold Company, 1971).
37. Desiraju, G. R. & Steiner, T. *The Weak Hydrogen Bond.* (Oxford University Press, 1999).
38. Melandri, S. 'Union is strength': How weak hydrogen bonds become stronger. *Phys. Chem. Chem. Phys.* **13**, 13901–13911 (2011).
39. Gardner, K. H. & Blackwell, J. The hydrogen bonding in native cellulose. *BBA - Gen. Subj.* **343**, 232–237 (1974).
40. The Cambridge Crystallographic Data Centre (CCDC). https://www.ccdc.cam.ac.uk/structures/.
41. Jeffrey, G. A. *An Introduction to Hydrogen Bonding.* (Oxford University Press, 1997).
42. Steiner, T. & Saenger, W. Geometric analysis of non-ionic O-H···O hydrogen bonds and non-bonding arrangements in neutron diffraction studies of carbohydrates. *Acta Crystallogr. Sect. B* **48**, 819–827 (1992).
43. Caminati, W. & Grabow, J.-U. Microwave Spectroscopy Molecular Systems. in *Frontiers of Molecular Spectroscopy* (ed. Laane, J.) 456–552 (Elsevier Inc., 2008).

44. Biswal, H. S., Shirhatti, P. R. & Wategaonkar, S. O−H···O versus O−H···S Hydrogen Bonding I: Experimental and Computational Studies on the p -Cresol·H2O and p -Cresol·H2S Complexes. *J. Phys. Chem. A* **113**, 5633–5643 (2009).

45. Biswal, H. S. & Wategaonkar, S. OH · · · X (X = O, S) hydrogen bonding in thetrahydrofuran and tetrahydrothiophene. *J. Chem. Phys.* **135**, 134306 (2011).

46. Biswal, H. S., Shirhatti, P. R. & Wategaonkar, S. O−H···O versus O−H···S Hydrogen Bonding. 2. Alcohols and Thiols as Hydrogen Bond Acceptors. *J. Phys. Chem. A* **114**, 6944–6955 (2010).

47. Biswal, H. S. & Wategaonkar, S. O−H···O versus O−H···S Hydrogen Bonding. 3. IR−UV Double Resonance Study of Hydrogen Bonded Complexes of p -Cresol with Diethyl Ether and Its Sulfur Analog. *J. Phys. Chem. A* **114**, 5947–5957 (2010).

48. Jouvet, C., Lardeux-Dedonder, C., Richard-Viard, M., Solgadi, D. & Tramer, A. Reactivity of molecular clusters in the gas phase: proton-transfer reaction in neutral phenol-(ammonia)n and phenol-(ethanamine)n. *J. Phys. Chem.* **94**, 5041–5048 (1990).

49. Iwasaki, A., Fujii, A., Watanabe, T., Ebata, T. & Mikami, N. Infrared Spectroscopy of Hydrogen-Bonded Phenol−Amine Clusters in Supersonic Jets. *J. Phys. Chem.* **100**, 16053–16057 (1996).

50. Biswas, N., Wategaonkar, S., Watanabe, T., Ebata, T. & Mikami, N. Fluorescence, REMPI, hole-burning, and FDIR spectroscopy of para-cyanophenol–water1 complex. *Chem. Phys. Lett.* **394**, 61–67 (2004).

51. Biswal, H. S. Hydrogen Bonding Involving Sulfur: New Insights from Ab Initio Calculations and Gas Phase Laser Spectroscopy. in *Noncovalent Forces* (ed. Scheiner, S.) (Springer Int. Pub., 2015).

52. Scheiner, S. *Hydrogen Bonding. A Theoretical Perspective.* (Oxford University Press, 1997).

53. Goebel, J. R., Ault, B. S. & Del Bene, J. E. Matrix Isolation and ab Initio Study of 1:1 Hydrogen-Bonded Complexes of H 2 O 2 with Phosphorus and Sulfur Bases. *J. Phys. Chem. A* **105**, 11365–11370 (2001).

54. Wierzejewska, M. Infrared matrix isolation studies of complexes formed between dimethylsulfide, dimethyldisulfide and nitrous acid. *J. Mol. Struct.* **520**, 199–214 (2000).

55. Bhattacharyya, S., Bhattacherjee, A., Shirhatti, P. R. & Wategaonkar, S. O–H···S Hydrogen Bonds Conform to the Acid–Base Formalism. *J. Phys. Chem. A* **117**, 8238–8250 (2013).

56. Das, A. *et al.* The H2S Dimer is Hydrogen-Bonded: Direct Confirmation from Microwave Spectroscopy. *Angew. Chemie Int. Ed.* **57**, 15199–15203 (2018).

57. Wategaonkar, S. & Bhattacherjee, A. N–H···S Interaction Continues To Be an Enigma: Experimental and Computational Investigations of Hydrogen-Bonded Complexes of Benzimidazole with Thioethers. *J. Phys. Chem. A* **122**, 4313–4321 (2018).

58. Sanz, M. E. *et al.* Conformation and Stability of Adducts of Sulfurated Cyclic Compounds with Water: Rotational Spectrum of Tetrahydrothiophene−Water. *J. Phys. Chem. A* **103**, 5285–5290 (1999).

59. Lobo, I. A., Robertson, P. A., Villani, L., Wilson, D. J. D. & Robertson, E. G. Thiols as Hydrogen Bond Acceptors and Donors: Spectroscopy of 2-Phenylethanethiol Complexes. *J. Phys. Chem. A* **122**, 7171–7180 (2018).

60. Martin, D. E., Robertson, E. G., Thompson, C. D. & Morrison, R. J. S. Resonant 2-photon ionization study of the conformation and the binding of water molecules to 2-phenylethanethiol (PhCH2CH2SH). *J. Chem. Phys.* **128**, 164301 (2008).

61. Mishra, K. K. *et al.* Observation of an Unusually Large IR Red-Shift in an Unconventional S–H···S Hydrogen-Bond. *J. Phys. Chem. Lett.* **12**, 1228–1235 (2021).

62. Bhattacharyya, S. & Wategaonkar, S. ZEKE Photoelectron Spectroscopy of p -Fluorophenol···H 2 S/H

2 O Complexes and Dissociation Energy Measurement Using the Birge–Sponer Extrapolation Method. *J. Phys. Chem. A* **118**, 9386–9396 (2014).

63. Bhattacherjee, A., Matsuda, Y., Fujii, A. & Wategaonkar, S. Acid–Base Formalism in Dispersion-Stabilized S–H···Y (Y=O, S) Hydrogen-Bonding Interactions. *J. Phys. Chem. A* **119**, 1117–1126 (2015).

64. Bhattacherjee, A., Matsuda, Y., Fujii, A. & Wategaonkar, S. The Intermolecular S-H···Y (Y=S,O) Hydrogen Bond in the H2S Dimer and the H 2 S-MeOH Complex. *ChemPhysChem* **14**, 905–914 (2013).

65. Juanes, M., Saragi, R. T., Caminati, W. & Lesarri, A. The Hydrogen Bond and Beyond: Perspectives for Rotational Investigations of Non-Covalent Interactions. *Chem. - A Eur. J.* **25**, (2019).

66. Caminati, W. & Grabow, J.-U. Advancements in Microwave Spectroscopy. in *Frontiers and Advancements in Microwave Spectroscopy* (ed. Laane, J.) 569–598 (Elsevier, 2018).

67. Cole, G. C., Møllendal, H. & Guillemin, J.-C. Microwave Spectrum of 3-Butyne-1-thiol: Evidence for Intramolecular S−H···π Hydrogen Bonding. *J. Phys. Chem. A* **110**, 9370–9376 (2006).

68. Juanes, M. *et al.* Rotational spectrum and intramolecular hydrogen bonding in 1,2-butanedithiol. *J. Mol. Struct.* **1211**, (2020).

69. Xu, L.-H. *et al.* Rotational spectra, conformational structures, and dipole moments of thiodiglycol by jet-cooled FTMW and ab initio calculations. *J. Mol. Spectrosc.* **228**, 243–250 (2004).

70. Ghosh, S., Bhattacharyya, S. & Wategaonkar, S. Dissociation Energies of Sulfur-Centered Hydrogen-Bonded Complexes. *J. Phys. Chem. A* **119**, 10863–10870 (2015).

71. Cooke, S. A., Corlett, G. K. & Legon, A. C. Comparisons of the interactions of benzene, furan and thiophene with Lewis acids: the rotational spectrum of thiophene···HF. *Chem. Phys. Lett.* **291**, 269–276 (1998).

72. Cocinero, E. J. *et al.* Weak hydrogen bonds C–H···S and C–H···F–C in the thiirane–trifluoromethane dimer. *Chem. Phys. Lett.* **402**, 4–10 (2005).

73. Tubergen, M. J., Flad, J. E. & Del Bene, J. E. Microwave spectroscopic and ab initio studies of the hydrogen-bonded trimethylamine–hydrogen sulfide complex. *J. Chem. Phys.* **107**, 2227–2231 (1997).

74. Wang, D., Chopra, P., Wategaonkar, S. & Fujii, A. Electronic and Infrared Spectroscopy of Benzene-(H 2 S) n (n = 1 and 2): The Prototype of the SH-π Interaction. *J. Phys. Chem. A* **123**, 7255–7260 (2019).

75. Arunan, E. *et al.* Rotational spectrum of the weakly bonded C6H6–H2S dimer and comparisons to C6H6–H2O dimer. *J. Chem. Phys.* **117**, 9766–9776 (2002).

76. Goswami, M. & Arunan, E. Microwave spectrum and structure of C6H5CCH···H2S complex. *J. Mol. Spectrosc.* **268**, 147–156 (2011).

77. Goswami, M., Neill, J. L., Muckle, M., Pate, B. H. & Arunan, E. Microwave, infrared-microwave double resonance, and theoretical studies of C2H4 ···H2S complex. *J. Chem. Phys.* **139**, 104303 (2013).

78. Crittenden, D. L. A Systematic CCSD(T) Study of Long-Range and Noncovalent Interactions between Benzene and a Series of First- and Second-Row Hydrides and Rare Gas Atoms. *J. Phys. Chem. A* **113**, 1663–1669 (2009).

79. Vila, A. & Mosquera, R. A. Are the hydrogen bonds involving sulfur bases inverse or anomalous? *Int. J. Quantum Chem.* **106**, 928–934 (2006).

80. Tauer, T. P., Derrick, M. E. & Sherrill, C. D. Estimates of the ab Initio Limit for Sulfur−π Interactions: The H 2 S−Benzene Dimer. *J. Phys. Chem. A* **109**, 191–196 (2005).

81. Wennmohs, F., Staemmler, V. & Schindler, M. Theoretical investigation of weak hydrogen bonds to sulfur. *J. Chem. Phys.* **119**, 3208–3218 (2003).

82. Kaur, D., Aulakh, D., Khanna, S. & Singh, H. Theoretical study on the nature of S···H and O ··· H hydrogen bonds. *J. Sulfur Chem.* **35**, 290–303 (2014).

83. Pauly, H. *Atom, Molecule, and Cluster Beams I*. vol. 28 (Springer Berlin Heidelberg, 2000).

84. Campargue, R. *Atomic and Molecular Beams*. (Springer Berlin Heidelberg, 2001). doi:10.1007/978-3-642-56800-8.

85. Scoles, G. *Atomic and Molecular Beam Methods, Vol. 1*. (Oxford University Press, 1988).

86. Scoles, G. *Atomic and Molecular Beam Methods: Vol. 2*. (Oxford University Press, 1992).

87. Shipman, S. T. & Pate, B. H. New Techniques in Microwave Spectroscopy. in *Handbook of High-resolution Spectroscopy* (eds. Quack, M. & Merk, F.) 801–827 (John Wiley & Sons, Ltd., 2011).

88. Grabow, J.-U. & Caminati, W. MICROWAVE SPECTROSCOPY EXPERIMENTAL TECHNIQUES. in *Frontiers of Molecular Spectroscopy* (ed. Laane, J.) 383–454 (Elsevier, 2009). doi:10.1016/B978-0-444-53175-9.X0001-3.

89. Gordy, W. & Cook, R. L. *Microwave Molecular Spectra*. (John Wiley & Sons, Ltd, 1984).

90. Kroto, H. W. *Molecular Rotation Spectra*. (Dover Publication Inc., 1992).

91. Townes, C. H. & Schawlow, A. L. *Microwave Spectroscopy*. (Dover Publication Inc., 1975).

92. Jensen, F. *Introduction to Computational Chemistry*. (John Wiley & Sons, Ltd, 1999).

93. Cleeton, C. E. & Williams, N. H. Electromagnetic Waves of 1.1 cm Wave-Length and the Absorption Spectrum of Ammonia. *Phys. Rev.* **45**, 234–237 (1934).

94. Dicke, R. H. & Romer, R. H. Pulse Techniques in Microwave Spectroscopy. *Rev. Sci. Instrum.* **26**, 915–928 (1955).

95. Ekkers, J. & Flygare, W. H. Pulsed microwave Fourier transform spectrometer. *Rev. Sci. Instrum.* **47**, 448–454 (1976).

96. Somers, R. M., Poehler, T. O. & Wagner, P. E. Microwave time domain Fabry–Perot emission spectrometer. *Rev. Sci. Instrum.* **46**, 719–725 (1975).

97. Legon, A. C. Isolation and characterisation of some transient complexes of chemical interest using pulsed-nozzle, Fourier-transform microwave spectroscopy. *J. Mol. Struct.* **266**, 21–37 (1992).

98. Balle, T. J., Campbell, E. J., Keenan, M. R. & Flygare, W. H. A new method for observing the rotational spectra of weak molecular complexes: KrHCl. *J. Chem. Phys.* **71**, 2723–2724 (1979).

99. Balle, T. J. & Flygare, W. H. Fabry-Perot cavity pulsed Fourier transform microwave spectrometer with a pulsed nozzle particle source. *Rev. Sci. Instrum.* **52**, 33–45 (1981).

100. Grabow, J. U., Stahl, W. & Dreizler, H. A multioctave coaxially oriented beam-resonator arrangement Fourier-transform microwave spectrometer. *Rev. Sci. Instrum.* **67**, 4072–4084 (1996).

101. Grubbs II, G., Moon, N., Persinger, T., Gillcrist, D. & Marshall, F. A chirped pulse fourier transform microwave (cp-ftmw) spectrometer with laser ablation source to search for actinide-containing molecules and noble metal clusters. in *Proceedings of the 71st International Symposium on Molecular Spectroscopy* 1–1 (University of Illinois at Urbana-Champaign, 2016).

doi:10.15278/isms.2016.MJ12.

102. Patterson, D., Schnell, M. & Doyle, J. M. Enantiomer-specific detection of chiral molecules via microwave spectroscopy. *Nature* **497**, 475–477 (2013).

103. Grabow, J.-U. Fourier Transform Microwave Spectroscopy Measurement and Instrumentation. in *Handbook of High-resolution Spectroscopy* (eds. Quack, M. & Merkt, F.) 724–799 (John Wiley & Sons, Ltd, 2011).

104. Neill, J. L. *et al.* Rotational spectroscopy of iodobenzene and iodobenzene–neon with a direct digital 2–8GHz chirped-pulse Fourier transform microwave spectrometer. *J. Mol. Spectrosc.* **269**, 21–29 (2011).

105. Watson, J. K. G. Simplification of the molecular vibration-rotation hamiltonian. *Mol. Phys.* **15**, 479–490 (1968).

106. Meyer, H. The Molecular Hamiltonian. *Annu. Rev. Phys. Chem.* **53**, 141–172 (2002).

107. Kleiner, I. Asymmetric-top molecules containing one methyl-like internal rotor: Methods and codes for fitting and predicting spectra. *J. Mol. Spectrosc.* **260**, 1–18 (2010).

108. Ruoff, R. S., Klots, T. D., Emilsson, T. & Gutowsky, H. S. Relaxation of conformers and isomers in seeded supersonic jets of inert gases. *J. Chem. Phys.* **93**, 3142–3150 (1990).

109. Grabow, J.-U., Heineking, N. & Stahl, W. The microwave spectrum of tert-butyl isocyanate. *J. Mol. Spectrosc.* **154**, 129–136 (1992).

110. Grabow, J. *Chemische Bindung und interne Dynamik in großen isolieren Molekülen: Rotationsspektroskopische Untersuchung*. (2004).

111. McGurk, J. C., Mäder, H., Hofmann, R. T., Schmalz, T. G. & Flygare, W. H. Transient emission, off-resonant transient absorption, and Fourier transform microwave spectroscopy. *J. Chem. Phys.* **61**, 3759–3767 (1974).

112. McGurk, J. C., Schmalz, T. G. & Flygare, W. H. Fast passage in rotational spectroscopy: Theory and experiment. *J. Chem. Phys.* **60**, 4181–4188 (1974).

113. Brown, G. G. *et al.* A broadband Fourier transform microwave spectrometer based on chirped pulse excitation. *Rev. Sci. Instrum.* **79**, 1–13 (2008).

114. Halgren, T. A. Merck molecular force field. I. Basis, form, scope, parameterization, and performance of MMFF94. *J. Comput. Chem.* **17**, 490–519 (1996).

115. Chang, G., Guida, W. C. & Still, W. C. An internal-coordinate Monte Carlo method for searching conformational space. *J. Am. Chem. Soc.* **111**, 4379–4386 (1989).

116. Kolossváry, I. & Guida, W. C. Low Mode Search. An Efficient, Automated Computational Method for Conformational Analysis: Application to Cyclic and Acyclic Alkanes and Cyclic Peptides. *J. Am. Chem. Soc.* **118**, 5011–5019 (1996).

117. Valatin, J. G. Generalized Hartree-Fock Method. *Phys. Rev.* **122**, 1012–1020 (1961).

118. Møller, C. & Plesset, M. S. Note on an Approximation Treatment for Many-Electron Systems. *Phys. Rev.* **46**, 618–622 (1934).

119. Leininger, M. L., Allen, W. D., Schaefer, H. F. & Sherrill, C. D. Is Mo/ller–Plesset perturbation theory a convergent ab initio method? *J. Chem. Phys.* **112**, 9213–9222 (2000).

120. Becke, A. D. Perspective: Fifty years of density-functional theory in chemical physics. *J. Chem. Phys.* **140**, (2014).

121. Goerigk, L. *et al.* A look at the density functional theory zoo with the advanced GMTKN55 database for general main group thermochemistry, kinetics and noncovalent interactions. *Phys. Chem. Chem. Phys.* **19**, 32184–32215 (2017).

122. Yu, H. S., He, X. & Truhlar, D. G. MN15-L: A New Local Exchange-Correlation Functional for Kohn–Sham Density Functional Theory with Broad Accuracy for Atoms, Molecules, and Solids. *J. Chem. Theory Comput.* **12**, 1280–1293 (2016).

123. Zhao, Y. & Truhlar, D. G. The M06 suite of density functionals for main group thermochemistry, thermochemical kinetics, noncovalent interactions, excited states, and transition elements: two new functionals and systematic testing of four M06-class functionals and 12 other function. *Theor. Chem. Acc.* **120**, 215–241 (2008).

124. Raghavachari, K. Perspective on 'Density functional thermochemistry. III. The role of exact exchange'. *Theor. Chem. Accounts Theory, Comput. Model. (Theoretica Chim. Acta)* **103**, 361–363 (2000).

125. Grimme, S. & Neese, F. Double-hybrid density functional theory for excited electronic states of molecules. *J. Chem. Phys.* **127**, 154116 (2007).

126. Chai, J.-D. & Head-Gordon, M. Long-range corrected hybrid density functionals with damped atom–atom dispersion corrections. *Phys. Chem. Chem. Phys.* **10**, 6615 (2008).

127. Grimme, S., Ehrlich, S. & Goerigk, L. Effect of the damping function in dispersion corrected density functional theory. *J. Comput. Chem.* **32**, 1456–1465 (2011).

128. Johnson, E. R. & Becke, A. D. A post-Hartree-Fock model of intermolecular interactions: Inclusion of higher-order corrections. *J. Chem. Phys.* **124**, 174104 (2006).

129. Weigend, F. & Ahlrichs, R. Balanced basis sets of split valence, triple zeta valence and quadruple zeta valence quality for H to Rn: Design and assessment of accuracy. *Phys. Chem. Chem. Phys.* **7**, 3297 (2005).

130. Frisch, M. J., Pople, J. A. & Binkley, J. S. Self-consistent molecular orbital methods 25. Supplementary functions for Gaussian basis sets. *J. Chem. Phys.* **80**, 3265–3269 (1984).

131. Frisch, M. J.; Trucks, G. W.; Schlegel, H. B.; Scuseria, G. E.; Robb, M. A.; Cheeseman, J. R.; Scalmani, G.; Barone, V.; Petersson, G. A.; Nakatsuji, H.; Li, X.; Caricato, M.; Marenich, A. V.; Bloino, J.; Janesko, B. G.; Gomperts, R.; Mennucci, B.; Hratch, D. *Gaussian 16, Revision C.01*. (J. Gaussian, Inc., 2016).

132. Contreras-García, J. *et al.* NCIPLOT: A Program for Plotting Noncovalent Interaction Regions. *J. Chem. Theory Comput.* **7**, 625–632 (2011).

133. Szalewicz, K. Symmetry-adapted perturbation theory of intermolecular forces. *Wiley Interdiscip. Rev. Comput. Mol. Sci.* **2**, 254–272 (2012).

134. Turney, J. M. *et al.* Psi4: an open-source ab initio electronic structure program. *Wiley Interdiscip. Rev. Comput. Mol. Sci.* **2**, 556–565 (2012).

135. Laplaza, R. *et al.* NCIPLOT and the analysis of noncovalent interactions using the reduced density gradient. *WIREs Comput. Mol. Sci.* **11**, (2021).

Chapter II

HYDRATION OF CYCLOHEXANOL:

(Cyclohexanol)* and (Cyclohexanol $\cdots$ H_2O) *

Adapted from:

(*): M. Juanes, W. Li, L. Spada, L. Evangelisti, A. Lesarri and W. Caminati, *Phys. Chem. Chem. Phys.* **2019**, *21*, 3676 – 3682

(The Electronic Supporting Information – ESI, can be found in the document: thesis-ESI.pdf)

I. Introduction

Alcohols, R-OH, are characterized by three energy minima upon a 360° internal rotation of the hydroxyl group. Depending on the symmetry of the R group, these three minima can be: (*i*) energetically equivalent to each other; (*ii*) two of them equivalent, but different from the third one; (*iii*) all of them with different energy values. In the last two cases a conformational equilibrium is obtained, while in the first cases tunneling and mixing of wavefunctions make the pattern of rotational levels very difficult to be interpreted. Further conformational species can appear when R has a high flexibility.

Rotational spectroscopy is a technique especially suitable to investigate conformational equilibria and to unveil tunneling effects in case of equivalent minima, which can also be analyzed to the formation of intermolecular clusters, in particular hydrates.

In methanol and *tert*-butanol the C_3 symmetry of R allows only one conformer to exist, but their rotational spectra have been found extremely difficult to analyze because of multiple tunneling effects.[1,2] Conversely, in ethanol and *iso*-propanol the C_s symmetry of R leads to the detection of the rotational spectra of the *trans* and *gauche* conformers, with a tunneling motion connecting the two equivalent *gauche* forms.[3,4] The R chain in *n*-propyl alcohol is flexible and it can adopt either a *trans* (with C_s symmetry) or a *gauche* shape (with C_1 symmetry). As in ethyl alcohol, *trans* generates, upon rotation of the hydroxyl group, a *trans-trans* and a *trans-gauche* (tunnelling) species (labelled *Tt* and *Tg*). *Gauche* generates, upon rotation of the hydroxyl group, three distinguished non-tunneling conformers, *Gt*, *Gg*, *Gg'*. All together, five conformers were assigned in the microwave spectrum.[5] For the larger *n*-pentan-2-ol and *n*-hexan-2-ol rotational spectroscopy has detected 5 and 14 conformers, respectively.[6]

Concerning cyclic alcohols, the rotational spectra of *gauche*-cyclopropanol[7] and of the *equatorial-trans* form of cyclobutanol[8] have been observed. The rotational spectrum of cyclopentanol is not reported. Finally, four conformers were assigned for 1-methylcyclohexanol,[9] denoted *Eg, Et, Ag, At* (*E* is the abbreviation of equatorial, and *A* is axial) For cyclohexanol (CHO) neither the monomer nor the water dimer have been reported. For this reason, we decided to study the conformational equilibria for the bare molecule and the hydrate using supersonic jet Fourier transform microwave spectroscopy.

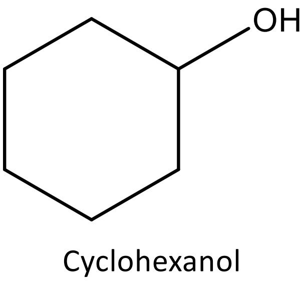

Figure 1. The molecule of cyclohexanol displays a characteristic chair conformation

Cyclohexanol (CHO) is an important feedstock in the polymer industry, as a precursor to nylons and various plasticizers. It is also used as a solvent. The chair form of the aliphatic ring is the by large the most stable one. However, the orientation of the hydroxyl group gives rise to four possible isomers. The hydroxyl group may be attached in the *equatorial* (*E*) or axial (*A*) positions of the cyclohexyl ring. In both cases R has a C_s symmetry, and it can generate *trans* and *gauche* (doubly degenerate) species, for a total of four conforners. James et al.[10] concluded from the temperature dependence of the Raman spectra that in the ordered phases the *equatorial* isomer dominates the structure of the phase. Andre et al.[11] found that there is an equal distribution of *axial* and *equatorial* forms in the glassy phase. More recently Ibberson et al.[12] found that the cyclohexanol molecules adopt only *equatorial* shapes in crystal, by using high-resolution neutron diffraction of powder, synchrotron X-ray diffraction of powder and single-crystal X-ray diffraction techniques.

II. Cyclohexanol and Cyclohexanol ··· H_2O adduct

1. Experimental set up:

	Cyclohexanol @ Bologna	Cyclohexanol @ Valladolid
Carrier Gas	He	Ne
Nozzle Ø (mm)	0.5	0.8
Sample T^a	Room temperature	60°C
Carrier Gas Pressure	3 bar	4 bar

Samples of CHO were obtained commercially (Aldrich) and used without further purification. The rotational spectrum has been measured in two different laboratories:

a) Bologna. A COBRA-type[13] Fourier-transform microwave spectrometer[14] (FTMW) was used to cover the frequency range 6.5-18 GHz.[15] Helium at a stagnation pressure of ~0.3 MPa was passed over a container with CHO under room temperature and expanded through a solenoid valve (Parker, Series 9, nozzle diameter 0.5 mm) into the Fabry-Pérot cavity. The gas-phase expansion formed a supersonic jet, cooling the molecules in their lowest vibrational state. The spectral line positions were determined after Fourier transformation of the time-domain signal with 8k data points, recorded with 100 ns sample intervals. Each rotational transition appears as doublets due to Doppler effect. The line positions are calculated as the arithmetic mean of the frequencies of the Doppler components. The estimated accuracy of the frequency measurements is better than 3 kHz. Lines separated by more than 7 kHz are resolvable.

b) Valladolid. The rotational spectrum has been recorded with a broadband direct-digital chirped-pulse FTMW spectrometer covering the frequency range 2-8 GHz, which follows Pate's design.[16] In this spectrometer a 5 µs chirp pulse created by an arbitrary waveform generator is amplified to 20 W and radiated perpendicular to the propagation of the jet expansion through a horn antenna. A molecular transient emission spanning 40 µs is then detected through a second horn, recorded with a digital oscilloscope and Fourier-transformed to the frequency domain. Sample preparation was similar to Bologna, with optimal conditions requiring backing pressures of ca. 0.4 MPa and neon as carrier gas. The accuracy of the frequency measurements is better than 15 kHz.

2. Rotational spectra of CHO

Guided by the predicted rotational constants in Table 3, a few rotational transitions for the two equatorial *Eg* and *Et* conformers were first assigned in the broadband spectrum in the range 2-8 GHz. More μ_a- and μ_c-type transitions for both conformers were then measured in the range 6-18.5 GHz using the cavity spectrometer. As illustrated in Figure 2, all the transitions for the *Eg* conformer appeared as doublets because of the hydroxyl group internal rotation. These splittings led to the assignment of the pair of ground torsional states, denoted 0^+ and 0^-. Searches for plausible axial conformers were performed unsuccessfully. We rationalized that collisional mechanisms in the jet produce an efficient conformational relaxation into the global minimum, as observed empirically when the interconversion barrier between equilibrium minima is below $2kT$.[17] Evidence for this argument comes from the fact that the Et/Eg population ratio should be 0.34 according to a Boltzmann distribution, while the $Et/Eg(0^+)$ spectra intensity ratio is lower, i.e., it is just 0.1 in the transition $3_{03} \leftarrow 2_{02}$. This implies the global minimum is more populated than expected.

Table 1. Experimental rotational parameters of the two equatorial conformers of the cyclohexanol

	Eg		**Et**
	0^+	0^-	
A / MHz[a]	4295.7884(8)	4293.3876(7)	4288.1884(5)
B / MHz	2231.4842(4)	2231.7890(5)	2215.7086(6)
C / MHz	1612.4343(5)	1612.4672(5)	1609.2335(5)
D_J / kHz	0.116(9)		0.120(12)
D_{JK} / kHz	0.25(3)		0.312(38)
D_K / kHz	0.52(9)		[0.] [c]
d_1 / kHz	-0.029(6)		-0.0422(94)
d_2 / kHz	-0.006(5)		-0.0171(55)
ΔE_{0+0-}/GHz	52(2)		
F_{ab}/MHz	11.16(2)		
F_{bc} /MHz	4.57(7)		
N[b]	53		27
σ / kHz	1.8		2.7

[a]Rotational constants (A, B, C), Watson's S-reduction centrifugal distortion constants (D_J, D_{JK}, D_K, d_1, d_2) and electric dipole moments (μ_α, α = a, b, c). [b]Number of transitions (N) and rms deviation (σ) of the fit. [d]Standard errors in units of the last digit. [c]Values in square brackets were fixed to zero. [f]B3LYP-D3(BJ) / def2-TZVP.

All equatorial *trans* transitions were fitted with Watson's semirigid-rotor Hamiltonian, including quartic centrifugal distortion constants (I^r representation and S reduction).[18,19] For the *gauche* conformer, the tunneling splittings were fitted using a two-state torsion-rotation coupled Hamiltonian, including semirigid rotor terms for each torsional state ($\boldsymbol{H}_0^R, \boldsymbol{H}_1^R$), common centrifugal distortion ($\boldsymbol{H}^{CD}$), the torsional energy difference ΔE_{0+0-}, and Coriolis coupling terms F_{bc} and F_{ab} determined in the reduced axis system of Pickett,[20] according to equations:

$$\boldsymbol{H} = \begin{pmatrix} \boldsymbol{H}_0^R + \boldsymbol{H}^{CD} & \boldsymbol{H}_{int} \\ \boldsymbol{H}_{int} & \boldsymbol{H}_1^R + \boldsymbol{H}^{CD} + \Delta E_{0^+0^-} \end{pmatrix} \tag{1}$$

where the interaction term is expressed:

$$\boldsymbol{H}_{int} = F_{bc}\,(\boldsymbol{P_b P_c} + \boldsymbol{P_c P_b}) + F_{ab}\,(\boldsymbol{P_a P_b} + \boldsymbol{P_b P_a}) \tag{2}$$

where $\boldsymbol{P}_\alpha$ (α=a, b, c) represents angular momentum operators. The fitted spectroscopic constants for the two equatorial species are reported in Table 1. All experimental transition frequencies are given in Tables S1 and S2 in the Electronic Supporting Information (ESI, see attached file).

The spectral measurements were extended to the monosubstituted ^{13}C and ^{18}O isotopic species in natural abundance for the most abundant *Eg* conformer, definitively confirming the spectral assignment. A single transition was observed the near-symmetric $^{13}C(2)/^{13}C(6)$ and $^{13}C(3)/^{13}C(5)$ positions. The rotational parameters and transition frequencies for the minor isotopologues are in Tables S3-S8 (ESI, see attached file).

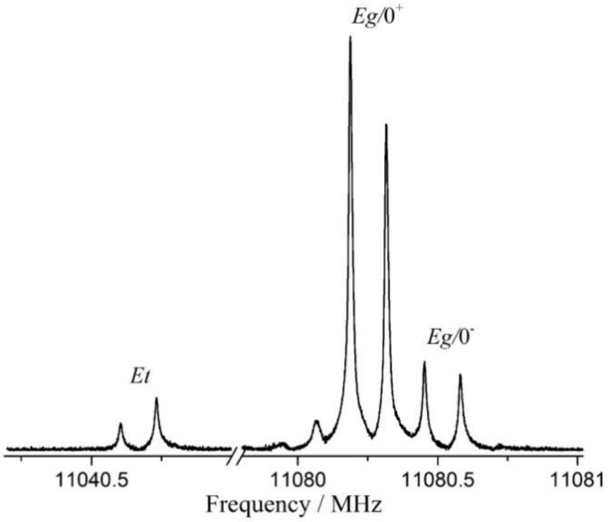

Figure 2. A typical rotational transition ($3_{03} \leftarrow 2_{02}$) of cyclohexanol recorded with the cavity spectrometer, showing two torsional tunneling components (0+/0-) for the equatorial gauche conformer (Eg) but a single component for the trans species (Et). Each transition is additionally doubled by the Doppler effect.

Table 2. Experimental rotational parameters of the dimer cyclohexanol - water

	0^{+}	0^{-}
A / MHz[a]	2555.2943(21)	2556.2312(50)
B / MHz	1130.35883(48)	1129.94502(59)
C / MHz	1113.24155(43)	1112.60936(75)
D_J / kHz	0.7549(63)	
D_{JK} / kHz	1.954(53)	
D_K / kHz	[0.]	
d_1 / kHz	0.0527(48)	
d_2 / kHz	-0.0415(51)	
ΔE_{0+0-}/GHz	-1.3293(57)	
F_{ab}/MHz	2.75(13)	
F_{bc} /MHz	-6.87(24)	
N	74	
σ / kHz	7.2	

[a]Parameter definition as in Table 1.

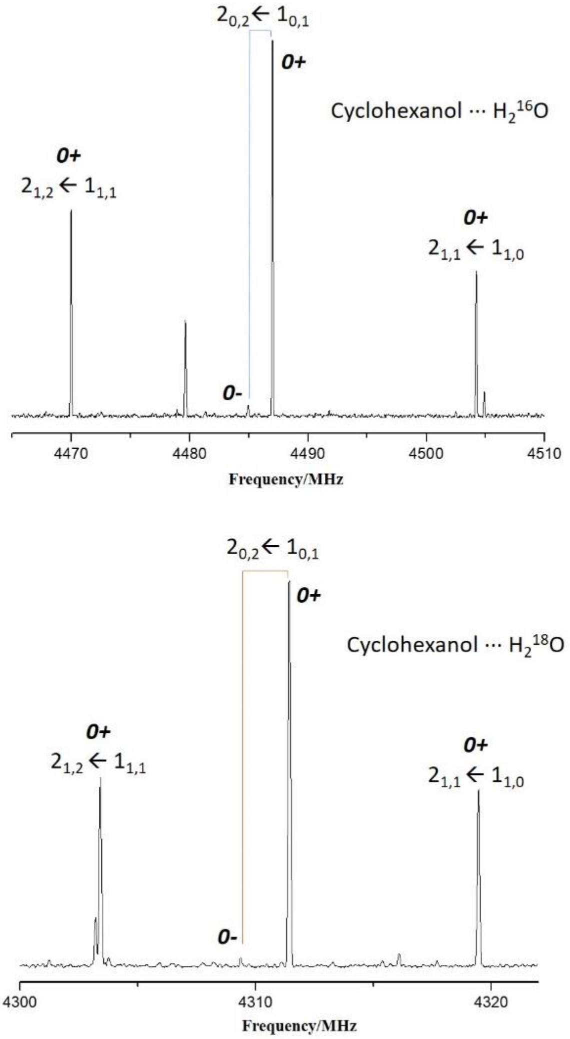

Figure 3. A section of the spectrum of cyclohexanol ··· $H_2{}^{16}O$ and cyclohexanol ··· $H_2{}^{18}O$ recorded with the broadband spectrometer, showing the isotopic shift caused by ^{18}O-water. The torsional splitting is observed only for the most intense $2_{02} \leftarrow 1_{01}$ transition.

Investigation of the monohydrated cyclohexanol-water dimer started with the ab initio predictions and the broadband spectrum. The spectral signature of an asymmetric rotor was then discovered, exhibiting torsional doublings similar to the parent species. Analysis of the spectrum required a two-state Hamiltonian, with the same Coriolis coupling terms as in the monomer. The assignment of water dimer was later confirmed by observation of the $H_2{}^{18}O$ cluster using an isotopically enriched water sample, as shown in Figure 3. The spectroscopic results for the dimer are collected in Tables 2 and S9 (ESI), while transition frequencies are presented in Tables S10 and S11 (ESI, see attached file).

3. Theoretical calculations

The conformational equilibrium of cyclohexanol is driven by the ring puckering, which can interconvert the *axial* or *equatorial* location of the OH group, and by the internal rotation of the hydroxyl group, which can generate *gauche* and *trans* orientations of the hydroxylic hydrogen with respect to the aliphatic hydrogen in C1. These two internal motions generate six energy minima, which correspond to four different conformers, labeled as, *Eg, Et, Ag, At* (*A*, *E*, *t* and *g* stand for *axial*, *equatorial*, *trans* and *gauche*). Each *gauche* form is doubly degenerated because of the two equivalent orientations of hydroxyl group around C-O bond. We performed ab initio calculations (MP2/6-311++G(d,p))[21] to determine the optimized structures, relative energies, rotational and centrifugal distortion constants, and the electric dipole moment components for the four conformers. Vibrational frequency analysis confirmed further that all these conformers are stable energy minima. All theoretical data are summarized in Table 3.

Table 3. Molecular structures, relative energies and spectroscopic predictions for the four conformers of cyclohexanol (MP2/6-311++G(d,p))

	Eg	***Et***
	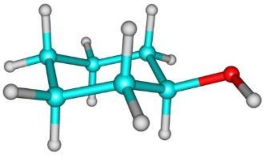	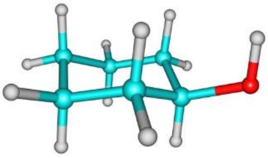
A, *B*, *C*/MHz	4309.1, 2238.5, 1617.8	4304.5, 2218.0, 1613.4
μ_a, μ_b, μ_c /D	0.5,1.5,1.0	1.4,0.0,1.4
$\Delta(E+\text{ZPE})$/ kJ mol^{-1}	0.00	0.96
ΔG/ kJ mol^{-1}	0.00	0.82
	Ag	***At***
	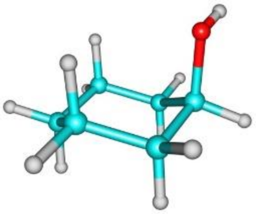	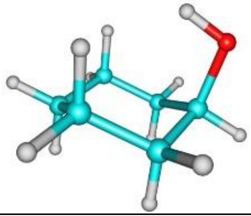
A, *B*, *C*/MHz	3556.0, 2671.7, 2006.3	3581.4, 2612.8, 1972.8
μ_a, μ_b, μ_c /D	0.5,1.5,0.2	1.2,0,1.6
$\Delta(E+\text{ZPE})$/ kJ mol^{-1}	1.78	5.73
ΔG/ kJ mol^{-1}	1.97	5.57

For the cyclohexanol-water dimer we performed an initial molecular mechanics conformational search followed by re-optimization with ab initio and dispersion-corrected density-functional theory. Table 4 presents the two most stable hydrated structures, with energetic and structural predictions according to MP2/6-311++G(d,p) level of calculation. For comparison purposes additional calculations were performed using the B3LYP-D3 method. In both cases *Eg*-water and *Et*-water turned out to be the most stable isomers of the hydrate.

Table 4. Molecular structures, relative energies and spectroscopic predictions of the most stable isomers of cyclohexanol-water (MP2/6-311++G(d,p))

	***Eg* ··· H_2O**	***Et* ··· H_2O**
	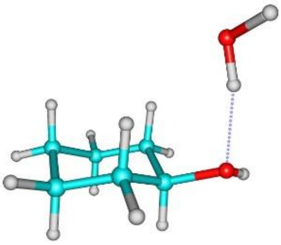	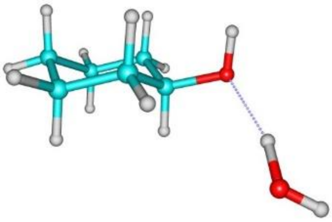
A, *B*, *C*/MHz	2553.7, 1166.6, 1139.8	3183.0, 1071.1, 889.1
μ_a, μ_b, μ_c/D	1.8, 0.6, 0.9	1.4, 0.9, 1.9
$\Delta(E+\text{ZPE})$/ kJ mol^{-1}	0.00	1.1
ΔG/ kJ mol^{-1}	0.1	0.00

4. Molecular Structure and Potential energy functions of the OH group internal rotation

Molecules exhibiting large-amplitude motions cannot be described by rigid structural parameters but for the potential function controlling the intramolecular dynamics. In equatorial cyclohexanol the observation of isotopic species and the torsional energy difference ΔE_{0+0-} allows determining both the heavy-atom skeleton and the hydroxyl internal rotation potential function.

The skeleton of cyclohexanol was determined with the substitution and effective structures. The results are presented in Tables S12 and S13 (ESI, see attached file), where they are also compared with ab initio results. The OH internal rotation potential function was calculated with the monodimensional flexible model of Meyer,[22] which allows the numerical calculation of the rotational and vibrational wave functions and eigenvalues (and then vibrational spacings). The internal rotation of the hydroxyl group, described by the dihedral angle HC-OH (τ), was first

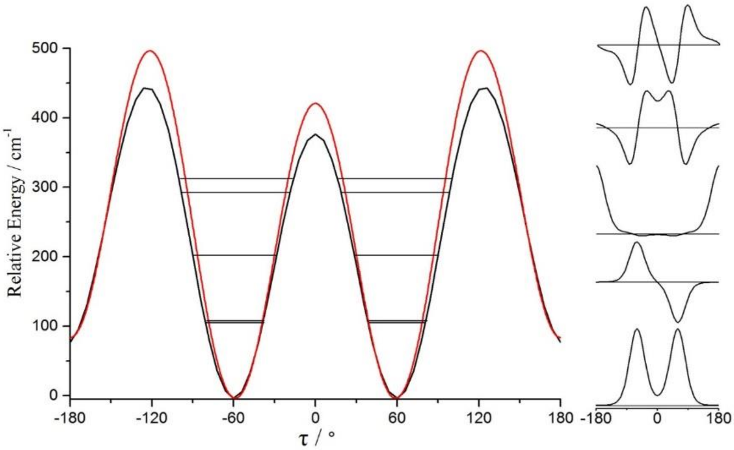

Figure 4. Ab initio (red trace) and experimental (black trace) potential energy curves as a function of dihedral angle HC–OH (cm^{-1} vs. degrees) when the OH group rotates around the CO bond in the equatorial conformers of cyclohexanol. The wavefunctions of the lower vibrational states are drawn on the right.

modelled using ab initio methods. The MP2/6-311++G(d,p) potential function of the *equatorial* conformer is represented by the red line in Figure 4. This function was parametrized as

$$V(\tau) = V_0 + V_1\cdot(1-\cos\tau) + V_2\cdot(1+\cos2\tau) + V_3\cdot(1+\cos3\tau) \qquad (3)$$

The values of the four parameters V_i, i= 0-3, are shown in Table 5. Guided by the theoretical calculations, we took into account the main structural relaxation parameters associated to the internal rotation, according to equations of the type:

$$S_i(\tau) = S^0_i + \Delta S_i(\tau) \qquad (4)$$

Table 5. MP2/6-311++G(d,p) values of the Vi coefficients in Eq. (3) for the internal rotation potential function. The energy values at the critical points, relative to the gauche energy minimum, are also given.

V_0/cm^{-1}	V_1/cm^{-1}	V_2/cm^{-1}	V_3/cm^{-1}	B_2/cm^{-1}	E_t-E_g/cm^{-1}	$B_{t\to g}$/cm^{-1}
-32.44	54.0	4.0	222.6	420.7	83.5	496.5

For a given parameter *S*, S^0 is the value at $\tau = 0$ while Δ*S* is its variation as a function of τ. All these values have been obtained from the *ab initio* geometries at the four critical points. Six structural relaxations have been taken into account for the model calculations. The corresponding detailed expressions, according to eq. (4), are given in the supporting information as Table S14 (ESI).

Meyer's model produced a reasonable reproduction of the torsional splitting by multiplying eq. (3) by a scale factor of 0.9 (the τ coordinate has been considered in the 2π cyclic range and solved into 61 mesh points). The barrier B_2 to the *gauche* ↔ *gauche* pathways resulted to be 377 cm^{-1}, which is slightly larger than that in 1-methylcyclohexanol (356 cm^{-1}, and 320 cm^{-1} for *axial* and *equatorial* species, respectively) but lower than the *ab initio* result of 420.7 cm^{-1}. All these data are shown in Table 6. The resulting potential energy function is given in Figure 4 (black trace), together with the wave functions of the lower energy levels.

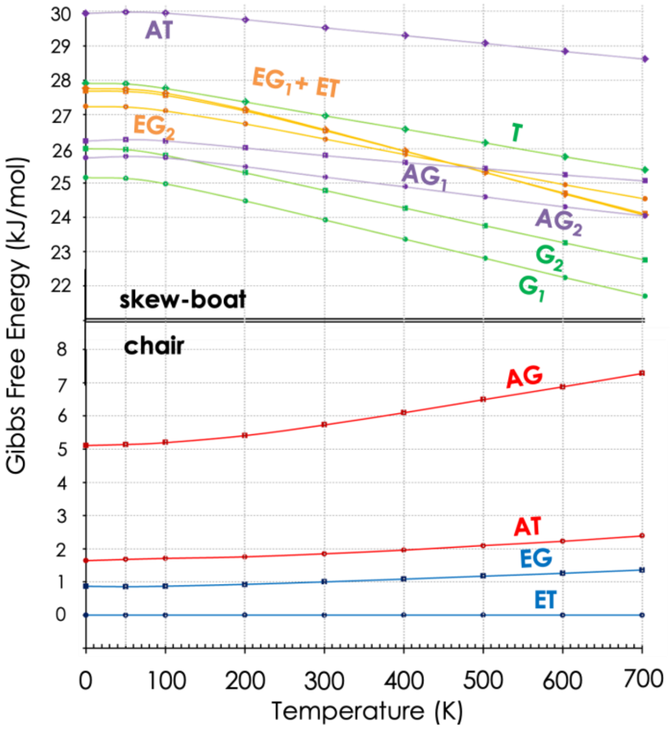

Figure 5. Relative stability of the cyclohexanol monomer as a function of temperature (M06-2X/6-311++G(d,p)).

5. Water dimer geometry and dynamics

As expected, a moderately strong O-H···O hydrogen bond will stabilize the adduct of cyclohexanol-water. However, the ab initio calculations did not offer a priori a clear structural prediction, as the two most stable dimer geometries (*Eg*-H_2O and *Et*-H_2O) in Table 4 are practically isoenergetic using the MP2 method in combination with the 6-311++G(d,p) basis set. Additional calculations for two more isomers obtained from the conformational search (*Ag*-H_2O and *Eg2*-H_2O) in Table S15 (ESI, see attached file) predicted larger relative energies. These structures were reoptimized with the dispersion-corrected B3LYP-D3 method for comparison purposes in the same table.

The spectrum provided definitive experimental evidence of the geometry of the cluster and its internal dynamics. The determined rotational constants in Tables 2 and S9 (ESI, see attached

Table 6. Results of the flexible model calculations for equatorial cyclohexanol

Tunneling splittings		
	Obs.	Calc.
ΔE_{0+0-}/ GHz	52.2	52.2
Parameters:		
Scale factor *f* (fitted)	0.895	
Barrier B_2 (extrapolated) /cm^{-1}	377	

file) unequivocally confirm the detection of isomer *Eg*-H_2O, based on the most stable *gauche* monomer. The water molecule acts as proton donor to the oxygen lone pair at the ring, as in other aliphatic alcohols. Interestingly, the tunneling effects in the dimer are evidence of a large-amplitude motion, which in principle could be related either to the monomer internal rotation or to water or both. The relative intensities of the two tunneling components ($0^+ >> 0^-$) are incompatible with an internal rotation of water in the dimer around its axis, which would result in nuclear spin statistical weights of 3:1. In consequence, the cluster dynamics is most probably associated to the internal rotation of the hydroxyl group. The most reasonable scenario is a concerted motion involving the internal rotation of water and a simultaneous rearrangement of the water molecule, as observed in the isopropanol-water dimer. The decrease in the torsional energy difference in the dimer (ΔE_{0+0-}= 32.7(4) < 52(2) GHz in the monomer) is consistent with this hypothesis.

Despite only two isotopic species were detected for the cyclohexanol-water dimer we estimated the hydrogen bond distance using an effective structure (Table S16, ESI, see attached file). The resulting value of r(O-H_w)=1.928(5) Å is slightly larger than the ab initio prediction (1.881 Å), but within the broad range observed for this interaction in crystal structures (1.40-2.18 Å).[23] The substitution coordinates of the water oxygen are calculated in Table S17 (ESI, see attached file). A recent review offers information on other water clusters detected by rotational spectroscopy.[24]

6. Discussion and Conclusions

We presented a rotational investigation on the internal dynamics of cyclohexanol and the adduct cyclohexanol–water. The conformational equilibria in cyclohexanol are displaced towards the two gauche and trans equatorial forms Eg and Et. This observation contrasts with the case of 1-methylcyclohexanol,[9] where we succeeded in also observing the axial conformers. This fact suggests that the presence of a methyl group adjacent to the OH group decreases the energy differences between the axial and equatorial forms. The detection of tunneling doublings was instrumental for the evaluation of the potential function for the internal rotation of the hydroxyl group. The comparison of the B_2 potential energy barriers hindering the motion between the equivalent Eg forms is also interesting. The ab initio values are B_2 = 420 and 410 cm^{-1} for cyclohexanol and 1-methylcyclohexanol,[9] respectively. However, the experimental data suggest quite larger B_2 values in cyclohexanol (377 cm^{-1}) than in 1-methylcyclohexanol (320 cm^{-1}). How can this be justified? It can be argued that the presence of a methyl group in the carbon atom to which the hydroxyl is attached lowers the barrier to internal rotation of the OH group in the section connecting the two gauche forms. By comparing the tunneling splitting with the values in the case of five other alcohols, we found that the order of torsional energy difference ΔE_{0+0-} is as: Cyclopropanol < Isopropanol < Cyclohexanol < n-Propanol < Ethanol < 1-Methycyclohexanol (see Table 6). All of the alcohols have both *trans* and *gauche* conformers. For the first three alcohols the hydrogen atom is adjacent to the OH group, whereas for the latter alcohols an alkyl group is replacing the H atom.

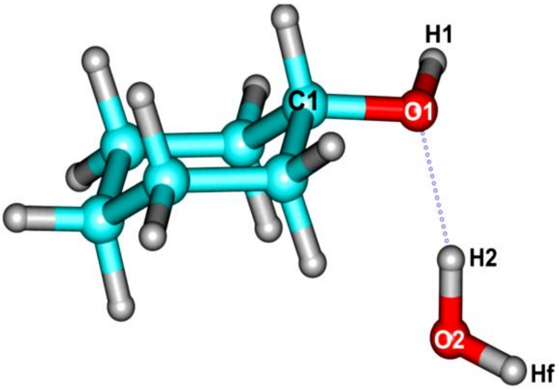

Figure 6. The observed cyclohexanol–water dimer and labelling of the atoms involved in the flexible model analysis of Eg-W. Hf indicates the "free" (not involved in the hydrogen bond) water hydrogen.

Table 6. Comparison of the cis-inversion tunnelling splitting energies ΔE_{0+0-} of alcohols

Species	ΔE_{0+0-}/ GHz
Cyclopropanol	4.1[a]
Isopropanol	46.8[b]
Cyclohexanol	52.2[c]
n-Propanol	91[d]
Ethanol	96.7[e]
1-Methylcyclohexanol	102.5/103[f,g]

[a]Ref. 7. [b]Ref. 4. [c]This work. [d]Ref. 5. [e]Ref. 3. [f]The values are for *axial* and *equatorial* forms, respectively. [g]Ref. 9.

At the same time, this is one of the few cases where the torsional barrier of the hydroxyl group can be compared between the bare molecule and the monohydrated adduct. The experimental observations combined with Meyer's flexible model indicate an increase of the barrier from 377 to 494 cm^{-1} on water complexation, associated with the more complex concerted motion of the hydroxyl group in the dimer.

This work also allow future analysis of other clusters of cyclohexanol, in particular the homodimers (see Chapter III), species with several water molecules and larger heteroclusters, providing experimental information on the properties of more complex alcohol aggregates.

Chapter II. References:

1. Baskakov, O. I. & Pashaev, M. A. O. Microwave and submillimeter-wave rotational spectrum of methyl alcohol in the ground torsional state. *J. Mol. Spectrosc.* **151**, 282–291 (1992).

2. Cohen, E. A. *et al.* The rotational spectrum of tertiary-butyl alcohol. *J. Mol. Spectrosc.* **260**, 77–83 (2010).

3. Kakar, R. K. & Quade, C. R. Microwave rotational spectrum and internal rotation in gauche ethyl alcohol. *J. Chem. Phys.* **72**, 4300–4307 (1980).

4. Hirota, E. & Kawashima, Y. Internal Rotation of the Hydroxyl Group in Isopropanol and the Chirality of the Gauche Form: Fourier Transform Microwave Spectroscopy of (CH3)2CHOD. *J. Mol. Spectrosc.* **207**, 243–253 (2001).

5. Kisiel, Z. *et al.* Determination of precise relative energies of conformers of n-propanol by rotational spectroscopy. *Phys. Chem. Chem. Phys.* **12**, 8329 (2010).

6. Tubergen, M. J. *et al.* Gas-phase conformational distributions for the 2-alkylalcohols 2-pentanol and 2-hexanol from microwave spectroscopy. *J. Mol. Spectrosc.* **251**, 330–338 (2008).

7. Macdonald, J. N., Norbury, D. & Sheridan, J. Microwave spectrum, dipole moment and internal rotation potential function of gauche-cyclopropanol. *J. Chem. Soc. Faraday Trans. 2* **74**, 1365 (1978).

8. Lin, W. *et al.* Microwave spectra and structural parameters of equatorial-trans cyclobutanol. *J. Mol. Struct.* **922**, 83–87 (2009).

9. Li, W., Spada, L., Evangelisti, L. & Caminati, W. Conformational Equilibrium and Potential Energy Functions of the O-H Internal Rotation in the Axial and Equatorial Species of 1-Methylcyclohexanol. *J. Phys. Chem. A* **120**, 4338–4342 (2016).

10. James, D. W., Shurvell, H. F. & Parry, R. M. Polymorphism in cyclohexanol: A Raman spectroscopic study. *J. Raman Spectrosc.* **5**, 201–209 (1976).

11. André, D., Ceccaldi, D. & Szwarc, H. Glassy crystals III : X-ray determination of the structures of the plastic and glassy crystalline phases of cyclohexanol. *J. Phys.* **45**, 731–737 (1984).

12. Ibberson, R. M., Parsons, S., Allan, D. R. & Bell, A. M. T. Polymorphism in cyclohexanol. *Acta Crystallogr. Sect. B Struct. Sci.* **64**, 573–582 (2008).

13. Grabow, J. U., Stahl, W. & Dreizler, H. A multioctave coaxially oriented beam-resonator arrangement Fourier-transform microwave spectrometer. *Rev. Sci. Instrum.* **67**, 4072–4084 (1996).

14. Balle, T. J. & Flygare, W. H. Fabry-Perot cavity pulsed Fourier transform microwave spectrometer with a pulsed nozzle particle source. *Rev. Sci. Instrum.* **52**, 33–45 (1981).

15. Caminati, W. *et al.* Molecular beam Fourier transform microwave spectrum of the dimethylether–xenon complex: tunnelling splitting and 131Xe quadrupole coupling constants. *Chem. Phys. Lett.* **392**, 1–6 (2004).

16. Neill, J. L. *et al.* Rotational spectroscopy of iodobenzene and iodobenzene–neon with a direct digital 2–8GHz chirped-pulse Fourier transform microwave spectrometer. *J. Mol. Spectrosc.* **269**, 21–29 (2011).

17. Ruoff, R. S., Klots, T. D., Emilsson, T. & Gutowsky, H. S. Relaxation of conformers and isomers in seeded supersonic jets of inert gases. *J. Chem. Phys.* **93**, 3142–3150 (1990).

18. Pickett, H. M. The fitting and prediction of vibration-rotation spectra with spin interactions. *J. Mol.*

Spectrosc. **148**, 371–377 (1991).

19. Watson, J. K. G. Vibrational Spectra and Structure. in (ed. Durig, J. R.) 1–89 (Elsevier Inc., 1977).

20. Pickett, H. M. Vibration—Rotation Interactions and the Choice of Rotating Axes for Polyatomic Molecules. *J. Chem. Phys.* **56**, 1715–1723 (1972).

21. Frisch, M. J., Trucks, G. W., Schlegel, H. B., Scuseria, G. E. & Robb, M. A. et al. *Gaussian 09, Revision A.02*. (Gaussian, Inc., 2016).

22. Meyer, R. Flexible models for intramolecular motion, a versatile treatment and its application to glyoxal. *J. Mol. Spectrosc.* **76**, 266–300 (1979).

23. Jeffrey, G. A. *An Introduction to Hydrogen Bonding*. (Oxford University Press, 1997).

24. Caminati, W. & Grabow, J.-U. Advancements in Microwave Spectroscopy. in *Frontiers and Advancements in Microwave Spectroscopy* (ed. Laane, J.) 569–598 (Elsevier, 2018).

Chapter III

DIMERIZATION OF CYCLOHEXANOL:

(Cyclohexanol)$_2$*

Adapted from:

(*): M. Juanes, I. Usabiaga, I. León, L. Evangelisti, J. A. Fernández and A. Lesarri, *Angew. Chem. Int. Ed.*, **2020**, *59*, 12412 – 12421

(The Electronic Supporting Information – ESI, can be found in the document: thesis-ESI.pdf)

I. Introduction

In Chapter II of this thesis we have studied molecular structure and the intramolecular dynamics of cyclohexanol and its monohydrate. Going one step further, this chapter proposes a delicate test model of the role of dispersion forces in intermolecular association using a well-known alcohol molecule (cyclohexanol) as analysis target for generating the larger complex of the homodimer in gas phase.

The formation of the cyclohexanol homodimer ($CHOL_2$) stabilizes the transient chirality of the gauche+/gauche- monomer conformations, as different chiral combinations donor-acceptor result in permanent chirality. This molecular complex represents a larger level of complexity compared with previous observations in aliphatic alcohol dimers[1,2] and similar molecular structures such as the phenol dimer.[3] While phenol produces a single dimer, suppression of π interactions and the larger conformational flexibility in cyclohexanol results in multiple isomerism, adopting six different conformations in a supersonic jet expansion.

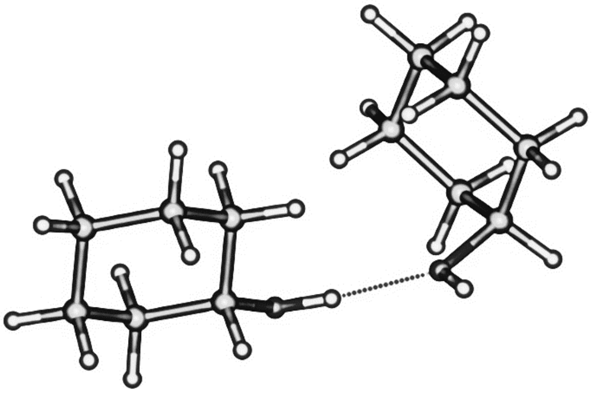

Figure 1. Conformational example of an equatorial-axial complexation isomer of Cyclohexanol$_2$.

Rotational spectroscopy reveals accurate structural data, specifically the formation of homo- and heterochiral diastereoisomers and the presence of both equatorial and axial forms in the dimers. Moreover, an extesive theoretical analysis has been carried out where four dispersion-corrected density-functional molecular orbital calculations were tested against the experiment, with B3LYP-D3(BJ) offering good structural reproducibility with an Alrich's triple-ζ basis set. However, the prediction of the dimer energetics is largely model-dependent, thus offering a testbed for the validation of dispersion-corrected computational models. Additionally, we have also carried out an analysis of the intermolecular interactions based in the electronic density topology (NCIPlot)[4] and a symmetry-adapted perturbation theory (SAPT)[5].

II. Cyclohexanol homodimer

1. Experimental set up:

	(Cyclohexanol)$_2$
Carrier Gas	Ne
Nozzle Ø (mm)	0.8
Sample Tª	85°C
Carrier Gas Pressure	3 bar

As in the previous study of the cyclohexanol and its water adduct (see Chapter II), the sample was obtained commercially (Aldrich) and used without further purification. The main difference in the experiments carried out for the experimental observation of conformations of the homodimer (compared to CHOL and CHOL···water) is based on the modification of some macroscopic experimental parameters such as: *temperature* (increased from 60°C to 85°C), carrier gas (Ne), *backing pressure* (reduced from 4 bar to 3 bar), *number of averages* recorded per experiment (1500k AVG vs 2000k AVG) and the *frequency range* covered per experiment neccesary to detect the noticeably less intense lines (between 5-10% compared to the monomer) of the rotational transitions of the homodimers (six independent experiments covering a frequency range of 1GHz from 2-8GHz, instead of a single 2-8GHz experiment performed in previous studies, achieving better signal-to-noise).

2. About Chirality

Chiral recognition is as a pervasive molecular player in biological and supramolecular Chemistry, directly influencing ligand binding and macromolecular assembly.[6] Experiments in gas-phase contribute with structural, dynamical and energetic information on the non-covalent interactions observed in the association of free chiral molecules,[7–9] with the ultimate goal

DISPERSION
HB

Figure 2. Ilustrative competition between a leading hydrogen bond (HB) and weak dispersive forces produces multiple isomerism in the cyclohexanol dimer, where six different species were observed in a jet expansion.

of understanding the molecular basis of enantioselectivity. However, the lack of a general aggregation model, the multiple intermolecular forces, the variety of interaction energies, the cooperative and competitive effects and the need of accurate empirical data to validate quantum mechanical models call for additional experiments on chiral recognition between isolated molecules.

Chiral recognition is primarily affected by the stereomutation barriers. Low stereomutation barriers are denoted transient chirality and the molecular recognition process, which might involve a structural readaptation, has been categorized as chirality synchronization.[8] Homodimers with transient chirality are interesting because the formation of the cluster quenches stereomutation, offering the possibility to detect separately the hetero- and homochiral diastereomeric clusters and insights into the recognition process.

Torsional chirality has been mostly studied in alcohols, because of the moderately strong O-H···O H-bond and the use of the O-H stretching vibration as structural probe in IR,[10] Raman,[11] IR/UV[12,13] or IR/IR/IR[14] spectroscopy. Microwave spectroscopy offers higher (sub-Doppler) resolution, unambiguous structural identification and general applicability.[9,15] However, the number of rotational studies on transiently chiral dimers is scarce.[1,2,16–22] The analysis of the cyclohexanol dimer explores the balance of intermolecular forces and the differences with phenol.[3] Our results reveal a rich isomerism, arising unexpected questions. In particular, how non-covalent forces affect isomerism? Can density functional theory (DFT) account for the energetics and structure? and, finally, can you invert a cyclohexanol ring in a jet expansion?

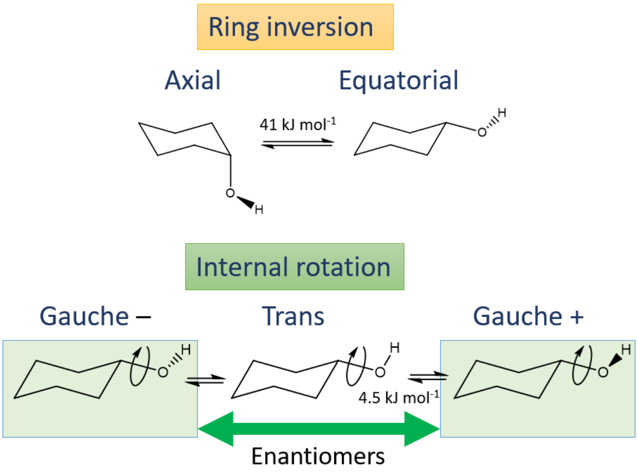

Figure 3. Large-amplitude motions in the cyclohexanol monomer.

Cyclohexanol offers a variety of structural families, based on axial (A) /equatorial (E) inversion chairs and large-amplitude vibration of the hydroxyl group in Figure 3. The most stable equatorial conformer is a fluxional structure tunneling between two symmetry-equivalent equatorial-gauche (EG+ and EG-) isomers, splitting the ground-vibrational state into two torsional-rotation sublevels (ΔE_{01}=52(2) GHz).[23] The equatorial-trans (ET) conformer adopts a non-degenerate rigid structure. The axial conformers (ca. 2-6 kJ mol^{-1}), previously observed for 3-methylcyclohexanol,[24] were not detected for cyclohexanol.[23] On formation of the cyclohexanol dimer the gauche stereomutation is broken and the two enantiomers become distinguishable, producing distinct diastereoisomers. Assuming that the dimer is primary stabilized by a conventional O-H···O hydrogen bond, the two oxygen lone-pairs in the proton acceptor offer six (2 E/A and 3 G+/G-/T) possibilities for each of the six proton donor cases, forming 72 isomer families in 36 enantiomeric pairs. However, previous vibrational investigations could only identify a single EG-EG isomer.[14] Recent FTIR and Raman jet spectra have suggested at least four isomers,[25] demanding conclusive investigations.

3. Rotational spectra of (Cyclohexanol)$_2$

Cyclohexanol was first probed in a neon jet expansion using a direct-digital chirp-pulse FTMW spectrometer covering the frequency range 2-8 GHz, which follows Pate's design[26] at the

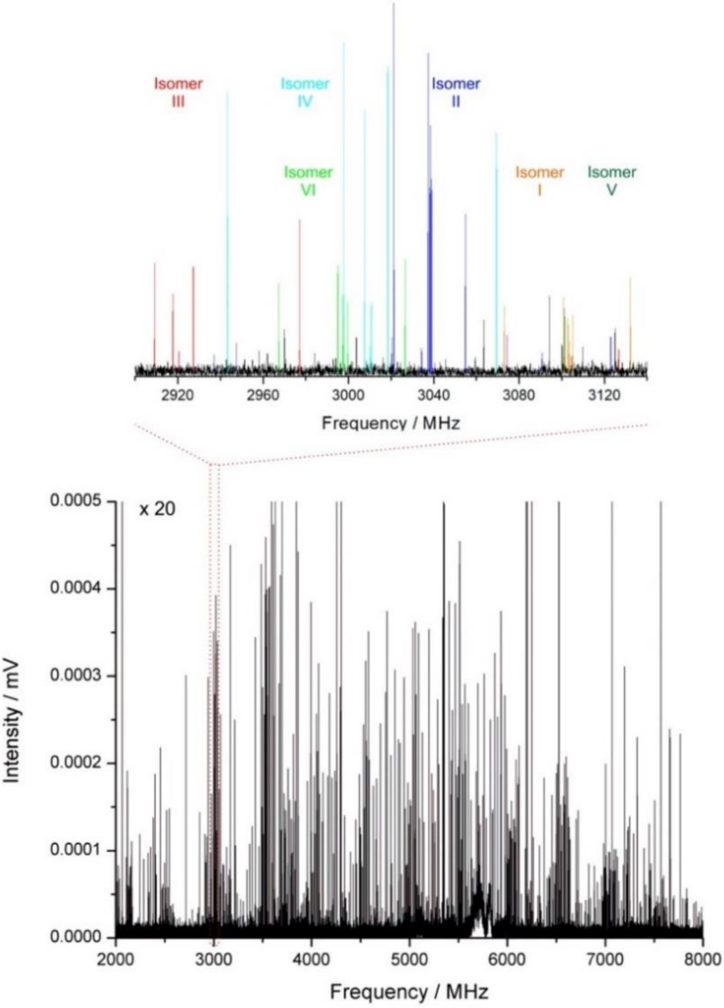

Figure 4. The microwave spectrum of the cyclohexanol dimer and a 120 MHz expansion, showing transitions from six different isomers.

University of Valladolid. The spectrum in Figures 4 and S2-S3 (ESI, see attached file) is dominated by the monomer, but contains other weak (5-10%) features from plausible clusters. The spectral assignment started from trial rotational constants and iteratively led to the identification of six isomers of the homodimer (I-VI). The rotational transitions (Tables S18-S23, ESI, see attached file) were fitted to a semirigid-rotor Hamiltonian,[27] with spectroscopic parameters in Table 7. A second experiment in helium did not identify additional species. Experiments with argon showed only isomers II, III and IV, confirming that the global minimum is one of these species and the presence of conformational relaxation.[28]

4. Dispersion model

The experiment was rationalized with molecular orbital calculations. The PES was expected quite shallow and corrugated, with multiple local minima of small energy, low isomerization barriers and multiple interconversion paths. Our computational strategy used DFT to probe the maximum conformational space. Following molecular mechanics screening (203 isomers), the 60 most stable structures were reoptimized with three hybrid or meta-GGA functionals, including B3LYP,[29] MN15-L[30] and M06-2X,[31]using Ahlrichs' polarized triple-zeta basis def2-TZVP.[32] Minnesota functionals were assumed parametrized for dispersion. B3LYP was supplemented with D3[33] dispersion corrections and Becke-Johnson damping.[33] Finally, the isomers located with each method were reoptimized with the other two functionals. Convergence difficulties were apparent, with minor changes in the initial geometries resulting in different final structures. Tables S24-S26 (ESI, see attached file) collect the computational results.

All observed isomers could be identified with one of the predicted structures. However, the three DFT methods approximate the experiment differently. MN15-L and M06-2X behaved similarly and reproduced the rotational constants with larger relative deviations (~2.0-5.0%). B3LYP-D3(BJ) offered the best agreement, with maximum relative deviations below 3% (i.e., IV and V) and best agreements of 0.1-1.0% (i.e., III and VI). Table S10 (ESI, see attached file) compares experiment and theory for B3LYP-D3(BJ). The results support the argument that Minnesota functionals might need corrections for long-range dispersion.[34] Despite the good agreement, both the convergence difficulties and the fact that small structural changes (exchange of donor/acceptor or hydroxyl internal rotation) may produce similar rotational constants and conformational energies, turning the structural conclusions model-dependent. Convergence difficulties were confirmed a posteriori by an independent search using PW6B95-D3[35] and a ωB97X-D[36] reoptimization of the six observed dimers in Table S10 (ESI).

Isomer identification is given in Table 1 and Figure 6, with labels indicating the equatorial/axial and gauche/trans orientations for the proton donor and acceptor, respectively, the (+/-) gauche chirality (relative to a $^1C_4$ chair) and the bridging oxygen lone pair position (1/2) at the proton acceptor. The equatorial-gauche appears in all isomers, as expected from its larger stability in the monomer. However, one of the two monomers occasionally adopts other geometries (see 3-D Figures S4-S9 and Tables S11-S16, ESI, ESI, see attached file). Specifically, three isomers contain an axial-gauche moiety (III=EG-(1)AG-, IV=EG-(1)AG+, V=AG-(1)EG+) and one isomer contains the axial-trans orientation (I=AT(2)EG-). The two remaining isomers are composed exclusively of equatorial-gauche forms (II=EG-(2)EG-, VI=EG-(1)EG+). The present computational model and the spectral intensities give population ratios of I:II:III:IV:V:VI = 1.0(4):0.7(4):0.6(3):0.5(2):0.3(1):0.3(1). This

Table 1. Experimental rotational parameters of the dimer (Cyclohexanol)$_2$

	Isomer I AT(2)EG-	Isomer II EG-(2)EG-	Isomer III EG-(1)AG-
A / MHz[a]	1218.11(23)[d]	1273.9599(22)	1203.5721(82)
B / MHz	316.22133(97)	255.99343(18)	303.99025(48)
C / MHz	304.41165(91)	250.38848(19)	279.76964(43)
D_J / kHz	0.0583(13)	0.05908(57)	0.06469(69)
D_{JK} / kHz	-0.1976(88)	-0.4638(99)	-0.2661(34)
D_K / kHz	[0.0][c]	1.45(34)	[0.0]
d_1 / kHz	-0.0043(19)	[0.0]	-0.01083(87)
N[b]	71	129	101
σ / kHz	13.0	13.3	10.3

	Isomer IV EG-(1)AG+	Isomer V AG-(1)EG+	Isomer VI EG-(1)EG+
	1167.877(41)	1039.694(67)	1311.72(22)
	313.51209(51)	328.52277(90)	254.73673(31)
	288.25106(51)	304.34728(85)	244.86010(34)
	0.06942(56)	0.2037(13)	0.06438(54)
	-0.2290(26)	-0.475(11)	-0.5107(72)
	[0.0]	[0.0]	[0.0]
	-0.01058(97)	-0.0286(20)	[0.0]
	106	69	100
	8.3	12.2	13.5

[a]Rotational constants (A, B, C), Watson's S-reduction centrifugal distortion constants (D_J, D_{JK}, D_K, d_1, d_2) and electric dipole moments (μ_α, α = a, b, c). [b]Number of transitions (N) and rms deviation (σ) of the fit. [c]Values in square brackets were fixed to zero. [d]Standard errors in units of the last digit.

Table 2. Theoretical[c] rotational parameters of the (Cyclohexanol)$_2$

	Isomer I AT(2)EG-	Isomer II EG-(2)EG-	Isomer III EG-(1)AG-	Isomer IV EG-(1)AG+	Isomer V AG-(1)EG+	Isomer VI EG-(1)EG+
A / MHz[a]	1228.97	1270.09	1202.20	1208.79	1030.73	1315.30
B / MHz	318.01	260.21	301.24	307.43	338.33	257.32
C / MHz	312.71	255.09	281.64	283.36	312.10	245.51
D_J / kHz	0.040	0.056	0.051	0.061	0.395	0.061
D_{JK} / kHz	-0.077	-0.428	0.032	-0.215	-0.740	-0.595
D_K / kHz	0.443	2.468	0.253	0.720	2.150	3.339
d_1 / kHz	-0.00097	-0.00092	-0.0037	-0.010	-0.060	-0.0041
d_2 / kHz	0.00001	-0.00040	-0.00022	-0.00067	0.0019	-0.00034
$\lvert\mu_a\rvert$ / D	1.10	1.83	2.07	2.97	2.12	2.06
$\lvert\mu_b\rvert$ / D	0.12	0.17	1.53	1.11	0.28	0.83
$\lvert\mu_c\rvert$ / D	1.34	1.09	1.89	0.54	0.42	0.85
ΔE / kJ mol^{-1}[b]	3.20	0.10	2.92	1.00	0.93	0.00
ΔG / kJ mol^{-1}	8.00	1.68	3.83	4.43	2.39	0.24
E_B / kJ mol^{-1}	-33.85	-31.76	-30.54	-33.10	-33.76	-31.84

[a]Parameter definition as in Table 1. [b]Relative energies corrected with the zero-point energy (ZPE), Gibbs energy (ΔG, 298K, 1 atm) and complexation energy (including BSSE corrections) relative to the monomers in the geometry of the dimer. [c] B3LYP-D3(BJ)/ def2-TZVP.

calculation is only approximate, as it additionally assumes a polarization regime proportional to the squared dipole moments and uniform instrumental response.[37]

The presence of axial forms is noticeable. Unlike 1-methylcyclohexanol, where the bulkier methyl group stabilizes the axial hydroxyl,[24] cyclohexanol has a preference for the equatorial conformations (Figure 5, Chapter II).[23] In order to explain the axial forms we compared the equatorial-to-axial potential barriers both in the monomer and the dimer. The inversion barrier for the cyclohexanol chair was predicted as 47-54 kJ mol^{-1} in a coordinate scan (no transient-state calculation: Figure S1, ESI, see attached file). A similar calculation in the dimer starting from each of the observed geometries and averaging over six inversion paths rendered comparatively similar barriers of 44-51 kJ mol^{-1} in Figure 5. We conclude that there are no plausible ring inversion paths of reduced energy, so the presence of axial forms is due to energetic collisions at the initial stages of the expansion. Collisional stabilization of specific isomers undetected in the monomers has been observed in jets for other clusters.[38–40]

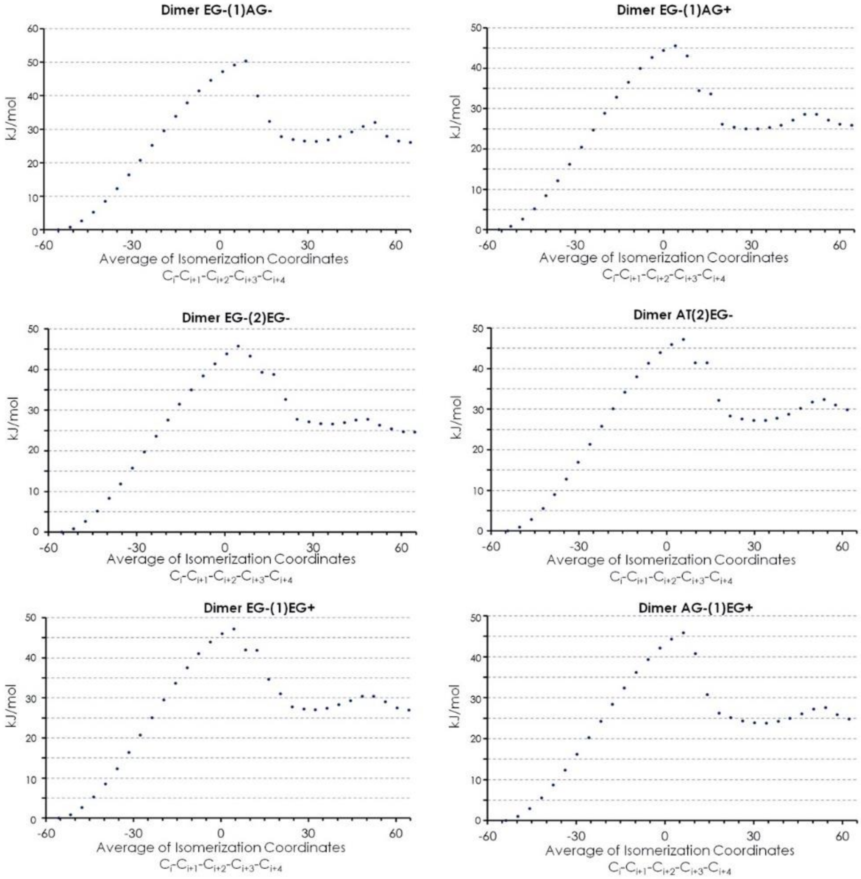

Figure 5. Equatorial-to-axial estimated interconversion barriers for the cyclohexanol dimer starting from the six observed dimer geometries. The reaction barriers are estimations, since no transition-state calculation has been performed. Each interconversion barrier is the average over six interconversion paths using as inversion coordinate the dihedrals C1-C2-C3-C4, C2-C3-C4-C5, C3-C4-C5-C6, C4-C5-C6-C1, C5-C6-C1-C2 and C6-C1-C2-C3. The conformational stabilities were calculated with M06-2X/6-311++G(d,p) and gave barriers heights of 44-51 kJ mol-1.

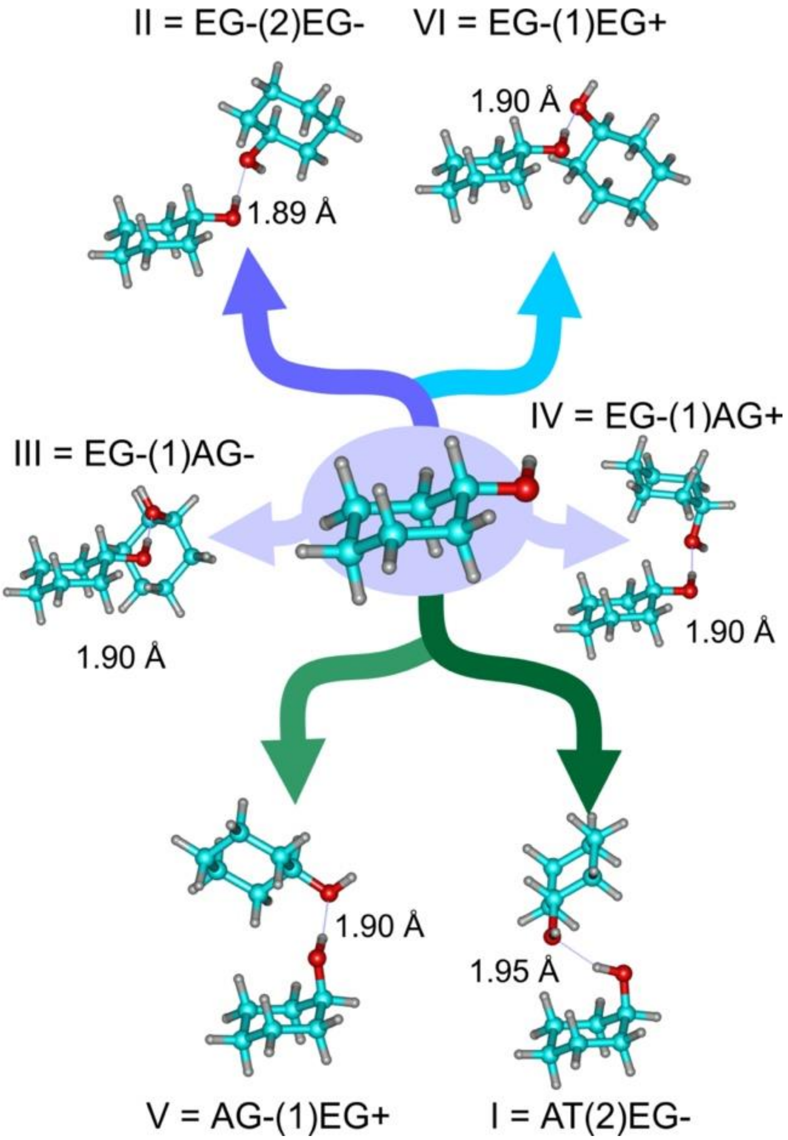
II = EG-(2)EG-
VI = EG-(1)EG+
1.90 Å
1.89 Å
IV = EG-(1)AG+
III = EG-(1)AG-
1.90 Å
1.90 Å
1.90 Å
1.95 Å
V = AG-(1)EG+
I = AT(2)EG-

Figure 6. Conformational assignment of the six isomers of the cyclohexanol dimer and hydrogen bond distances according to B3LYP-D3(BJ).

5. Non-covalent interactions

The intermolecular interactions have been mapped using non-covalent-interactions plots in Figures 7, based on a reduced gradient $s\left(=\frac{1}{1(3\pi^2)^{1/3}}\frac{|\nabla\rho|}{\rho^{4/3}}\right)$ of the electron density.[41] All the observed structures exhibit an O-H···O hydrogen bond with predicted distances r_e=1.891-1.904 Å (B3LYP-D3(BJ)), except for the AT proton donor (1.948 Å). In some isomers additional weak C-H···O hydrogen bonds are apparent (2.65-2.82 Å). In all cases, the two cyclohexyl moieties avoid near-stacking structures. The hydrogen bond distance is intermediate between the phenol dimer[3] (O···H: r_0=1.837(23)-1.879(38) Å, r_e=1.87-89 Å; O···O: r_0=2.830(36)-2.833(21) Å) and the water dimer (O···O: r_0=2.976 Å, r_e=2.952 Å). Additional insight into the nature of the non-covalent interactions was obtained by energy decomposition. SAPT2+(3)/aug-cc-pVDZ[42] results in Table 3 show that, while the primary interaction in both cases is electrostatic (159% of a binding energy of -29.2 kJ mol^{-1}), the dispersion component is very significant (91%) and similar to that of the phenol dimer (104%).

Table 3. Results from a second-order intramonomer / third-order intermonomer Symmetry-Adapted Perturbation Theory (SAPT2+(3)/aug-cc-pVDZ) binding energy decomposition of (cyclohexanol)$_2$ and related dimers, comparing the magnitude of the electrostatic and dispersion contributions, together with available reference values from the S22 database (all values in kJ mol^{-1}).

	$\Delta E_{\mathrm{Electrostatic}}$	$\Delta E_{\mathrm{Induction}}$	$\Delta E_{\mathrm{Dispersion}}$	$\Delta E_{\mathrm{Exchange}}$	$\Delta E_{\mathrm{Total}}$	ΔE_{S22}[f]
$(H_2O)_2$ [a]	-35.7 [191.9%]	-9.5 [50.8%]	-11.1	37.7	-18.6	-21.0
(Cyclohexanol)$_2$ [b]	-46.5 [159.2%]	-26.6 [91.2%]	-16.6	60.5	-29.2	
(Phenol)$_2$ [c]	-41.8 [151.3%]	-28.8 [104.3%]	-15.9	58.9	-27.6	-29.5
(2-Adamantanol)$_2$ [b]	-44.8 [136.2%]	-35.2 [107.0%]	-16.2	63.3	-32.9	
(Cyclohexylamine)$_2$ [b]	-30.0 [138.1%]	-31.4 [144.5%]	-9.3	48.9	-21.7	
$(H_2S)_2$ [d]	-12.1 [223.7%]	-7.8 [144.5%]	-4.7	19.2	-5.4	
Pyridine-CH_4 [e]	-3.0 [57.5%]	-10.9 [208.1%]	-0.7	9.4	-5.2	

[a]T. R. Dyke, K. M. Mack, J. S. Muenter, *J. Chem. Phys.*, 1977, **66**, 498–510. [b]This work. [c]N. A. Seifert, A. L. Steber, J. L. Neill, C. Pérez, D. P. Zaleski, B. H. Pate, A. Lesarri, *Phys. Chem. Chem. Phys.* **2013**, *15*, 11468-11477. [d]A. Das, P. K. Mandal, F. J. Lovas, C. Medcraft, N. R. Walker, E. Arunan, *Angew. Chem. Int. Ed.*, 2018, **57**, 15199–15203. [e]Q. Gou, L. Spada, M. Vallejo-López, A. Lesarri, E. J. Cocinero, W. Caminati, *Phys. Chem. Chem. Phys.*, 2014, **16**, 13041–13046. [f] ΔE_{S22} corresponds to the interaction energies calculated in Hobza's S22 database, recalculated by Sherrill: T. Takatani, E. G. Hohenstein, M. Malagoli, M. S. Marshall, C. D. Sherrill, *J. Chem. Phys.*, 2010, **132**, 144104.

In conclusion, we characterized the association between two neutral free molecules of cyclohexanol in a jet expansion. Compared to the phenol dimer,[3] the suppression of π-π or C-H···π stabilization forces and larger flexibility results in multiple isomerism. Stereomutation of the alcohol is quenched in the dimers, so the gauche chiral species collapse into different diastereoisomers. However, there is no indication of a dominant stereoselectivity as both homochiral and heterochiral species are observed in the dimer. In other small-alcohol dimers both homochiral[16,17] and heterochiral[1,2,20] preferences have been observed, anticipating sensitive isomerization equilibria in shallow multiconformational PES.

Because of the competition between multiple low-energy species the computational survey was of difficult convergence. Moreover, the DFT dimer energetics turned out model-dependent and show deficiencies to assess the observed minima. In this sense, the cyclohexanol dimer proves an interesting testbed for the predictability of computational models describing non-covalent interactions. This issue can be related to the most general search of benchmark clusters and appropriate dispersion models within the "DFT zoo", as advocated by Grimme.[34] This result evidences how the combination of rotational data with computational methods offers a synergic benefit to characterize weakly-bound chirality recognition models in gas phase.

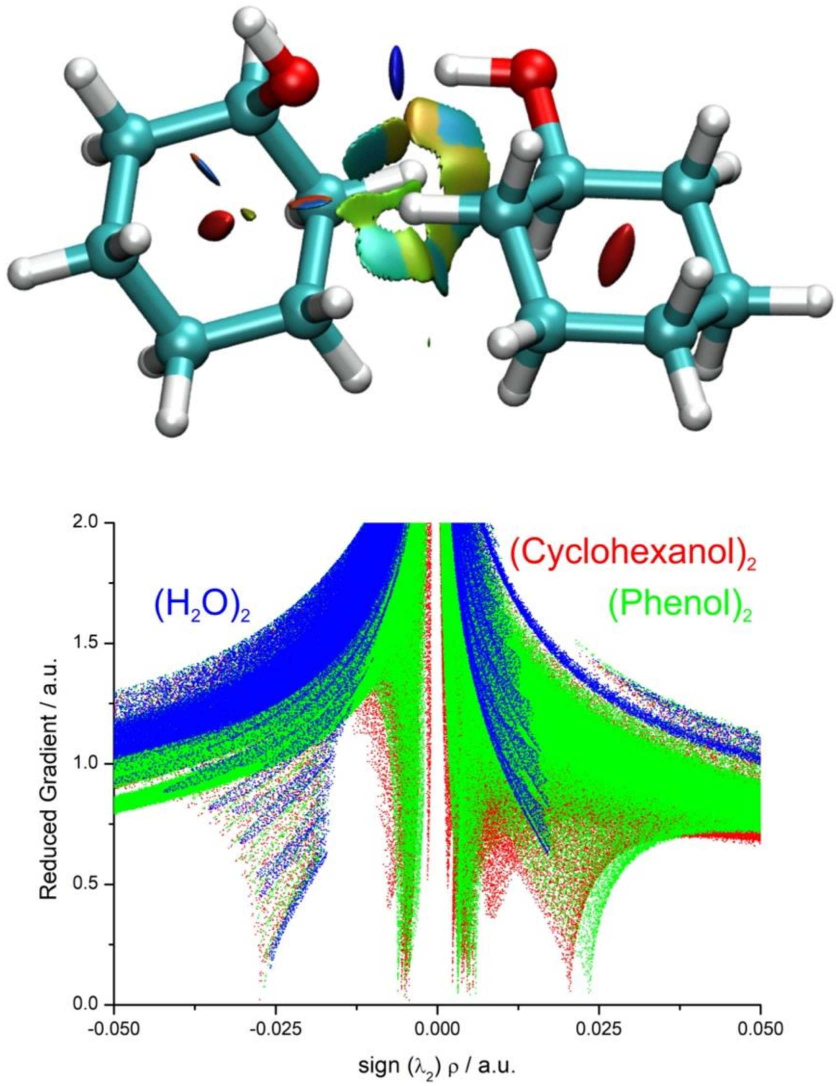

Figure 7. The spatial distribution of the non-covalent interactions in isomer IV of the cylohexanol dimer, according to a NCIPlot analysis. The O-H···O H-bond (blue) is accompanied by broad weak dispersive interactions (green shades) and repulsive zones (red). The lower graphic shows the reduced electronic density gradient representation for the water (blue), phenol (green) and cyclohexanol dimers (red), see SI.

Chapter III. References:

1. Snow, M. S., Howard, B. J., Evangelisti, L. & Caminati, W. From Transient to Induced Permanent Chirality in 2-Propanol upon Dimerization: A Rotational Study. *J. Phys. Chem. A* **115**, 47–51 (2011).
2. King, A. K. & Howard, B. J. A microwave study of the hetero-chiral dimer of butan-2-ol. *Chem. Phys. Lett.* **348**, 343–349 (2001).
3. Seifert, N. A. *et al.* The interplay of hydrogen bonding and dispersion in phenol dimer and trimer: Structures from broadband rotational spectroscopy. *Phys. Chem. Chem. Phys.* **15**, 11468–11477 (2013).
4. Contreras-García, J. *et al.* NCIPLOT: A Program for Plotting Noncovalent Interaction Regions. *J. Chem. Theory Comput.* **7**, 625–632 (2011).
5. Garcia, J., Podeszwa, R. & Szalewicz, K. SAPT codes for calculations of intermolecular interaction energies. *J. Chem. Phys.* **152**, 184109 (2020).
6. Morrow, S. M., Bissette, A. J. & Fletcher, S. P. Transmission of chirality through space and across length scales. *Nat. Nanotechnol.* **12**, 410–419 (2017).
7. Zehnacker, A. *Chiral Recognition in the Gas Phase*. (CRC Press, 2010).
8. Zehnacker, A. & Suhm, M. A. Chirality Recognition between Neutral Molecules in the Gas Phase. *Angew. Chemie Int. Ed.* **47**, 6970–6992 (2008).
9. Juanes, M., Saragi, R. T., Caminati, W. & Lesarri, A. The Hydrogen Bond and Beyond: Perspectives for Rotational Investigations of Non-Covalent Interactions. *Chem. - A Eur. J.* **25**, (2019).
10. Adler, T. B., Borho, N., Reiher, M. & Suhm, M. A. Chirality-Induced Switch in Hydrogen-Bond Topology: Tetrameric Methyl Lactate Clusters in the Gas Phase. *Angew. Chemie Int. Ed.* **45**, 3440–3445 (2006).
11. Wassermann, T. N., Zielke, P., Lee, J. J., Cézard, C. & Suhm, M. A. Structural Preferences, Argon Nanocoating, and Dimerization of n -Alkanols As Revealed by OH Stretching Spectroscopy in Supersonic Jets †. *J. Phys. Chem. A* **111**, 7437–7448 (2007).
12. Usabiaga, I., Camiruaga, A., Calabrese, C., Maris, A. & Fernández, J. A. Exploring Caffeine–Phenol Interactions by the Inseparable Duet of Experimental and Theoretical Data. *Chem. – A Eur. J.* **25**, 14230–14236 (2019).
13. Rijs, A. M. & Oomens, J. Gas-Phase IR Spectroscopy and Structure of Biological Molecules. in *Gas-Phase IR Spectrosc. Struct. Biol. Mol.* (eds. Rijs, A. M. & Oomens, J.) 1–42 (Springer Int. Pub., 2015).
14. León, I., Montero, R., Longarte, A. & Fernández, J. A. IR mass-resolved spectroscopy of complexes without chromophore: Cyclohexanol·(H 2 O) n , n = 1–3 and cyclohexanol dimer. *J. Chem. Phys.* **139**, 174312 (2013).
15. Caminati, W. & Grabow, J.-U. Advancements in Microwave Spectroscopy. in *Frontiers and Advancements in Microwave Spectroscopy* (ed. Laane, J.) 569–598 (Elsevier, 2018).
16. Hearn, J. P. I., Cobley, R. V. & Howard, B. J. High-resolution spectroscopy of induced chiral dimers: A study of the dimers of ethanol by Fourier transform microwave spectroscopy. *J. Chem. Phys.* **123**, 1–7 (2005).
17. Loru, D., Peña, I. & Sanz, M. E. Ethanol dimer: Observation of three new conformers by broadband rotational spectroscopy. *J. Mol. Spectrosc.* **335**, 93–101 (2017).
18. Su, Z., Borho, N. & Xu, Y. Chiral self-recognition: Direct spectroscopic detection of the homochiral and

heterochiral dimers of propylene oxide in the gas phase. *J. Am. Chem. Soc.* **128**, 17126–17131 (2006).

19. Maris, A., Giuliano, B. M., Bonazzi, D. & Caminati, W. Molecular recognition of chiral conformers: A rotational study of the dimers of glycidol. *J. Am. Chem. Soc.* **130**, 13860–13861 (2008).

20. Liu, X., Borho, N. & Xu, Y. Molecular self-recognition: Rotational spectra of the dimeric 2-fluoroethanol conformers. *Chem. - A Eur. J.* **15**, 270–277 (2009).

21. Thomas, J. & Xu, Y. Chirality synchronization in trifluoroethanol dimer revisited: The missing heterochiral dimer. *J. Phys. Chem. Lett.* **5**, 1850–1855 (2014).

22. Seifert, N. A. *et al.* Chiral recognition and atropisomerism in the sevoflurane dimer. *Phys. Chem. Chem. Phys.* **17**, 18282–18287 (2015).

23. Juanes, M. *et al.* Internal dynamics of cyclohexanol and the cyclohexanol-water adduct. *Phys. Chem. Chem. Phys.* **21**, (2019).

24. Li, W., Spada, L., Evangelisti, L. & Caminati, W. Conformational Equilibrium and Potential Energy Functions of the O-H Internal Rotation in the Axial and Equatorial Species of 1-Methylcyclohexanol. *J. Phys. Chem. A* **120**, 4338–4342 (2016).

25. Gawrilow, M. & Suhm, M. A. 2-Methoxyethanol: harmonic tricks, anharmonic challenges and chirality-sensitive chain aggregation. *Phys. Chem. Chem. Phys.* **22**, 15303–15311 (2020).

26. Neill, J. L. *et al.* Rotational spectroscopy of iodobenzene and iodobenzene–neon with a direct digital 2–8GHz chirped-pulse Fourier transform microwave spectrometer. *J. Mol. Spectrosc.* **269**, 21–29 (2011).

27. Watson, J. K. G. Vibrational Spectra and Structure. in (ed. Durig, J. R.) 1–89 (Elsevier Inc., 1977).

28. Godfrey, P. D., Rodgers, F. M. & Brown, R. D. Theory versus Experiment in Jet Spectroscopy: Glycolic Acid. *J. Am. Chem. Soc.* **119**, 2232–2239 (1997).

29. Becke, A. D. Perspective: Fifty years of density-functional theory in chemical physics. *J. Chem. Phys.* **140**, (2014).

30. Yu, H. S., He, X. & Truhlar, D. G. MN15-L: A New Local Exchange-Correlation Functional for Kohn–Sham Density Functional Theory with Broad Accuracy for Atoms, Molecules, and Solids. *J. Chem. Theory Comput.* **12**, 1280–1293 (2016).

31. Zhao, Y. & Truhlar, D. G. The M06 suite of density functionals for main group thermochemistry, thermochemical kinetics, noncovalent interactions, excited states, and transition elements: two new functionals and systematic testing of four M06-class functionals and 12 other function. *Theor. Chem. Acc.* **120**, 215–241 (2008).

32. Weigend, F. & Ahlrichs, R. Balanced basis sets of split valence, triple zeta valence and quadruple zeta valence quality for H to Rn: Design and assessment of accuracy. *Phys. Chem. Chem. Phys.* **7**, 3297 (2005).

33. Grimme, S., Ehrlich, S. & Goerigk, L. Effect of the damping function in dispersion corrected density functional theory. *J. Comput. Chem.* **32**, 1456–1465 (2011).

34. Goerigk, L. *et al.* A look at the density functional theory zoo with the advanced GMTKN55 database for general main group thermochemistry, kinetics and noncovalent interactions. *Phys. Chem. Chem. Phys.* **19**, 32184–32215 (2017).

35. Bannwarth, C., Ehlert, S. & Grimme, S. GFN2-xTB—An Accurate and Broadly Parametrized Self-Consistent Tight-Binding Quantum Chemical Method with Multipole Electrostatics and Density-Dependent Dispersion Contributions. *J. Chem. Theory Comput.* **15**, 1652–1671 (2019).

36. Chai, J.-D. & Head-Gordon, M. Long-range corrected hybrid density functionals with damped atom–atom dispersion corrections. *Phys. Chem. Chem. Phys.* **10**, 6615 (2008).

37. Grabow, J.-U. *Fourier Transform Microwave Spectroscopy Measurement and Instrumentation. Handbook of High-resolution Spectroscopy* (2011). doi:10.1002/9780470749593.hrs037.

38. Thomas, J., Seifert, N. A., Jäger, W. & Xu, Y. A Direct Link from the Gas to the Condensed Phase: A Rotational Spectroscopic Study of 2,2,2-Trifluoroethanol Trimers. *Angew. Chemie Int. Ed.* **56**, 6289–6293 (2017).

39. Seifert, N. A., Thomas, J., Jäger, W. & Xu, Y. Rotational spectra and theoretical study of tetramers and trimers of 2-fluoroethanol: dramatic intermolecular compensation for intramolecular instability. *Phys. Chem. Chem. Phys.* **20**, 27630–27637 (2018).

40. Oswald, S. *et al.* The Chiral Trimer and a Metastable Chiral Dimer of Achiral Hexafluoroisopropanol: A Multi-Messenger Study. *Angew. Chemie Int. Ed.* **58**, 5080–5084 (2019).

41. Johnson, E. R. *et al.* Revealing Noncovalent Interactions. *J. Am. Chem. Soc.* **132**, 6498–6506 (2010).

42. Hohenstein, E. G. & Sherrill, C. D. Density fitting of intramonomer correlation effects in symmetry-adapted perturbation theory. *J. Chem. Phys.* **133**, 014101 (2010).

Chapter IV

HYDRATION OF FURFURYL COMPOUNDS:

(Furfuryl Mercaptan $\cdots H_2O$) and (Furfuryl Alcohol $\cdots H_2O$)*

Adapted from:

(*): M. Juanes, A. Lesarri, R. Pinacho, E. Charro, J. E. Rubio, L. Enríquez and M. Jaraíz, *Chem. Eur. J.* **2018**, *24*, 6564 – 6571

(The Electronic Supporting Information – ESI, can be found in the document: thesis-ESI.pdf)

I. Introduction

Non-covalent interactions (NCI) involving sulfur centers are still undercharacterized,[1,2] despite recent theoretical and experimental investigations signalling a variety of chemical roles as σ and π hydrogen-bond (HB) donor (S-H···O, S-H···S, S-H···π, etc)[3] and acceptor (O-H···S, N-H···S, etc), the participation of σ/π holes of Group 16 atoms as electrophilic attractors in chalcogen bonds[4–6] and the influence of sulfur contacts in the functional properties of proteins and organic crystals.[7,8] In this chapter, we further discuss the behavior and structural preferences of different monohydrated dimers of alcohol/thiol five-membered aromatic ring molecules that bear oxygen and/or sulfur as heteroatoms. The objective of this chapter is to provide experimental results and analysis for better understanding the interactions involving sulfur. The solvation of these derivatives will therefore allow comparing the strength of the interaction of water with the OH and SH groups. The hydrogen bond differences of these water dimers have been compared and studied depending on the presence of sulfur or oxygen atoms.

Here we report on the monohydrated dimers of furfuryl mercaptan (FM···H_2O) and furfuryl alcohol (FA···H_2O). These complexes with water offer competing intra/intermolecular HB possibilities through their thiol and alcohol groups. The furfuryl compounds display a simplified (two-rotor) bi-dimensional potential energy surface, providing alternative O/S/π binding sites and sufficient conformational flexibility to establish different, even simultaneous, HBs with water. Since both FM and FA themselves can be stabilized by O/S-H···O or O/S-H···π intramolecular HBs, the insertion of a water molecule may disrupt the conformational preferences of the bare molecules, offering a possibility to investigate the influence of water addition on the conformational balance and intramolecular hydrogen bonding. The solvation of both furfuryl derivatives will therefore allow comparing the donor/acceptor strength of water against the OH and SH groups.

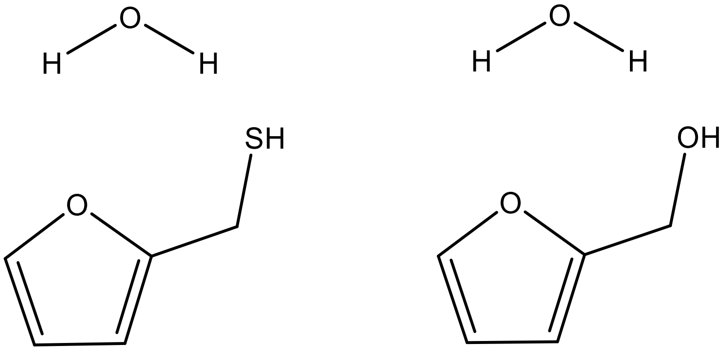

(1) (2)

Figure 1. Molecular formulas of the dimers analyzed in this chapter, including the furfuryl mercaptan (1) and furfuryl alcohol (2) hydrates.

All the experiments have been assisted by molecular-orbital quantum chemical calculations with different dispersion-corrected density functional theory (DFT) models and/or ab initio methods, simultaneously assessing the theoretical calculations.

II. Furfuryl Mercaptan and Furfuryl alcohol

1. Experimental set up:

The monohydrated FM and FA dimers were created by a near-adiabatic jet expansion of the sample vapors and a carrier gas seeded with water. The supersonic jet was probed using both fast-passage[11–13] and cavity (see Chapter I) Fourier-transform microwave (FTMW) spectrometers, covering the frequency regions 2-8 GHz and 8-18 GHz, respectively. In the fast-passage spectrometer (see Chapter I) a microwave chirped pulse (4 µs, 20 W) simultaneously excites the full bandwidth in a single experimental event. In the cavity spectrometer the jet expands within a tuned multi-pass Fabry-Perot resonator and is probed at individual frequencies by bandwidth-limited pulses (1 µs, 0.1 W). The free-induction decay is recorded in the time-domain and Fourier transformed to produce the frequency spectrum. The collinear arrangement of the jet and the resonator axis in the cavity spectrometer results in longer decays and associated smaller linewidths (full widths at half maximum ca. 10 kHz), but restricted to short bandwidths of about 1 MHz. Conversely, the perpendicularly expanding jet in the chirped-pulse experiment produces much shorter decays and enlarges the typical linewidths to about 100 kHz. Frequency oscillators in the two systems are locked to a rubidium standard, providing frequency accuracies of the rotational transitions below 5 kHz.

	Furfuryl Mercaptan	FM···H_2O	Furfuryl Alcohol	FA···H_2O
Carrier Gas	Ne		Ne	
Nozzle Ø (mm)	0.5		0.8	
Sample Tª	Room temperature		36°C	
Carrier Gas Pressure	2.5 bar		2 bar	

2. Computational methods

In addition to the spectroscopic results obtained, the experimental work was supported by a combination of molecular mechanics and quantum mechanical methods. The conformational space of the two dimers was first explored with the MMFFs[14] force field, generating a set of plausible initial structures within a 25 kJ mol^{-1} window. All isomers of FM···H_2O and FA···H_2O were later reoptimized using both ab initio (MP2) and DFT (B3LYP). Empirical dispersion terms using the Grimme correction (D3)[15] or Becke-Johnson (D3(BJ)[16]) damping function were added to the B3LYP functional. Vibrational frequency calculations (harmonic approximation) and basis-set superposition errors were later calculated for each method. The computational models used both Ahlrichs' def2TZVP and Pople's 6-311++G(d,p) triple-ζ basis sets, implemented in Gaussian09.[17] Zero-order symmetry-adapted perturbation theory[10] (SAPT(0) implemented in Psi4)[18] and a truncated double-ζ aug-cc-pVDZ (denoted jun-cc-pVDZ) basis set was used for energy partition in both complexes, as this calculation level is reported to provide acceptable error cancellation.[19]

3. **Rotational spectra of FM and FA**

As a preliminary step in the analysis of the two hydrates we reinvestigated the rotational spectra and conformational and energetic properties of both FM and FA in a cooled supersonic expansion, extending the previous measurements on thermalized static samples (-15°C and 5°C, respectively) conducted in the K_a band (26.5-39.5 GHz).[20,21]

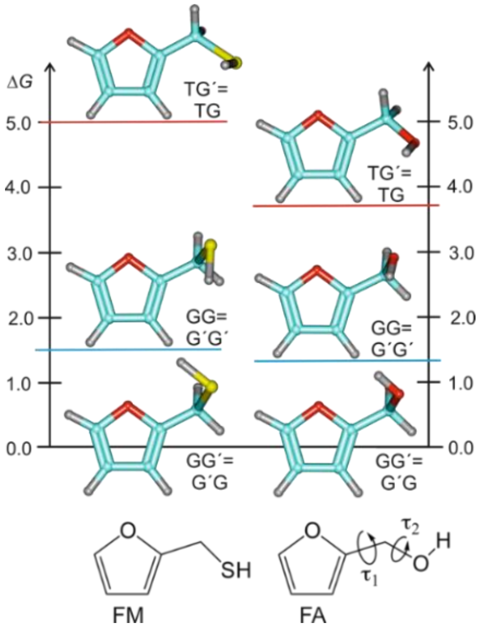

Figure 2. Theoretical Gibbs energies (MP2, kJmol^{-1}) for the lowest-lying conformations of furfuryl mercaptan (FM) and furfuryl alcohol (FA), as collected in Table S5 and S6 (ESI). Molecular conformations are labeled according to the O-CC-S/O (t_1) and C-C-S/O-H (t_2) dihedrals (G=+gauche, G'=-gauche T=trans).

The rotational spectra of the monomers revealed a dominant skew conformation in which the thiol or alcohol groups are nearly perpendicular to the ring plane and the terminal hydrogen atom is oriented towards the ring heteroatom, forming a S-H···O or O-H···O intramolecular hydrogen bond in FM and FA, respectively (+*gauche*/-*gauche* or GG´ in Figure 2 for dihedrals τ_1=S/O-C-C-O and τ_2=H-S/O-C-C, respectively). The second most stable conformation shares the heavy-atom skeleton, but the terminal hydrogen atom points to the ring, consistent with a weak S-H···π or O-H···π hydrogen bond (+*gauche*/+*gauche* or GG). Tables S1-S4 (ESI, see attached file) show the predicted atomic coordinates. The energy separation between the two most stable GG´ and GG conformations was previously estimated as 2.3(5) and 1.5(4) kJ mol^{-1}, respectively, for FM[20] and FA.[21] These values are comparable to the theoretical MP2 estimations in Tables S5 and S6 (ESI, see attached file), giving relative Gibbs energies of 1.5 and 1.3 kJ mol^{-1}, respectively. Noticeably, the GG isomer, previously detected in a static sample for the two compounds, was observed in the jet for FM but not for FA. This fact is consistent with a lower interconversion barrier in FA, permitting the conformational relaxation[22] to the global minimum GG´. Interconversion barriers GG´→GG were previously available only for FA[23] (B3LYP) and have now been extended to both molecules in Figure 3 using MP2. For the most abundant GG´ isomer of FM and FA all ^{13}C isotopologues were detected in natural abundance, together with the ^{34}S and one of the ^{18}O species in FM and FA, respectively. Finally, a new third conformer could be assigned for FM (*trans*/-*gauche* or TG´ in Figure 2). The spectroscopic parameters, effective and substitution structures and transition frequencies for FM and FA are collected in Tables S7-S31 (ESI, see attached file).

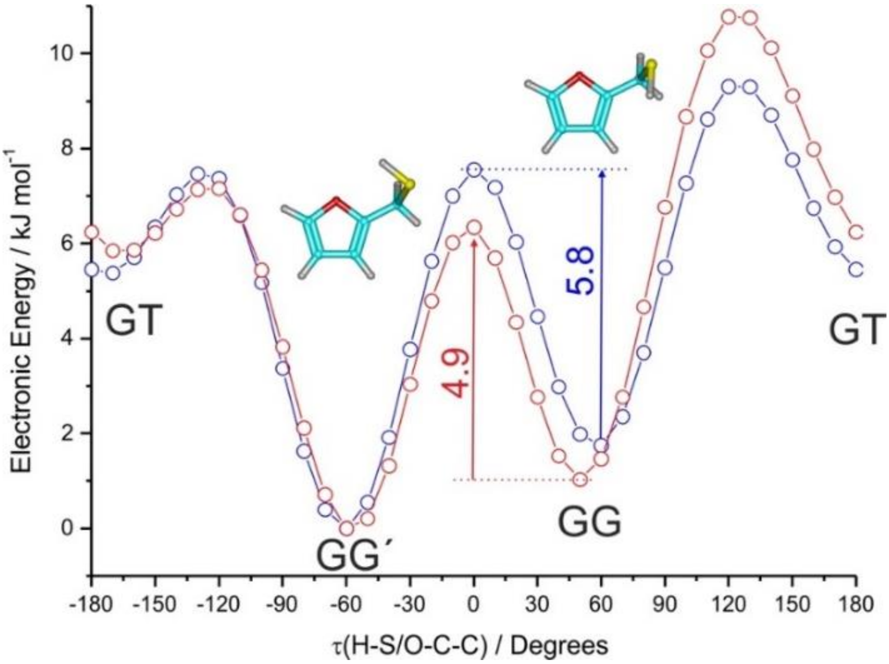

Figure 3. Interconversion barriers (MP2/6-311++G(d,p)) for the internal rotation of the terminal hydrogen atom in the thiol/alcohol group of furfuryl mercaptan (FM, blue trace) and furfuryl alcohol (FA, red trace). The exocyclic sulfur/oxygen atom is kept fixed to the O-C-C-S/O *gauche* position. The FA barrier for the GG-GG´conversion is 4.9 kJ mol^{-1}, ca. 0.9 kJ mol^{-1} smaller than in FM.

4. Rotational spectra of the of the FM and FA monohydrates

We generated the neutral monohydrates of furfuryl mercaptan and furfuryl alcohol coexpanding the ring compounds and water vapor with a pressurized neon carrier gas. The near-adiabatic expansion into an evacuated chamber created the dimers by many-body intermolecular collisions in the vicinity of the nozzle, later freezing the clusters in the transient expansion. The rotational spectra shown in Figures 4-7 were analyzed in the region 2-18 GHz, with support from three DFT/ab initio molecular models. The most stable isomers for FM···H_2O and FA···H_2O (and adopted notation) are shown in Figure 8, with predicted rotational parameters in Tables 3-4 (B3LYP-D3(BJ)/def2-TZVP; see Tables S32-S33 (ESI, see attached file) for alternative B3LYP-D3/6-311++G(d,p) and MP2/6-311++G(d,p) predictions). For both complexes two types of dimers with water resulted from the conformational search:

1) insertion complexes, in which the water molecule bridges the two polar groups of FM or FA, establishing two simultaneous HBs and closing a seven-membered ring, or, alternatively:

2) addition complexes, in which water is primarily attached to the thiol/alcohol group but not to the endocyclic oxygen, eventually forming secondary weak interactions with the furfuryl ring. Intermolecular interactions between the thiol/alcohol groups and the water molecule may proceed in both cases either through donor (S-H/O-H···O$_{water}$) or acceptor (O$_{water}$-H···S/O) HBs. Water may exhibit the well-known donor/acceptor role, while the furfuryl monomers may favor the most stable GG´ or GG conformations or eventually become distorted by hydration. This sum of factors made difficult to establish *a priori* which of the isomers in Figure 3 could be most stable. The theoretical calculations predicted close relative energies between all isomers (ΔG < 5-8 kJ mol^{-1} in Tables 3 and 4 for both FM···H_2O and FA···H_2O), but with different energy orderings depending on the quantum chemical model (compare with Tables S32-S33, ESI, see attached file).

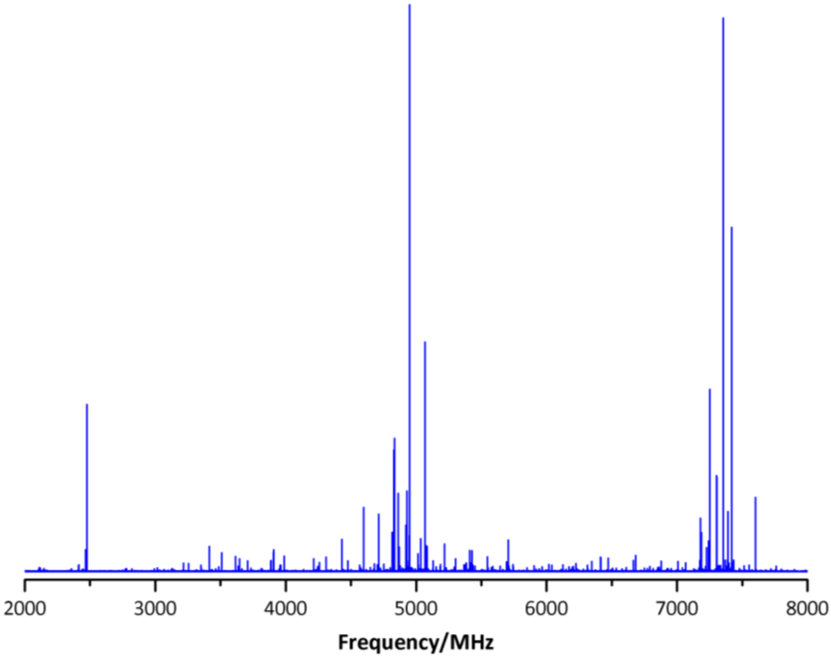

Figure 4. Microwave spectrum of the dimer furfuryl mercaptan – water in the 2-8 GHz region

Since the conformational predictions were model dependent and could not totally ascertain the identity of the global minima, the initial spectral surveys of the FM and FA hydrates targeted systematically all the isomers predicted in Tables 3 and 4. In FM···H_2O we observed the spectra from two asymmetric rotors denoted isomers I and II, comprising both μ_a- and μ_b-type *R*-branch ($J+1 \leftarrow J$, J=0-8, $\mu_a > \mu_b$) rotational transitions (Figure 5). The spectral dataset was fitted to experimental accuracy with a semirigid-rotor Watson's Hamiltonian[24] (S reduction), determining all quartic centrifugal distortion constants (except d_2 for isomer I). In order to check the assignment, we added isotopically labeled $H_2{}^{18}O$ water to the jet. A new spectrum at lower frequencies of the parent species was consistent with the expected shifts in the moments of inertia, confirming unequivocally the spectral identification (Figure 3).

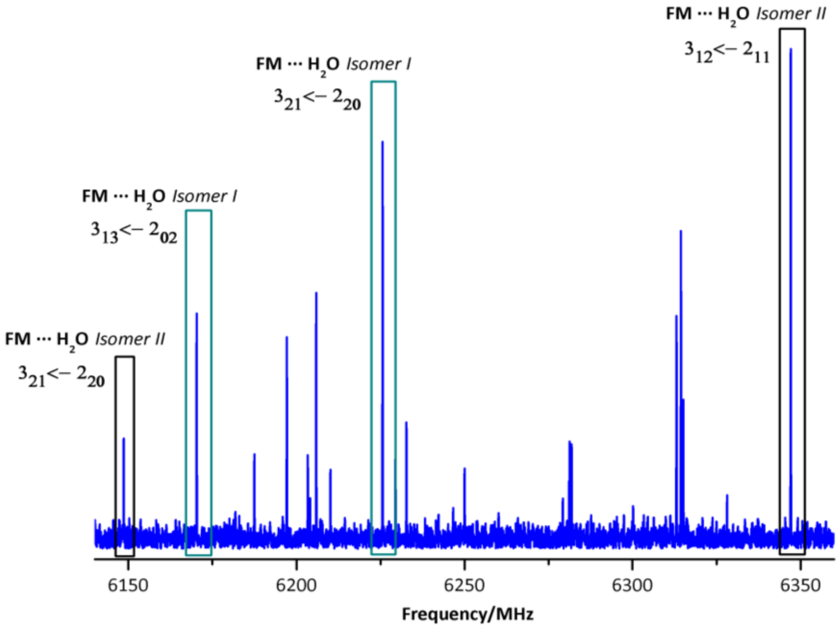

Figure 5. Illustrative rotational transitions of the dimer furfuryl mercaptan – water: section of 200 MHz showing transitions from isomers I and II.

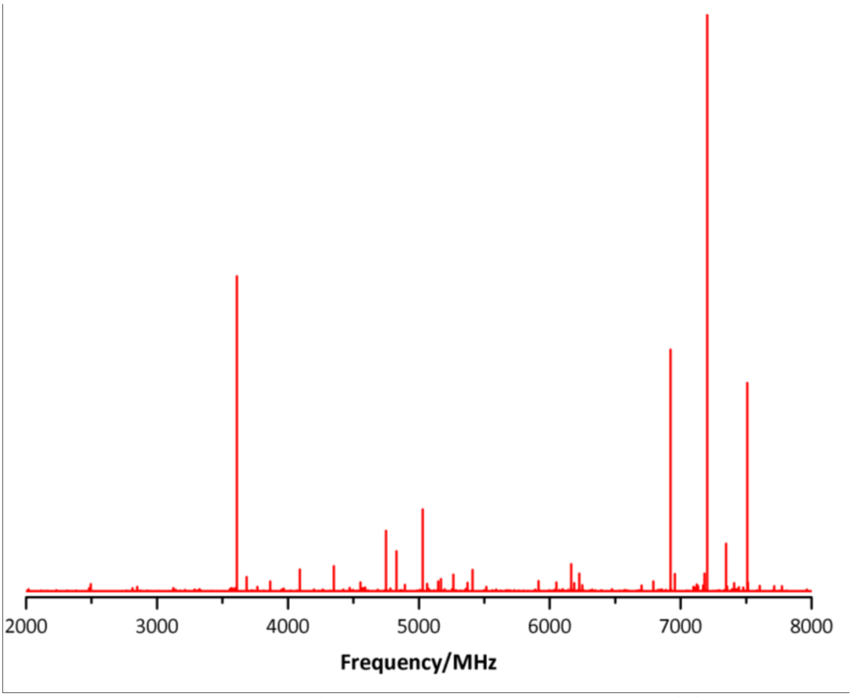

Figure 6. Microwave spectrum of the dimer furfuryl alcohol – water in the 2-8 GHz region

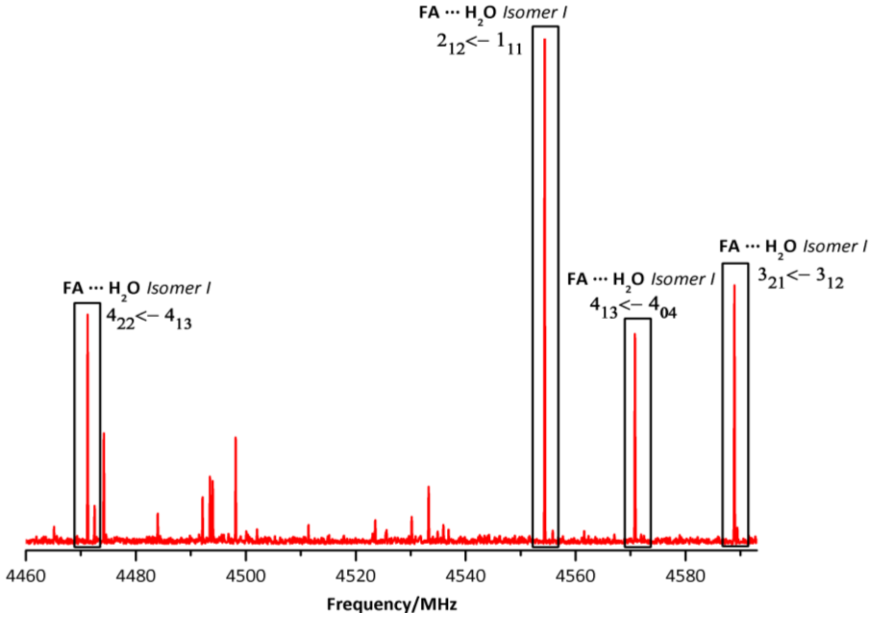

Figure 7. Illustrative rotational transitions of the dimer furfuryl alcohol – water: section of 140 MHz showing transitions from isomer I.

Conversely, the spectrum of FA···H$_2$O (Figure 6) revealed a single isomer with *R*-branch transitions ($\mu_a > \mu_b > \mu_c$), that was analyzed similarly. The spectral identification was again verified by detection of the H$_2{}^{18}$O isotopologue (Figure S5, ESI, see attached file). The experimental spectroscopic parameters for FM···H$_2$O and FA···H$_2$O are collected in Tables 1 and 2 and S34-S35 (ESI, see attached file), while the observed transitions are listed in Tables S36-S41 (ESI, see attached file). The observation of the H$_2{}^{18}$O isotopic species allowed determining the atomic coordinates of the water oxygen atom in the monohydrate for the three detected species. The resulting coordinates obtained from the Kraitchman[25] equations are presented in Tables S42 and S43 (ESI, see attached file).

The conformational assignment relied on a comparison of the experimental rotational constants and water oxygen coordinates with the theoretical DFT/ab initio predictions in Tables 3 and 4, S32-S33 and S42-S43 (ESI, see attached file). The assignment of the furfuryl alcohol monohydrate FA···H$_2$O was relatively straightforward, as the rotational constants clearly pointed to the identification of the observed cluster as the insertion complex GG´-W$_{da}$, predicted as global minimum using B3LYP-D3(BJ). This isomer exhibits a network of two consecutive O-H···O HBs, in which the hydroxyl group acts as proton donor to the water oxygen and water similarly behaves as proton donor to the ring oxygen atom. On the other hand, the conformational assignment of the two observed furfuryl mercaptan hydrates FM···H$_2$O I/ II was more difficult, as the theoretical predictions were not totally consistent and the rotational constants of the three predicted insertion complexes were relatively close. Finally, inspection of the experimental evidence led to the identification of isomer I as GG´-W$_{da}$ and isomer II as GG-W$_{dd}$. In both complexes water simultaneously binds to the ring oxygen and to the thiol group, with the thiol group engaging to water either as proton donor (isomer I) or proton acceptor (isomer II). Vibrationally-averaged effective structures were calculated for the three observed dimers by a least-squares fit of the moments of inertia.[26,27] For FA···H$_2$O we could fit both the position of the water oxygen and the orientation of the water moiety (using an

Table 1. Experimental rotational parameters of the dimer furfuryl mercaptan - water

	Isomer I	Isomer II
A / MHz[a]	2164.0642(22)[d]	2183.8117(29)
B / MHz	1160.11174(62)	1142.99515(73)
C / MHz	828.46438(29)	830.52727(40)
D_J / kHz	0.1795(44)	0.2285(46)
D_{JK} / kHz	0.409(44)	0.554(49)
D_K / kHz	2.03(18)	5.05(25)
d_1 / kHz	-0.0236(27)	-0.0599(31)
d_2 / kHz	[0.][c]	-0.0184(18)
$\|\mu_a\|$ / D	+ + +	+ + +
$\|\mu_b\|$ / D	+	+
$\|\mu_c\|$ / D		
N[b]	29	30
σ / kHz	9.2	8.3

[a]Rotational constants (A, B, C), Watson's S-reduction centrifugal distortion constants (D_J, D_{JK}, D_K, d_1, d_2) and electric dipole moments (μ_α, α = a, b, c). [b]Number of transitions (N) and rms deviation (σ) of the fit. [c]Values in square brackets were fixed to zero. [d]Standard errors in units of the last digit.

Table 2. Experimental rotational parameters of the dimer furfuryl alcohol - water

	FA ··· $H_2{}^{16}O$
A / MHz[a]	3053.15493(75)
B / MHz	1444.99486(39)
C / MHz	1036.46161(16)
D_J / kHz	0.3881(43)
D_{JK} / kHz	-0.289(28)
D_K / kHz	5.59(14)
d_1 / kHz	-0.1252(28)
d_2 / kHz	-0.02017(69)
$\|\mu_a\|$ / D	++ +
$\|\mu_b\|$ / D	++
$\|\mu_c\|$ / D	+
N	50
σ / kHz	5.4

[a]Parameter definition as in Table 1.

auxiliary dummy atom in the C_2 water axis), satisfactorily reproducing all observed rotational constants with a five parameters fit, as observed in Tables S44 (ESI, see attached file). For FM···H_2O a reduced set of three parameters adjusting only the water oxygen position was determinable (Tables S45 and S46, ESI, see attached file). In all cases the rest of the dimer was frozen at the B3LYP-D3(BJ) geometry. A comparison of the equilibrium, vibrationally-averaged structures and water oxygen substitution coordinates is shown in Figure 8. The atomic coordinates from the effective structure can be compared with the DFT predictions in Tables S47-S49 (ESI, see attached file).

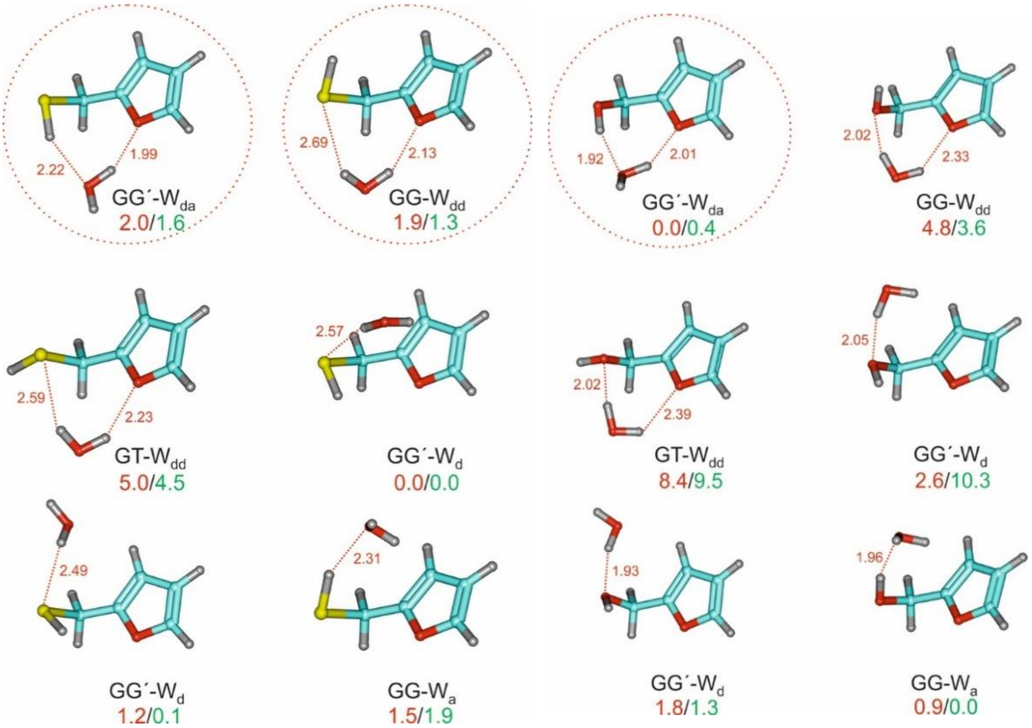

Figure 8. Conformational preferences of the furfuryl mercaptan monohydrate (FM···H_2O) on the right and the furfuryl alcohol monohydrate (FA···H_2O) on the left, showing relative Gibbs energies (kJ mol^{-1}) and hydrogen bond distances (Å, B3LYP-D3(BJ)). Isomers are labeled according to the conformation of the monomer (GG'/GG/GT) and the donor/acceptor ($W_{d/a}$) character of water. The red circles indicate the two isomers observed experimentally Energy values (in red and green) denote the B3LYP-D3(BJ) and MP2 predictions, respectively

5. Discussion

We have examined the non-covalent interactions stabilizing the water adduct of furfuryl mercaptan and observed the binding consequences of replacing a thiol by an alcohol group in the furfuryl monomer. Two isomers of monohydrated furfuryl mercaptan (GG´-W_{da} and GG-W_{dd}) and one isomer of the analog alcohol dimer (GG´-W_{da}) were detected in the isolation conditions of a supersonic jet. Several structural and energetic arguments rationalize these observations. The detection of two different isomers in FM···H_2O is partly due to the different conformational composition of the monomers in the jet. FM and FA display similar preferences for the thiol or alcohol group, with the exocyclic S/O heteroatom *gauche* to the ring (monomer structures in Tables S1-S4, ESI, see attached file) and terminal hydrogen atoms pointing to the ring heteroatom. The thiol/alcohol internal rotation barriers are apparently similar (5.8 vs 4.9 kJ mol^{-1}, respectively, in Figure 3), but the slightly larger value in FM effectively prevents conformational relaxation between the GG and GG´ isomers, since both monomers are detected in the jet. Conversely, the lower interconversion barrier in FA, closer to the empirical threshold of $2kT_{nozzle}$,[22] actually depopulates the higher energy isomer GG by relaxation to the global minimum GG´. The availability in the expansion of two isomers of FM kinetically favors the formation of two dimers with water, while in FA only the global minimum appears bound to water.

Table 3. Theoretical[c] rotational parameters of the dimer furfuryl mercaptan – water

	GG′-W$_d$	GG′-W$_d$	GG-W$_a$	GG-W$_{dd}$	GG′-W$_{da}$	GT-W$_{dd}$
A / MHz[a]	2289.26	2279.40	2214.48	2289.88	2168.91	2307.36
B / MHz	1187.61	1119.12	1171.58	1140.09	1173.86	1139.52
C / MHz	957.38	826.22	936.03	835.82	823.46	840.96
D_J / kHz	0.201	0.260	0.390	0.159	0.206	0.179
D_{JK} / kHz	1.784	0.940	6.328	0.618	0.929	0.783
D_K / kHz	0.883	1.969	-1.058	2.350	3.080	1.625
d_1 / kHz	-0.022	-0.072	0.054	-0.038	-0.070	-0.054
d_2 / kHz	0.017	-0.020	0.028	-0.012	-0.015	-0.018
$\|\mu_a\|$ / D	1.3	0.0	2.6	3.1	2.8	2.2
$\|\mu_b\|$ / D	3.3	0.3	0.8	2.6	0.4	2.2
$\|\mu_c\|$ / D	0.4	0.4	0.1	0.5	0.5	0.6
ΔE / kJ mol^{-1}[b]	0.0	2.5	3.9	2.9	3.6	5.0
ΔG / kJ mol^{-1}	0.0	1.2	1.5	1.9	2.0	5.0
E_B / kJ mol^{-1}	-23.5	-24.2	-21.5	-22.8	-23.8	-24.7

[a]Parameter definition as in Table 1. [b]Relative energies corrected with the zero-point energy (ZPE), Gibbs energy (ΔG, 298K, 1 atm) and complexation energy (including BSSE corrections) relative to the monomers in the geometry of the dimer. [c] B3LYP-D3(BJ)/ def2-TZVP.

Table 4.[a] Theoretical rotational parameters of the dimer furfuryl alcohol – water

	GG′-W$_{da}$	GG-W$_a$	GG′-W$_d$	GG′-W$_d$	GG-W$_{dd}$	GT-W$_{dd}$
A / MHz	3019.26	2688.69	3218.56	2545.14	3150.80	3117.54
B / MHz	1478.45	1539.60	1300.37	1581.06	1376.40	1400.42
C / MHz	1055.00	1232.59	998.93	1255.77	1016.39	1026.29
D_J / kHz	0.42	0.92	0.78	2.05	0.55	0.62
D_{JK} / kHz	-0.48	4.47	-2.89	12.29	-1.76	-2.06
D_K / kHz	6.51	-2.58	10.94	-11.75	8.25	10.74
d_1 / kHz	-0.12	0.01	-0.22	-0.31	-0.19	-0.22
d_2 / kHz	-0.03	-0.02	-0.02	0.06	-0.02	-0.02
$\|\mu_a\|$ / D	2.2	2.7	0.6	2.4	4.5	2.5
$\|\mu_b\|$ / D	1.9	1.9	1.2	2.7	2.2	2.4
$\|\mu_c\|$ / D	0.3	0.1	0.3	0.3	0.6	1.0
ΔE / kJ mol^{-1}	0.0	1.4	4.5	5.5	5.7	10.3
ΔG / kJ mol^{-1}	0.0	0.9	1.8	2.6	4.8	8.4
E_B / kJ mol^{-1}	-35.0	-32.1	-29.9	-25.0	-26.2	-26.7

[a]Parameter definition as in Table 3

The formation of insertion complexes with a network of two simultaneous HBs is preferred to addition complexes. The strongest HB in the FA monohydrate is formed by the ring alcohol, acting as proton donor to water (O-H···O$_w$). Simultaneously water binds as proton donor to the ring (O$_w$-H···O$_r$), reminiscent of the conformation of the furan monohydrate. The stronger character of the alcohol HB is apparent in the geometry of the complex, with the water oxygen considerably displaced with respect to the furfuryl plane and shorter hydrogen bond distances to the alcohol group ($r(\mathrm{OH\cdots O_w})$=1.956(3) Å vs. $r(\mathrm{O_wH\cdots O_r})$=2.16(1) Å in Figure 9). The O-H···O_w hydrogen bond distance is close to that observed in the gas-phase for water adducts with cyclic ethers and alcohols, where only a main HB is formed (ethylene oxide:[28] 1.92(1) Å; propylene oxide:[29] 1.908(7) Å; oxetane:[30] 1.86(2) Å; tetrahydropyrane:[31] 1.91(2) Å; 1,4-dioxane:[32] 1.90(3) Å; tert-butyl alcohol:[33] 1.903 Å). In the FM hydrate the situation is reversed, as evidenced in the bonding distances and the oxygen position, now closer to the furfuryl ring. In isomer I (GG´-W_{da}) the primary HB is now formed by water acting as proton donor to the ring ($r(\mathrm{O_wH\cdots O_r})$=1.99(2) Å), while the thiol forms a weaker secondary HB ($r(\mathrm{SH\cdots O_w})$=2.44(3) Å). For comparison, the analysis of the furan monohydrate found an effectively planar dimer with a slightly shorter hydrogen bond (r_{OwOr}=2.8561(18) Å, $r(\mathrm{O_wH\cdots O_r})$=1.95 Å).[29] The thiol group preferentially behaves as proton donor to water, as observed by comparison of isomers GG´-W_{da} and GG-W_{dd}. The predicted binding energies favor GG´-W_{da} by 1.0 kJ mol^{-1} (B3LYP-D3(BJ)) to 2.9 kJ mol^{-1} (MP2). When the thiol group behaves as proton acceptor in isomer GG-W_{dd} the water molecule is weakly bound to the sulfur atom ($r(\mathrm{O_wH\cdots S})$=2.95(3) Å), and the water oxygen similarly sits close to the furfuryl plane ($r(\mathrm{O_wH\cdots O_r})$=1.95 Å), as in the furan hydrate. In tetrahydrothiophene-water the only O_wH···S hydrogen bond was found much shorter ($r(\mathrm{O_wH\cdots S})$=2.37(4) Å).[34] For comparison, in the prototype hydrogen sulfide dimer the hydrogen bond distance is $r(\mathrm{SH\cdots S})$=2.779(4) Å. However, a systematic structural comparison of gas-phase sulfur HBs is presently not possible considering the limited experimental data. Our results for furfuryl alcohol qualitatively confirm the tendency of aromatic alcohols to behave as proton donors to water,[35] as opposed to aliphatic alcohols,[32,36] where the alcohol behaves as proton acceptor. Additional comparison with the glycidol monohydrate[37] is worth noting because both an alcohol and an endocyclic oxygen are available for water binding, making the dimer chemically similar to FA···H_2O. Interestingly, the water insertion in glycidol···H_2O produces a considerable (9 degree) rearrangement of the O-C-C-O side chain (a torsional change of 18 degrees was previously reported for the hydrate of 2-aminoethanol).[38] In the FA and FM hydrates the experimental rotational constants were reproduced considering that the monomer is not modified on complexation. The theoretical predictions suggest changes in the S/O-C-C-O dihedral on complexation below 2 degrees.

The computational results emphasize the need to properly account for dispersion contributions for weak non-covalent interactions like the sulfur HBs. The B3LYP functional with the Grimme-Becke-Johnson empirical corrections[15,16] (D3(BJ)) provided a satisfactory approximation to the experimental rotational constants in terms of efficiency and cost. As an example, the relative deviations for FM···H_2O I and FA ··· H_2O amount to 0.2-1.2% and 1.1-2.3%, respectively (for comparison the MP2 relative differences represent 0.3-3.2% and 0.5-1.2%, respectively). On the other hand, neither B3LYP-D3(BJ) nor MP2 could correctly identify the global minimum in FM ··· H_2O and establish a definitive energy ordering.

We found in Tables 3, S32 and S33 (ESI, see attached file) much larger binding energies for the B3LYP models than for MP2 (i.e., -27.5, -23.8 and -17.9 kJ mol^{-1}, respectively, for B3LYP-D3(BJ), B3LYP-D3 and MP2 in the GG´-W_{da} isomer of FM···H_2O). Previous estimations of binding energies involving sulfur HBs depend considerably on the molecular groups. The complexation energies of dimethylsulfide with methanol or water were estimated at -22.8[39] and -16.1 kJ mol^{-1},[40] respectively, using CCSD(T) and G2-MP2. The binding energies in a series of p-cresol dimers and sulfides are in the range -10.4 to -26.1 kJ mol^{-1}.[2] Noticeably, the predicted binding

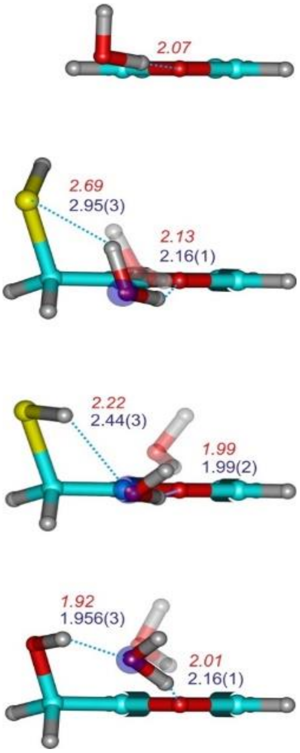

Figure 9. Hydrogen bonding in the monohydrates of furan (top), FM and FA (bottom), comparing the vibrationally-averaged effective structures (solid water molecules), the theoretical predictions (transparent water molecules), and the substitution coordinates of the water oxygen (blue spheres). For the furan hydrate the only structure corresponds to the theoretical calculations (all predictions B3LYP-D3(BJ)/def2-TZVP). The hydrogen bond distances represent both the effective (blue digits) and theoretical equilibrium values (red digits).

energies indicate a consistent increase in complexation energies of 11.2-12.2 kJ mol^{-1} (B3LYP-D3(BJ)) or 8.2-11.1 (MP2) when passing from the furfuryl mercaptan hydrate I/II to furfuryl alcohol, confirming the weaker character of the interactions involving sulfur in the furfuryl mercaptan adducts. Comparative values have been reviewed,[2] including cases where the sulfur HB strength presents stabilizations energies comparable to the alcohol group.[39]

Finally, information on the nature of the non-covalent interactions in the furfuryl – water dimers was obtained from an energy partition analysis[41] based on symmetry-adapted perturbation theory[19,42] (SAPT). The energy decomposition in Table 5 shows dominant electrostatic contributions for FA···H_2O, FM···H_2O-I and FM-H_2O-II, representing 184%, 196% and 171%, respectively, of the total binding energy. The dispersion terms are of smaller magnitude, but considerably larger in the sulfur compound than in the alcohol (56%-59% vs 42% of the binding energy, respectively). Differences can also be observed between the two hydrates of furfuryl mercaptan, with less electrostatic and more dispersion components in the second isomer, which correlates satisfactorily with the structural data. For comparison purposes Table 5 offers additional results for the dimers of water[43] and hydrogen sulfide, together with two clusters dominated by dispersion (pyridine-methane)[44] or mixed-regime (sevoflurane-benzene)[45] forces. In consequence, while the interactions in the three clusters can be categorized as dominantly hydrogen bonding, we appreciate a noticeable decrease in binding energy and larger dispersion character in the interactions involving sulfur.

In conclusion, the synergy between rotational spectroscopy and quantum mechanical calculations has revealed the structural and energetic differences between the thiol and alcohol groups in the furfuryl monohydrates. Rotational data complement the electronic and vibrational experiments in the gas-phase, providing a test-bed for selection and adjustment of molecular orbital methods. Additional theoretical and experimental investigations of other thiol clusters will be necessary to gain a systematic view of the hydrogen bonding and non-covalent interactions involving sulfur.

Table 5. Binding energy decomposition for the monohydrates of furfuryl alcohol and furfuryl mercaptan (SAPT(0)/jun-cc-pVDZ, kJ mol^{-1}), and comparison with dimers dominated by electrostatic (water dimer), dispersion (pyridine-methane) or mixed (sevoflurane-benzene) intermolecular interactions.

	$\Delta E_{\text{Electrostatic}}$	$\Delta E_{\text{Induction}}$	$\Delta E_{\text{Dispersion}}$	$\Delta E_{\text{Exchange}}$	ΔE_{Total}
FM···H_2O – GG´-W_{da}[a]	-41.8	-12.4	-12.9	45.8	-21.3
FM···H_2O – GG-W_{dd}[a]	-35.3	-7.0	-11.8	33.5	-20.6
FA···H_2O – GG´-W_{da}[a]	-61.3	-17.7	-14.6	60.1	-33.4
$(H_2O)_2$	-37.0	-9.0	-5.3	29.4	-21.8
$(H_2S)_2$ [b]	-12.9	-4.4	-5.2	18.0	-4.5
Pyridine-methane[c]	-17.9	-4.1	-42.0	46.1	-17.8
Sevoflurane-benzene[d]	-36.9	-10.5	-37.0	59.4	-25.0

[a]This work. [b]Ref. 43. [c]Ref. 44. [d]Ref. 45.

Chapter IV. References:

1. Biswal, H. S., Bhattacharyya, S., Bhattacherjee, A. & Wategaonkar, S. Nature and strength of sulfur-centred hydrogen bonds: laser spectroscopic investigations in the gas phase and quantum-chemical calculations. *Int. Rev. Phys. Chem.* **34**, 99–160 (2015).

2. Biswal, H. S. Hydrogen Bonding Involving Sulfur: New Insights from Ab Initio Calculations and Gas Phase Laser Spectroscopy. in *Noncovalent Forces* (ed. Scheiner, S.) (Springer Int. Pub., 2015).

3. Gilli, G. & Gilli, P. *The Nature of the Hydrogen Bond.* (2009).

4. Aakeroy, C. B. *et al.* Definition of the chalcogen bond (IUPAC Recommendations 2019). *Pure Appl. Chem.* **91**, 1889–1892 (2019).

5. Alkorta, I., Elguero, J. & Frontera, A. Not only hydrogen bonds: Other noncovalent interactions. *Crystals* **10**, (2020).

6. Legon, A. C. Tetrel, pnictogen and chalcogen bonds identified in the gas phase before they had names: a systematic look at non-covalent interactions. *Phys. Chem. Chem. Phys.* **19**, 14884–14896 (2017).

7. Zhou, P., Tian, F., Lv, F. & Shang, Z. Geometric characteristics of hydrogen bonds involving sulfur atoms in proteins. *Proteins Struct. Funct. Bioinforma.* **76**, 151–163 (2009).

8. Mundlapati, V. R., Ghosh, S., Bhattacherjee, A., Tiwari, P. & Biswal, H. S. Critical Assessment of the Strength of Hydrogen Bonds between the Sulfur Atom of Methionine/Cysteine and Backbone Amides in Proteins. *J. Phys. Chem. Lett.* **6**, 1385–1389 (2015).

9. Contreras-García, J. *et al.* NCIPLOT: A Program for Plotting Noncovalent Interaction Regions. *J. Chem. Theory Comput.* **7**, 625–632 (2011).

10. Garcia, J., Podeszwa, R. & Szalewicz, K. SAPT codes for calculations of intermolecular interaction energies. *J. Chem. Phys.* **152**, 184109 (2020).

11. Pérez, C. *et al.* Broadband Fourier transform rotational spectroscopy for structure determination: The water heptamer. *Chem. Phys. Lett.* **571**, 1–15 (2013).

12. Neill, J. L. *et al.* Rotational spectroscopy of iodobenzene and iodobenzene–neon with a direct digital 2–8GHz chirped-pulse Fourier transform microwave spectrometer. *J. Mol. Spectrosc.* **269**, 21–29 (2011).

13. Shipman, S. T. & Pate, B. H. New Techniques in Microwave Spectroscopy. in *Handbook of High-resolution Spectroscopy* (eds. Quack, M. & Merk, F.) 801–827 (John Wiley & Sons, Ltd., 2011).

14. Halgren, T. A. Merck molecular force field. I. Basis, form, scope, parameterization, and performance of MMFF94. *J. Comput. Chem.* **17**, 490–519 (1996).

15. Grimme, S., Antony, J., Ehrlich, S. & Krieg, H. A consistent and accurate ab initio parametrization of density functional dispersion correction (DFT-D) for the 94 elements H-Pu. *J. Chem. Phys.* **132**, 154104 (2010).

16. Grimme, S., Ehrlich, S. & Goerigk, L. Effect of the damping function in dispersion corrected density functional theory. *J. Comput. Chem.* **32**, 1456–1465 (2011).

17. Frisch, M. J., Trucks, G. W., Schlegel, H. B., Scuseria, G. E. & Robb, M. A. et al. *Gaussian 09, Revision A.02.* (Gaussian, Inc., 2016).

18. Turney, J. M. *et al.* Psi4: an open-source ab initio electronic structure program. *Wiley Interdiscip. Rev.*

Comput. Mol. Sci. **2**, 556–565 (2012).

19. Parker, T. M., Burns, L. A., Parrish, R. M., Ryno, A. G. & Sherrill, C. D. Levels of symmetry adapted perturbation theory (SAPT). I. Efficiency and performance for interaction energies. *J. Chem. Phys.* **140,** 094106 (2014).

20. Marstokk, K.-M. *et al.* Microwave Spectrum, Conformational Equilibrium, Intramolecular Hydrogen Bonding and Ab Initio Calculations for 2-Furanmethanethiol (Furfuryl Mercaptan). *Acta Chem. Scand.* **48**, 298–305 (1994).

21. Marstokk, K.-M. *et al.* Microwave Spectrum, Conformational Equilibrium and Ab Initio Calculations for 2-Furanmethanol (Furfuryl Alcohol). *Acta Chem. Scand.* **48**, 25–31 (1994).

22. Ruoff, R. S., Klots, T. D., Emilsson, T. & Gutowsky, H. S. Relaxation of conformers and isomers in seeded supersonic jets of inert gases. *J. Chem. Phys.* **93**, 3142–3150 (1990).

23. Araujo-Andrade, C., Gómez-Zavaglia, A., Reva, I. D. & Fausto, R. Conformers, Infrared Spectrum and UV-Induced Photochemistry of Matrix-Isolated Furfuryl Alcohol. *J. Phys. Chem. A* **116**, 2352–2365 (2012).

24. Watson, J. K. G. Vibrational Spectra and Structure. in (ed. Durig, J. R.) 1–89 (Elsevier Inc., 1977).

25. Kraitchman, J. Determination of Molecular Structure from Microwave Spectroscopic Data. *Am. J. Phys.* **21**, 17–24 (1953).

26. Rudolph, H. D. & Demaison, J. Equilibrium Molecular Structures: From Spectroscopy to Quantum Chemistry. in *Equilibrium Molecular Structures: From Spectroscopy to Quantum Chemistry* (eds. Demaison, J., Boggs, J. E. & Császár, A. G.) 125–158 (CRC Press, 2011).

27. MOMSTRUC Structural Package.

28. Caminati, W., Moreschini, P., Rossi, I. & Favero, P. G. The O···H− O Hydrogen Bond in the Gas Phase. Microwave Structure of Ethylene Oxide− Water. *J. Am. Chem. Soc.* **120**, 11144–11148 (1998).

29. Su, Z., Wen, Q. & Xu, Y. Conformational Stability of the Propylene Oxide− Water Adduct: Direct Spectroscopic Detection of O− H···O Hydrogen Bonded Conformers. *J. Am. Chem. Soc.* **128**, 6755–6760 (2006).

30. Ottaviani, P., Giuliano, M., Velino, B. & Caminati, W. Interactions Between Organic Molecules and Water: Rotational Spectrum of the 1:1 Oxetane?Water complex. *Chem. - A Eur. J.* **10**, 538–543 (2004).

31. Spoerel, U., Stahl, W., Caminati, W. & Favero, P. G. Jet-Cooled Rotational Spectra and Ab Initio Investigations of the Tetrahydropyran-Water System. *Chem. - A Eur. J.* **4**, 1974–1981 (1998).

32. Caminati, W., Dell'Erba, A., Melandri, S. & Favero, P. G. Conformation and Stability of Ether− Water Adducts: Free Jet Absorption Millimeter Wave Spectrum of 1,4-Dioxane− Water. *J. Am. Chem. Soc.* **120**, 5555–5558 (1998).

33. Evangelisti, L. & Caminati, W. Internal dynamics in complexes of water with organic molecules. Details of the internal motions in tert-butylalcohol–water. *Phys. Chem. Chem. Phys.* **12**, 14433 (2010).

34. Sanz, M. E. *et al.* Conformation and Stability of Adducts of Sulfurated Cyclic Compounds with Water: Rotational Spectrum of Tetrahydrothiophene− Water. *J. Phys. Chem. A* **103**, 5285–5290 (1999).

35. Melandri, S., Maris, A., Favero, P. G. & Caminati, W. Free jet absorption millimetre-wave spectrum and model calculations of phenol–water. *Chem. Phys.* **283**, 185–192 (2002).

36. Stockman, P. A., Blake, G. A., Lovas, F. J. & Suenram, R. D. Microwave rotation-tunneling spectroscopy of the water–methanol dimer: Direct structural proof for the strongest bound conformation. *J. Chem.*

Phys. **107**, 3782–3790 (1997).

37. Conrad, A. R., Teumelsan, N. H., Wang, P. E. & Tubergen, M. J. A Spectroscopic and Computational Investigation of the Conformational Structural Changes Induced by Hydrogen Bonding Networks in the Glycidol− Water Complex. *J. Phys. Chem. A* **114**, 336–342 (2010).

38. Tubergen, M. J., Torok, C. R. & Lavrich, R. J. Effect of solvent on molecular conformation: Microwave spectra and structures of 2-aminoethanol van der Waals complexes. *J. Chem. Phys.* **119**, 8397–8403 (2003).

39. Wennmohs, F., Staemmler, V. & Schindler, M. Theoretical investigation of weak hydrogen bonds to sulfur. *J. Chem. Phys.* **119**, 3208–3218 (2003).

40. Kaur, D., Aulakh, D., Khanna, S. & Singh, H. Theoretical study on the nature of S···H and O ··· H hydrogen bonds. *J. Sulfur Chem.* **35**, 290–303 (2014).

41. Scheiner, S. *Hydrogen Bonding. A Theoretical Perspective*. (Oxford University Press, 1997).

42. Hohenstein, E. G. & Sherrill, C. D. Density fitting of intramonomer correlation effects in symmetry-adapted perturbation theory. *J. Chem. Phys.* **133**, 014101 (2010).

43. Dyke, T. R., Mack, K. M. & Muenter, J. S. The structure of water dimer from molecular beam electric resonance spectroscopy. *J. Chem. Phys.* **66**, 498–510 (1977).

44. Gou, Q. *et al*. Interactions between alkanes and aromatic molecules: a rotational study of pyridine–methane. *Phys. Chem. Chem. Phys.* **16**, 13041–13046 (2014).

45. Seifert, N. A. *et al*. Probing the C-H ··· π Weak Hydrogen Bond in Anesthetic Binding: The Sevoflurane-Benzene Cluster. *Angew. Chemie Int. Ed.* **53**, 3210–3213 (2014).

Chapter V

HYDRATION OF THENYL COMPOUNDS:

$(Thenyl\ Mercaptan \cdots H_2O)^*$ and $(Thenyl\ Alcohol \cdots H_2O)^*$

Adapted from:

(*): M. Juanes, R. T. Saragi, R. Pinacho, J. E. Rubio and A. Lesarri, *Phys. Chem. Chem. Phys.*, **2020**, 22, 12412 – 12421

(The Electronic Supporting Information – ESI, can be found in the document: thesis-ESI.pdf)

I. Introduction

The analysis of thenyl mercaptan (TM), thenyl alcohol (TA) and their complexes with water (see Figure 1) follows the previous study of the hydrates of furfuryl mercaptan (FM) and furfuryl alcohol (FA), FM ··· H_2O and FA ··· H_2O, described in Chapter IV. These molecules are composed by the same number of heavy-atoms, share a similar molecular skeleton and differ in the heteroatom in the aromatic ring plane: sulfur in the thenyl derivatives, instead of oxygen in the furfuryl compounds.

As described in Chapter IV, furfuryl alcohol forms a single insertion dimer with water, stabilized by two simultaneous H-bonds of dominant electrostatic character. In the primary interaction the alcohol acts as proton donor to water ($O\text{-}H\cdots O_w$), while water donates a proton to the oxygen ring ($O_w\text{-}H\cdots O_r$). Conversely, two isomers are observed when furfuryl mercaptan binds to water, the stronger interaction now being the water-to-ring ($O_w\text{-}H\cdots O_r$) H-bond. In this case the thiol group may act both as H-bond donor ($SH\cdots O_w$) or acceptor ($O_w\text{-}H\cdots S$) to water, forming a secondary H-bond. The mercaptan dimer is still dominantly electrostatic, but with a larger dispersion contribution. Would the further replacement of the ring oxygen by sulfur enhance the interaction between water and the thiol group? Moreover, could water establish two simultaneous hydrogen bonds with sulfur atoms as it does with oxygen in furfuryl alcohol? These questions were addressed in the comparative study of thenyl mercaptan (TM), thenyl alcohol (TA) and their monohydrates (TM···H_2O and TA···H_2O), which confirmed a floppy interaction and a dynamic torsional behavior of water in the two dimers, quite different to the furfuryl hydrates.

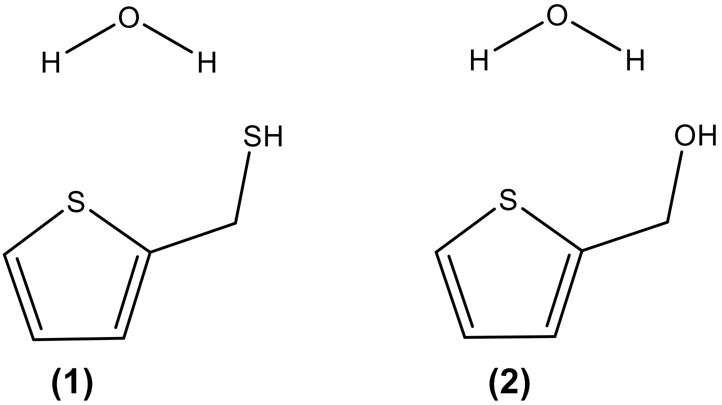

Figure 1. Molecular formulas of the dimers analysed in this chapter, including the thenyl mercaptan (1) and thenyl alcohol (2) hydrates.

The analisys of the thenyl mercaptan (TM···H_2O) and the thenyl alcohol (TA···H_2O) dimers could be understood as a continuation of the previous study which involve intra/intermolecular interactions though the thiol and alcohol groups in the main role, offering different interactions and HB forces. The solvation of both thenyl derivatives will therefore allow comparing the strength of the water interaction between the OH and SH groups. Furthermore, some unexpected tunneling motion and quantum effects due to the internal rotation of the H_2O have been observed in the rotational spectrum.

All the experiments have been, again, assisted by molecular-orbital quantum chemical calculations with different dispersion-corrected density functional theory (DFT) models and/or ab initio methods, simultaneously assessing the theoretical calculations. Additionally, we have also carried out an analysis of the intermolecular interactions based in the electronic density topology (NCIPlot)[1] and a symmetry-adapted perturbation theory (SAPT)[2] energy decomposition to examine the underlying basis of the intermolecular interactions originated by the thiol and alcohol groups.

II. Thenyl Mercaptan and Thenyl alcohol

1. Experimental set up:

Thenyl mercaptan (2-thiophenemethanethiol, >95% GC, b.p. 76°C) and thenyl alcohol (2-thiophenemethanol, >98% GC, b.p. 207°C) were obtained commercially and used without further purification. The vapors of each compound were diluted within a stream of pure neon (backing pressures of 0.25 MPa), forming a supersonic jet by expansion through a pin-hole nozzle (f=0.5-0.8 mm) into a high-vacuum chamber (ultimate pressures of 10-7 hPa). The mercaptan sample was volatile enough to be placed in an external reservoir inserted in the gas line, but the alcohol required a heating nozzle (45°C) to obtain sufficient vapor pressure. For the water clusters either H_2O or $H_2{}^{18}O$ were added to the gas line. The jet was probed with a broadband chirped-pulse Fourier transform microwave (CP-FTMW) spectrometer, operating in the region 2-8 GHz, and a Balle-Flygare cavity FTMW spectrometer, working in 8-18 GHz.

	Thenyl Mercaptan	TM···H_2O	Thenyl Alcohol	TA···H_2O
Carrier Gas	Ne		Ne	
Nozzle Ø (mm)	0.5		0.8	
Sample Tª	Room temperature		45°C	
Carrier Gas Pressure	2.5 bar		2.5 bar	

2. Rotational spectra of TM and TA

The experimental work initially examined the conformational landscape and rotational spectrum of the thenyl monomers TM and TA, previously unreported. Similarly to the furfuryl derivatives,[3] the bidimensional potential energy surface is defined by two dihedrals describing the elevation of the side chain with respect to the thenyl ring (τ_1(S1- C2-C6-S7/O7) and the orientation of the terminal thiol/alcohol hydrogen atom (τ_2(C2-C6- S7/O7-H). Molecular orbital calculations in Tables S1-S2 (ESI, see attached file) predicted elevation angles close to +60° (τ_1 +gauche or G) for the side chain (as in the furfuryl derivatives) and staggered orientations for the terminal alcohol/thiol. However, the terminal hydrogen atom now preferentially orients to the adjacent carbon-carbon bond in the ring π system (τ_2 +gauche or G) of TM or TA instead of pointing to the ring oxygen, inverting the conformational stability of the furfuryl compounds. DFT energetic predictions in Tables S3-S4 (ESI, see attached file) and Figures 2-3 suggest that the second GG´ conformation is 1.2-1.9 kJmol^{-1} above the global minimum GG at B3LYP-D3(BJ) level.

The jet-cooled microwave spectra of water-seeded TM and TA is shown in Figures 4 and 5. Following the initial predictions the rotational spectra of the two monomers were readily assigned based on their dominant μ_a and μ_b selection rule transitions. A smaller set of weaker μ_c transitions were added later. The spectrum was analyzed using a conventional Watson's (S-

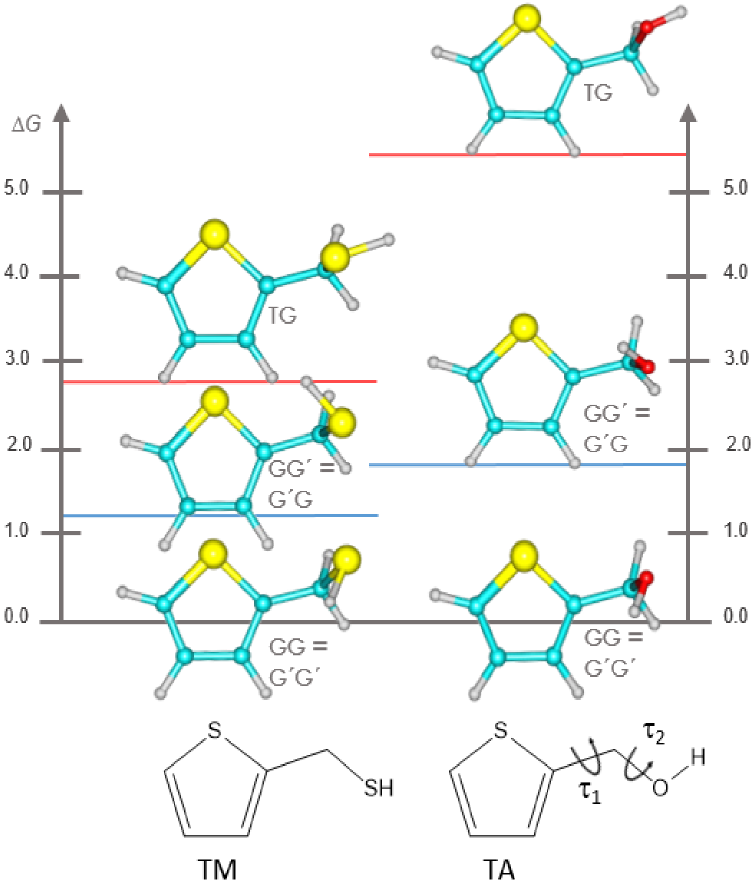

Figure 2. Theoretical Gibbs energies (B3LYP-D3(BJ), kJmol^{-1}) for the lowest-lying conformations of thenyl mercaptan (TM) and thenyl alcohol (TA), as collected in Table S3 and S4 (ESI). Molecular conformations are labeled according to the O-CC-S/O (t_1) and C-C-S/O-H (t_2) dihedrals (G=+gauche, G'=-gauche T=trans).

reduced) semirigid-rotor Hamiltonian[4] including up to quartic terms in the centrifugal distortion, implemented with Pickett's SPFIT program.[5] In the two molecules the spectral intensity was sufficient to assign independently the parent and all monosubstituted ^{13}C and ^{34}S isotopologues in natural abundance (1% and 4%, respectively). The resulting rotational parameters for TM and TA are collected in Tables S5 and S6 (ESI ESI, see attached file), while the present dataset of measured transitions are collected in Tables S7-S14 (TM) and S15-S21 (TA), ESI (see attached file). A structural analysis using effective and substitution methods[6] in Tables S22 and S27 (ESI, see attached file) was consistent with the detection of the predicted global minimum GG for the two thenyl monomers. The structural calculations used Rudolph's MOMSTRUC programs.[7]

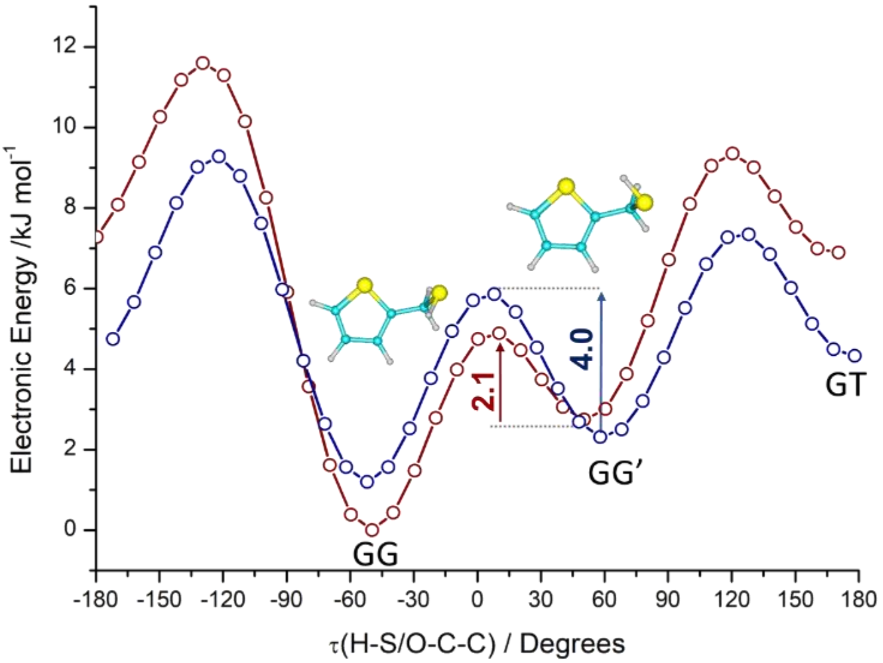

Figure 3. Interconversion barriers (B3LYP-D3(BJ)/def2-TZVP) for the internal rotation of the terminal hydrogen atom in the thiol/alcohol group of thenyl mercaptan (TM, blue trace) and thenyl alcohol (TA, red trace). The exocyclic sulfur/oxygen atom is kept fixed to the O-C-C-S/O *gauche* position. The TA barrier for the GG-GG´conversion is 2.1 kJ mol^{-1}, ca. 1.9 kJ mol^{-1} smaller than in TM.

3. Rotational spectra of the monohydrates

The investigation of the TM and TA monohydrates started from the computational molecular models in Tables 3-4. For TA···H_2O five isomers were found with Gibbs energy below 8 kJ mol^{-1}. As expected, the microsolvation of the alcohol always involves a primary H-bond between the water molecule and the hydroxyl group in the side chain, as shown in Figure 6. Conversely, attractive contacts with the thenyl sulfur atom are avoided, so water forms addition complexes either on top or laterally to the ring, which occasionally allows a secondary interaction with the p ring system. While water may act both as proton donor or acceptor to the alcohol the predictions suggest a marked preference for the alcohol to behave as proton donor to water, with other isomers well separated in energy (B3LYP-D3(BJ): 4-5 kJ mol^{-1}, MN15-L: 1-8 kJ mol^{-1}). The conformational options for the mercaptan monohydrate TM···H_2O in Figure 4 of Chapter IV are less clearly defined. According to B3LYP-D3(BJ) four isomers are very close in energy (< 1.8 kJ mol^{-1}), while the fifth isomer is located at 3.4 kJ mol^{-1}. Using MN15-L two isomers are practically isoenergetic (0.9 kJ mol^{-1}) and the rest have conformational energies of 2.7-5.2 kJ mol^{-1}.

In both cases the global minimum corresponds to the thiol group acting as proton donor to water, establishing a primary S-H···O_w hydrogen bond, which is accompanied by water interactions to the ring. In all isomers there are no direct interactions between water and the thenyl sulfur atom, except in the less stable isomer, where water simultaneously links to this atom and the π electronic cloud.

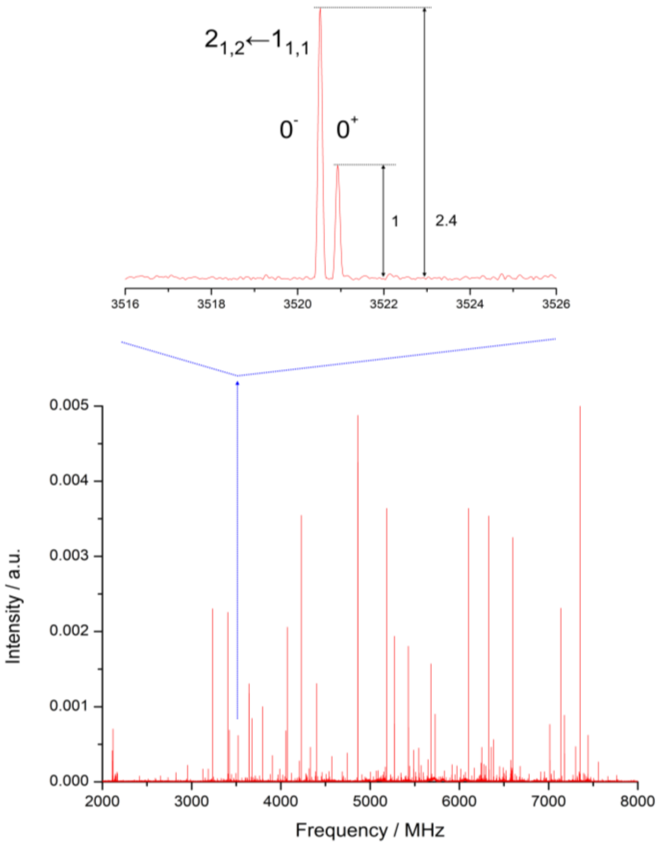

Figure 4. The microwave spectrum (2-8 GHz) of water seeded thenyl mercaptan, showing transitions from the TM monomer and the monohydrate TM···H_2O. Torsional tunneling doublings in TM···H_2O are exemplified here for the transition $2_{1,2} \leftarrow 1_{1,1}$.

The close conformational energies demanded an experimental verification of the computational models. The microwave spectrum of TA···H_2O in Figure 5 was first analyzed, using the predicted rotational constants of Table 4. A single isomer was then assigned, characterized by a set of both R- ($J+1 \leftarrow J$) and Q-branch ($J \leftarrow J$) μ_b and additional R-branch μ_a rotational transitions, spanning quantum numbers J=0-7 and $K_{-1}<3$. The most relevant spectral feature was a small (0.1-0.6 MHz) tunnelling doubling in both μ_a and μ_b transitions, confirming a large-amplitude internal motion connecting two symmetry-equivalent structures. The relative intensities of the two tunneling components were close to 3:1, coincident with the nuclear spin statistical weights associated to the exchange of two fermions with spin $I=1/2$. In consequence, the spectral doublings confirm an internal rotation of water around its symmetry axes in the cluster, splitting the ground vibrational state in two torsional sublevels 0^+ and 0^-.

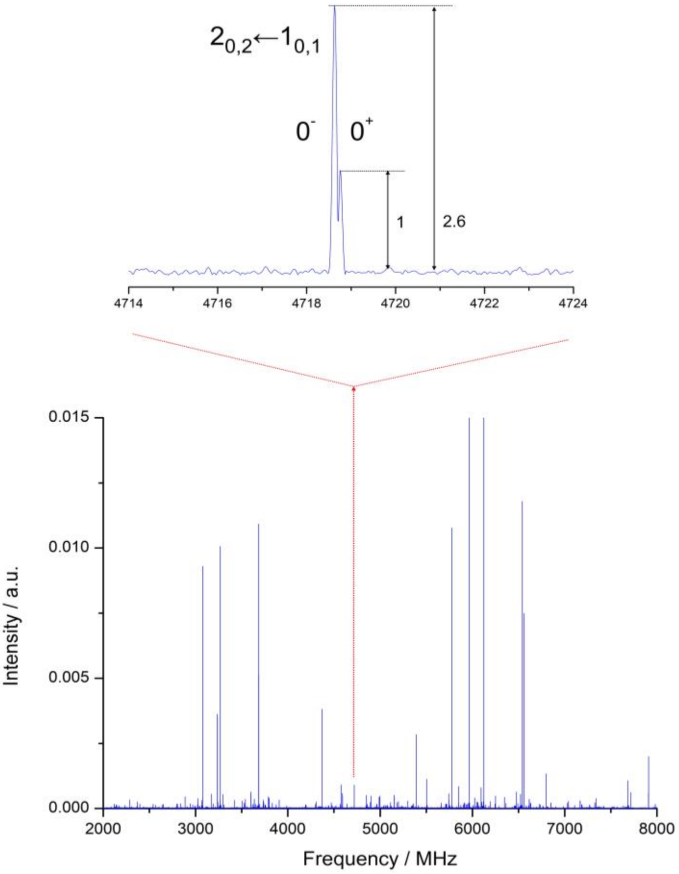

Figure 5. The microwave spectrum (2-8 GHz) of water-seeded thenyl alcohol, showing transitions from the TA monomer and the monohydrate TA···H_2O. The horizontal expansion (upper trace, 10 MHz) shows a typical torsional tunneling doubling in the rotational transition $2_{0,2}\leftarrow 1_{0,1}$.

The observed splittings correspond to intra-state $0^{\pm} \leftrightarrow 0^{\pm}$ torsional-rotational transitions, with interstate transitions $0^{\mp} \leftrightarrow 0^{\pm}$ forbidden. The rovibrational analysis used a two-state Hamiltonian $\boldsymbol{H}_{\mathrm{RV}}$ comprising rigid ($\boldsymbol{H}_{0+}^{R}$, $\boldsymbol{H}_{0-}^{R}$) and semirigid-rotor ($\boldsymbol{H}_{0+}^{CD}$, $\boldsymbol{H}_{0-}^{CD}$) Watson terms[4] for both states, the energy separation ($\Delta E_{0^{\pm}}$) and plausible interaction terms ($\boldsymbol{H}_{\mathrm{int}}$) according to:

$$\boldsymbol{H}_{RV} = \begin{pmatrix} \boldsymbol{H}_{0+}^{CD} + \boldsymbol{H}_{0-}^{CD} & \boldsymbol{H}_{\mathrm{int}} \\ \boldsymbol{H}_{\mathrm{int}} & \boldsymbol{H}_{0+}^{CD} + \boldsymbol{H}_{0-}^{CD} + \Delta E_{0^{\pm}} \end{pmatrix} \qquad \textit{(1)}$$

However, neither the interaction terms or the energy separation were determinable from our experimental dataset, which effectively behaved like two independent rotors. The final spectroscopic results are collected in Table 2. Because of the good intensity of the cluster the ^{34}S-thenyl isotopologue was additionally measured in natural abundance. The investigation proceeded also to the ^{18}O-water cluster, unequivocally confirming the assignment. The rotational parameters of ^{34}S-TA···$H_2{}^{16}O$ and TA···$H_2{}^{18}O$ are shown in Tables S28-S29 (ESI, see attached file), while all the measured transitions are collected in Tables S30-S32 (ESI, see attached file).

Table 1. Experimental rotational parameters of the dimer thenyl mercaptan - water

	0^+		0^-
A / MHz[a]	1861.917(15)		1862.708(35)
B / MHz	983.1121(11)		983.02830(98)
C / MHz	845.80994(56)		845.97410(80)
D_J / kHz		0.2403(63)	
D_{JK} / kHz		3.122(17)	
D_K / kHz		[0.][c]	
d_1 / kHz		0.0228(44)	
d_2 / kHz		[0.]	
$\|\mu_a\|$ / D	+ + +		+ + +
$\|\mu_b\|$ / D			
$\|\mu_c\|$ / D			
N[b]		41	
σ / kHz	8.1		3.5

[a]Rotational constants (A, B, C), Watson's S-reduction centrifugal distortion constants (D_J, D_{JK}, D_K, d_1, d_2) and electric dipole moments (μ_α, α = a, b, c). [b]Number of transitions (N) and rms deviation (σ) of the fit. [c]Values in square brackets were fixed to zero. [d]Standard errors in units of the last digit.

Table 2. Experimental rotational parameters of the dimer thenyl alcohol - water

	0^+		0^-
A / MHz[a]	2194.4109(12)[d]		2194.4803(13)
B / MHz	1265.93393(63)		1265.93612(25)
C / MHz	1103.18197(37)		1103.23363(13)
D_J / kHz		0.7549(63)	
D_{JK} / kHz		1.954(53)	
D_K / kHz		[0.]	
d_1 / kHz		0.0527(48)	
d_2 / kHz		-0.0415(51)	
$\|\mu_a\|$ / D	+ + +		+ + +
$\|\mu_b\|$ / D	+		+
$\|\mu_c\|$ / D			
N		72	
σ / kHz	9.6		11.1

[a]Parameter definition as in Table 1.

The study of the thenyl mercaptan monohydrate TM···H_2O was based in the microwave spectrum in Figure 4, which revealed a single isomer with only R-branch μ_a transitions and quantum numbers in the range J=1-9 and K_{-1}<5. Small tunnelling splittings of 0.2-0.4 MHz with relative intensities close to 3:1 were also apparent, similarly leading to the conclusion that water is engaging internally in internal rotation around its axis, symmetrically inverting two half spin fermions. A fit of the rotational transitions to the two-state Hamiltonian of eqn. (1) did not show noticeable couplings, and the two torsional states again behaved as independent rotors. The assignment was confirmed by observation of the ^{18}O-water dimer TM···$H_2{}^{18}O$. The derived rotational parameters are found in Table 1 and Table S33 (ESI, see attached file), with the full listing of transitions in Tables S34 and S35 (ESI, see attached file).

4. Molecular structures

The structural analysis of the monohydrates of thenyl alcohol and thenyl mercaptan used the effective (r_0) and substitution methods (r_s), described elsewhere.[6] In both cases the rotational constants, the substitution coordinates of the water oxygen atom and the derived effective structures give an unambiguous identification of the thenyl-water dimers. In the thenyl alcohol hydrate the conformational assignment immediately pointed to the predicted global minimum GG-Wa in Fig. 5, as observed by comparison between the experimental and predicted rotational constants in Tables 2 and 4. In this dimer the B3LYP-D3(BJ) predictions performed much better than MN15-L (relative deviations of 0.4-1.4% compared to 3.6-7.4%, respectively). Comparative B2PLYP and ωB97XD predictions are given in Table S42 (ESI, see attached file). This assignment is consistent with the substitution coordinates of the thenyl sulfur and water oxygen atoms in Table S37 (ESI, see attached file). An effective structure for TA···H_2O was derived by fitting three molecular parameters: the $r(H\cdots O_w)$ distance between the water oxygen and the bridging hydrogen atom, the $\angle(O\text{-}H\cdots O_w)$ linearity angle between the alcohol group and the water oxygen and the $\tau(C\text{-}O\text{-}H\cdots O_w)$ dihedral angle between the alcohol side chain and the water oxygen. The resulting fit in Table S36 (ESI, see attached file) reproduces the nine rotational constants below 1 MHz, with a root-mean-square (rms) residual

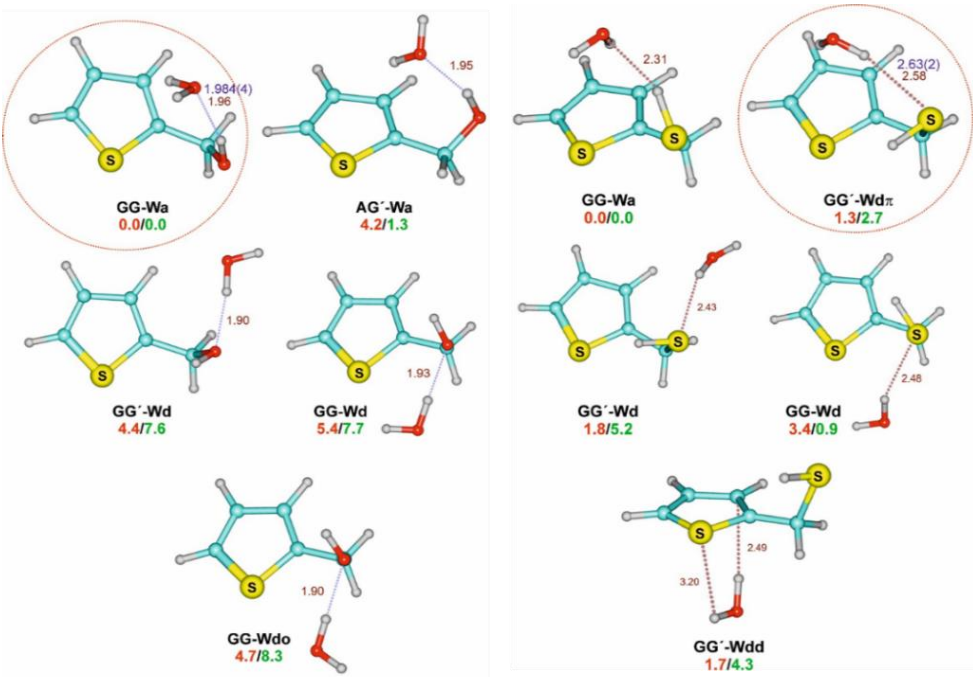

Figure 6. Conformational preferences of the thenyl mercaptan monohydrate (TM···H_2O) on the right and the thenyl alcohol monohydrate (TA···H_2O) on the left, relative Gibbs energies (kJ mol^{-1}) and hydrogen bond distances (Å, B3LYP-D3(BJ)). Isomers are labeled according to the conformation of the monomer (Figure 2) and the donor/acceptor ($W_{d/a}$) character of water. The red circles indicate the two isomers observed experimentally Energy values (in red and green) denote the B3LYP-D3(BJ) and MN15-L predictions, respectively

of 0.4 MHz. Non-fitted parameters were constrained to the B3LYP-D3(BJ) structure in Table S38 (ESI, see attached file).

Table 3. DFT predictions[c] for the dimer thenyl mercaptan monohydrate TM···H_2O

	GG-Wa	GG'-Wdπ	GG'-Wd	GG-Wd	GG-Wd
A / MHz[a]	1942.58/1919.45	1885.74/1923.67	1991.10/1915.80	2030.83/2013.83	1874.66/1892.87
B / MHz	977.68/981.78	990.07/980.92	915.11/968.76	956.48/937.22	852.91/895.10
C / MHz	864.93/865.63	844.35/852.33	677.68/704.67	706.99/721.49	750.21/800.86
D_J / kHz	0.197/0.103	0.172/0.124	0.187/0.129	0.139/0.242	0.610/0.916
D_{JK} / kHz	1.735/0.962	1.343/0.855	0.0025/1.769	0.868/0.332	-0.760/15.231
D_K / kHz	-0.137/0.0545	0.037/0.250	1.889/-0.505	0.651/1.164	14.894/-14.319
d_1 / kHz	0.015/-0.004	0.0052/-0.006	-0.058/-0.033	-0.034/-0.037	-0.256/0.012
d_2 / kHz	0.012/0.005	0.0010/0.004	-0.008/-0.030	-0.016/-0.069	-0.032/-0.048
$\|\mu_a\|$ / D	2.53/1.95	1.36/1.80	0.03/0.72	2.81/2.87	0.52/1.32
$\|\mu_b\|$ / D	1.09/2.15	3.03/2.31	0.28/0.63	1.12/0.67	2.06/1.24
$\|\mu_c\|$ / D	0.60/0.85	1.07/1.22	0.45/0.28	0.86/0.53	0.32/0.15
ΔE / kJ mol^{-1}[b]	0.00/0.00	0.06/2.66	1.99/6.93	3.37/5.95	7.14/11.17
ΔG / kJ mol^{-1}	0.00/0.00	1.27/2.65	1.79/5.22	3.37/0.90	1.68/4.33
E_B / kJ mol^{-1}	-23.10/-29.37	-24.14/-28.87	-25.44/-26.02	-21.00/-22.89	-15.36/-21.13

[a]Rotational constants (A, B, C), Watson's S-reduction centrifugal distortion constants (DJ, DJK, DK, d1, d2) and electric dipole moments (μα, α = a, b, c). [b]Relative energies corrected with the zero-point energy (ZPE), Gibbs energy (ΔG, 298K, 1 atm) and complexation energy (including BSSE corrections). [c]B3LYP-D3(BJ) and MN15-L values, respectively (basis set def2TZVP)).

Table 4. DFT predictions for the dimer thenyl alcohol monohydrate TA···H_2O

	GG-Wa	AG'-Wa	GG'-Wd	GG-Wd	GG-Wdo
A / MHz	2224.81/2118.75	2326.65/2288.30	2756.11/2635.40	2741.88/2720.89	2799.37/2721.54
B / MHz	1277.88/1331.33	1178.67/1204.17	1062.90/1092.20	1142.00/1146.75	1119.26/1152.50
C / MHz	1108.11/1191.07	1049.50/1142.67	809.05/822.05	851.03/857.78	842.44/858.43
D_J / kHz	0.5956 /0.2682	0.5736 /0.6810	0.3619/0.5402	0.5013/0.3077	0.8553/0.3692
D_{JK} / kHz	1.9458/1.1121	1.1601/0.9880	-1.4185/-2.5696	-1.2617/-0.4079	-3.2094/-0.6546
D_K / kHz	-1.0729/-0.1603	0.1530/0.4825	4.9560/7.2458	4.8963 /2.2772	7.4737/2.6473
d_1 / kHz	0.0874/-0.0222	0.0441/-0.1796	-0.1017/-0.1512	-0.1635/-0.1011	-0.2861/-0.1225
d_2 / kHz	-0.0648/0.0120	-0.0524/-0.0174	-0.0067/-0.0088	-0.0151/-0.0136	-0.0206/-0.0133
$\|\mu_a\|$ / D	2.57/2.74	1.62/1.69	0.63/0.44	3.65/3.17	1.20/0.90
$\|\mu_b\|$ / D	1.63/0.10	2.22/2.48	1.08/0.79	1.34/0.90	2.23/2.07
$\|\mu_c\|$ / D	0.21/0.62	0.02/0.29	0.36/0.55	1.43/1.49	0.29/0.45
ΔE / kJ mol^{-}	0.00/0.00	4.31/3.79	5.46/10.27	6.52/9.49	6.97/11.20
ΔG / kJ mol^{-1}	0.00/0.00	4.24/1.32	4.44/7.57	5.43/7.73	4.70/8.30
E_B / kJ mol^{-1}	-33.22/-34.56	-32.26/-34.39	-31.38/-28.83	-25.69/-24.89	-26.44/-23.77

[a]Parameter definition as in Table 3.

The identification of the thenyl mercaptan hydrate was more difficult, as more isomers are expected within a small energy range. However, the comparison of the rotational constants in Tables 1 and 3 clearly points to the second isomer GG´-Wdπ of Figure 6, identified as second most stable structure. The predicted global minimum, which was actually similar to that of TA···H_2O, was not observed, reflecting deficiencies of the DFT energetic calculations to identify the lowest-lying geometry for the weaker sulfur interaction. B3LYP-D3(BJ) and MN-15L predict the second isomer at 1.3-2.7 kJ mol-1 above the global minimum, which may be within the calculation uncertainty. Additional B2PLYP-D3(BJ) and ωB97XD in Table S43 (ESI, see attached file) suggest relative energies of 2.5-2.7 kJ mol-1. No other low-energy isomers were observed. The absence of additional isomers for $TA\cdots H_2O$ and $TA\cdots H_2O$ cannot be attributed to thermodynamic stability alone, as populations in jet experiments are affected by the pathways and energy barriers involved in conformational interconversion, making collisional relaxation a significant kinetic factor.[8]

Structurally, the prediction of rotational constants showed again better accuracy for the B3LYP-D3(BJ) method (0.2-1.3% vs 0.2-3.2 for MN15-L). The identification of isomer GG´-Wdπ was confirmed by the water oxygen substitution coordinates of Table S40 (ESI) and the effective structure of Table S41 (ESI, see attached file). For $TM\cdots H_2O$ the structural fit included the $r(H_w\cdots S)$ distance between the water hydrogen to the thiol sulfur atom, the $\angle(C\text{-}S\cdots H_w)$ orientation angle of the bridging hydrogen and the $\tau(C\text{-}C\text{-}S\cdots H_w)$ dihedral, all other parameters fixed to the B3LYP-D3(BJ) coordinates of Table S39 (ESI, see attached file). Because only two isotopologues were available for $TM\cdots H_2O$ the effective structure gives a worse reproduction of the experimental rotational constants (deviations <2.2 MHz, rms residual of 1.1 MHz) compared to $TA\cdots H_2O$.

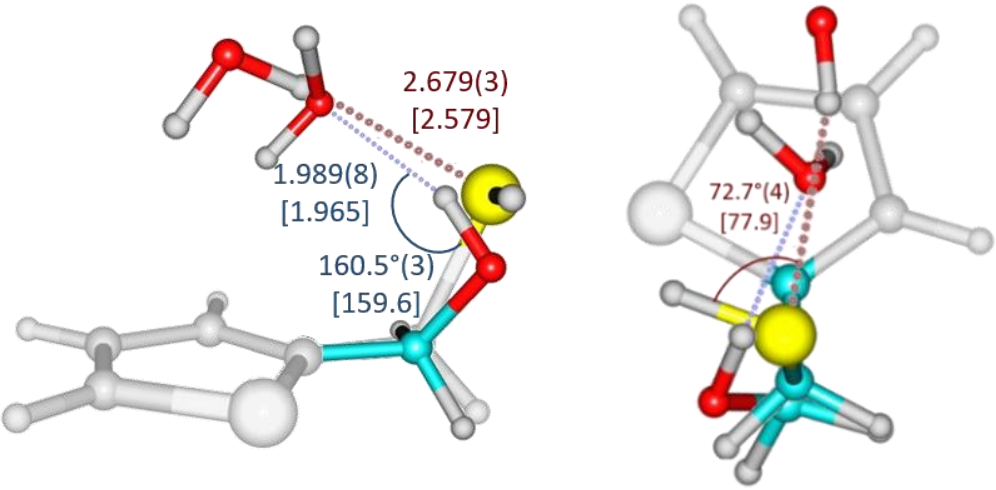

Figure 7. Hydrogen bonding in the monohydrates of thenyl mercaptan and thenyl alcohol, comparing the vibrationally-averaged effective calculated structures distances, the theoretical predictions (inside brackets), and the effective calculated structure angles of the alcohol/thiol groups respect to the hydrogen bond plane (all predictions B3LYP-D3(BJ)/def2-TZVP).

5. Non-covalent interactions

The non-covalent interactions in $TA\cdots H_2O$ and $TM\cdots H_2O$ have been analyzed structurally, energetically and using the electronic density topology. For comparison purposes Figure 8 shows the monohydrates of the two thenyl and the two furfuryl compounds of ref. 46. From a structural point of view thenyl alcohol forms a O-H···O-H bond to water, which behaves as proton acceptor (r_0: r(H···O$_w$)=1.984(4) Å, B3LYPD3(BJ): 1.965 Å). This situation is similar to furfuryl alcohol (r_0: r(H···O$_w$)=1.956(3), B3LYP-D3(BJ): 1.925 Å). However, while in the furfuryl compounds water may bind secondarily to the ring oxygen, the interaction of water with the thenyl compounds avoids the ring sulfur atom and gives priority to the interaction with the p electronic cloud through O$_w$-H···π interactions. In thenyl mercaptan there is no leading hydroxyl interaction and water is forced to behave as proton donor to the thiol group though a long O-H···S H-bond (r_0: r(H···Ow)= 2.634(18) Å, B3LYP-D3(BJ): 2.579 Å). The situation is reminiscent of the primary interaction in the furfuryl mercaptan - water cluster, where O-H ···S and S-H···O H-bonds both were detected. Interestingly, the conformation of thenyl alcohol in the monohydrate retains the most stable conformation of the monomer (GG), while in the thenyl mercaptan hydrate the monomer changes its conformation to the higher-energy structure GG´ to accommodate the O-H···S H-bond. This fact is consistent with collisionally affordable barriers for the GG⟷GG´ interconversion (Figure 3). Conformational changes induced by molecular aggregation have been occasionally reported.[9,10]

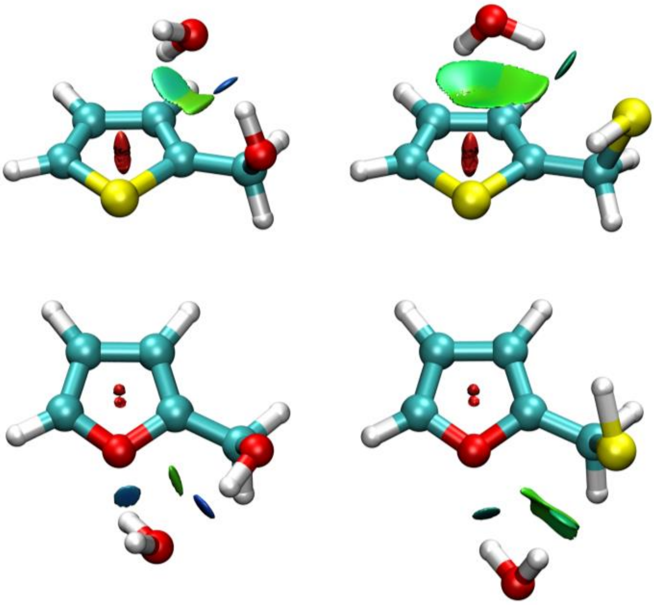

Figure 8. NCIPlot for the hydrates of thenyl alcohol and thenyl mercaptan (upper row), compared to furfuryl alcohol and furfuryl mercaptan (lower row), mapping noncovalent interactions. In this color scale blue shades indicate attractive interactions (associated to bond critical points), green colors indicate weak interactions and red represents repulsive interactions (like the ring critical points).

From the energetic point of view two aspects are noticeable. The (B3LYP-D3(BJ)) complexation energies in Tables 4-5 and Ref. 3 (relative to the monomer conformations in the complexes) are ca. 9-12 kJ mol^{-1} weaker in the thenyl compounds than in the furfuryl equivalents, following the trend: FA···H_2O (-35.0 kJ mol^{-1}) > TA···H_2O (-33.2 kJ mol^{-1}) > TM···H_2O (-24.1 kJ mol^{-1}) ~ FM···H_2O (-23.8 kJ mol^{-1}). In consequence, the absence of the alcohol group considerably decreases the magnitude of the intermolecular interactions in the dimer, reflecting the weaker H-bonds established by sulfur. Experimental binding energies for the O-H···S H-bond have been determined only for phenol···H_2S and fluorophenol···H_2S, using ZEKE photoelectron spectroscopy.[11,12] The experimental ground-state value of D_0 = -13.2(4) kJ mol^{-1} in phenol···H_2S is ca. 6% lower than our B3LYP-D3(BJ) calculations for this cluster (D_0 = -14.1 kJ mol^{-1}, De = -18.8 kJ mol^{-1}), suggesting that the computational complexation energies for the mercaptans may be larger by a similar factor. A second point concerns the contribution of dispersive interactions. All four furfuryl and thenyl monohydrates are dominantly electrostatic, as observed in Table 5 of Chapter III from a binding energy decomposition using SAPT(0)/jun-cc-pVDZ.[13,14] However, there is a considerable increase in the dispersion contribution when passing from the theny alcohol to the thenyl mercaptan hydrates, moving from 55.4% to 83.3% of the total binding energy. This increment was less notorious in the hydrates of furfuryl alcohol (43.6%) and furfuryl mercaptan (57.3-60.6%),[3] which both retain a O-H···O H-bond, absent in thenyl mercaptan. This calculation confirms the weaker and more dispersive character of the sulfur interactions in these molecules,[11,12,15–20] also observed in Table 5 for the dimers of water[21] and hydrogen sulphide.[22] A calculation on the dominantly dispersive pyridine-methane[23] dimer is given also for comparison.

Table 5. Binding energy decomposition for the hydrates of tenyl alcohol (TA) and thenyl mercaptane (TM), and comparison with the hydrates of furfuryl alcohol (FA) and furfuryl mercaptan (FM), the dimers of H_2O and H_2S and the pyridine-methane dimer. The interaction energy is decomposed into electrostatic (ΔE_{elec}), inductive (multipole interactions/charge transfer, ΔE_{ind}), exchange repulsion (ΔE_{exch}) and dispersion (ΔE_{disp}) energy terms, using SAPT(0)/jun-cc-pVDZ (all values in kJ mol^{-1}). See Tables 1-2 for a comparison of complexation energies for TA···H_2O and TM···H_2O using DFT.

	$\Delta E_{\text{Electrostatic}}$	$\Delta E_{\text{Induction}}$	$\Delta E_{\text{Dispersion}}$	$\Delta E_{\text{Exchange}}$	ΔE_{Total}
TM···H_2O – GG'-Wdπ[b]	-27.1 [154.4%][f]	-8.0	-14.7 [83.3%]	32.2	-14.3
TA···H_2O – GG-Wa[b]	-52.0 [179.9%]	-15.0	-15.9 [55.4%]	54.1	-25.4
FM···H_2O – GG´-W_{da}[a]	-41.8 [196.2%]	-12.4	-12.9 [60.6%]	45.8	-21.3
FM···H_2O – GG-W_{dd}[a]	-35.3 [171.4%]	-7.0	-11.8 [57.3%]	33.5	-20.6
FA···H_2O – GG´-W_{da}[a]	-61.3 [183.0%]	-17.7	-14.6 [43.6%]	60.1	-33.4
$(H_2O)_2$[c]	-37.0 [169.7%]	-9.0	-5.3 [24.3%]	29.4	-21.8
$(H_2S)_2$[e]	-12.9 [286.7%]	-4.4	-5.2 [115.6%]	18.0	-4.5
Pyridine-methane[d]	-17.9 [100.6%]	-4.1	-42.0[236%]	46.1	-17.8

[a]Ref.3. [b]This work. [c]Ref.21. [d]Ref.23. [e]Ref.22. [f]Percentage of the total binding energy.

Non-covalent interactions have been analyzed also using NCIPlot electronic density mapping.[24,25] This method evaluates a reduced electronic density gradient $s \left(= \frac{1}{1(3\pi^2)^{1/3}} \frac{|\nabla \rho|}{\rho^{4/3}}\right)$ *versus* a signed electronic density (sign $(\lambda_2)\rho$) using the second eigenvalue (λ_2) of the electron density Hessian. The NCIPlots in Figure 8 and Figure S1 (ESI) compare the four furfuryl and thenyl hydrates, revealing well-defined O-H···O H-bond regions (associated to bond critical points), together with weaker interactions associated to the O-H···S H-bond and, finally, broad surfaces of weak interactions between the water molecule and the π ring, most notorious in thenyl mercaptan. The NCIPlot analysis thus confirms the presence of multiple interactions in the hydrates and the gradation of attractive interactions on passing from oxygen to sulfur in these five-membered ring molecules.

6. Conclusion

The combination of jet-cooled (chirped-pulsed) broadband rotational spectroscopy,[26,27] molecular orbital calculations,[28–32] binding energy decomposition[2,66] and electronic density topological analysis[14] provided a comprehensive description of the non-covalent interactions in the monohydrates of thenyl alcohol and thenyl mercaptan, simultaneously emphasizing the role of gas-phase intermolecular clusters as functional and size-specific models of molecular aggregation.

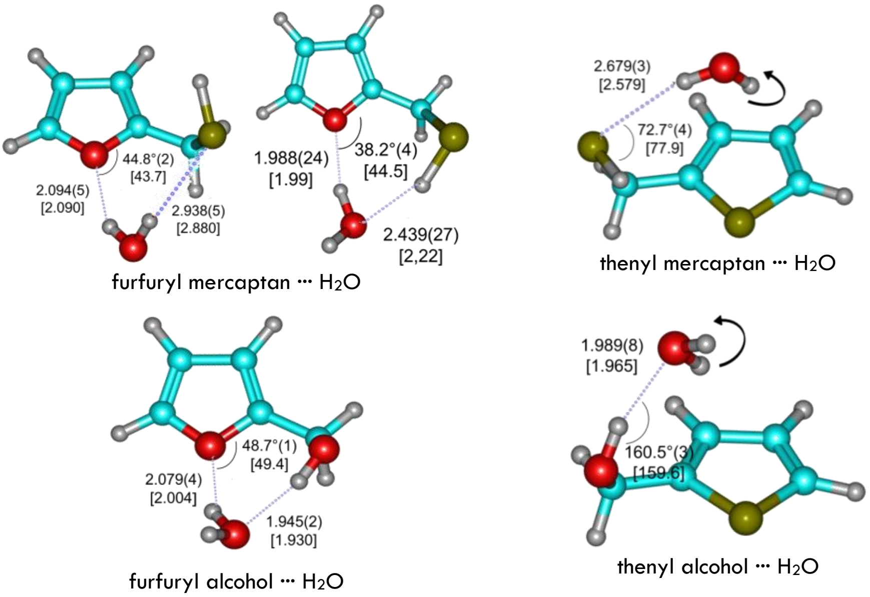

furfuryl mercaptan ··· H_2O

thenyl mercaptan ··· H_2O

furfuryl alcohol ··· H_2O

thenyl alcohol ··· H_2O

Figure 9. Different conformational preferences between the monohydrates of furfuryl (mercaptan and alcohol) on the left and thenyl (mercaptan and alcohol) on the right.

The molecular data on the two thenyl hydrates and the previous analysis of furfuryl alcohol and furfuryl mercaptan[3] allowed a comparative study in which the oxygen atoms were successively replaced by one or two sulfur atoms, offering quantitative information on the decrease in binding energy, increment of the role of dispersion interactions and structural rearrangement associated to the loss of the strong O-H···O hydroxyl to water H-bond. In addition, the presence of a thenyl group instead of the furfuryl ring prevented the interactions of water to the ring heteroatom, resulting in a floppy character of the two thenyl hydrates, where water retains the capacity to engage in large-amplitude internal motions, as revealed by the torsional tunneling splittings in the rotational spectra. The nature of hydrogen bonding to sulfur centers and other low-electronegativity atoms,[15,16,33] together with the correlation between weaker interactions and increased isomerism and intramolecular large-amplitude motions,[34] remains a topic still under-investigated, calling for additional high-resolution molecular studies.

Finally, the importance of accurate DFT dispersion models for the description of weakly-bound complexes should be stressed. As illustration, the worse behavior of the MN15-L functional in the present study may suggest the need to introduce explicit long-range dispersion corrections in the Minnesota functionals.[35] This fact illustrates the contribution and complementary role of empirical data from high-resolution rotational data for the development of DFT computational models of molecular aggregation.

Chapter V. References:

1. Contreras-García, J. *et al.* NCIPLOT: A Program for Plotting Noncovalent Interaction Regions. *J. Chem. Theory Comput.* **7**, 625–632 (2011).

2. Garcia, J., Podeszwa, R. & Szalewicz, K. SAPT codes for calculations of intermolecular interaction energies. *J. Chem. Phys.* **152**, 184109 (2020).

3. Juanes, M. *et al.* Sulfur Hydrogen Bonding in Isolated Monohydrates: Furfuryl Mercaptan versus Furfuryl Alcohol. *Chem. - A Eur. J.* **24**, 6564–6571 (2018).

4. Watson, J. K. G. Vibrational Spectra and Structure. in (ed. Durig, J. R.) 1–89 (Elsevier Inc., 1977).

5. Pickett, H. M. The fitting and prediction of vibration-rotation spectra with spin interactions. *J. Mol. Spectrosc.* **148**, 371–377 (1991).

6. Rudolph, H. D. & Demaison, J. Equilibrium Molecular Structures: From Spectroscopy to Quantum Chemistry. in *Equilibrium Molecular Structures: From Spectroscopy to Quantum Chemistry* (eds. Demaison, J., Boggs, J. E. & Császár, A. G.) 125–158 (CRC Press, 2011).

7. MOMSTRUC Structural Package.

8. Godfrey, P. D., Rodgers, F. M. & Brown, R. D. Theory versus Experiment in Jet Spectroscopy: Glycolic Acid. *J. Am. Chem. Soc.* **119**, 2232–2239 (1997).

9. Thomas, J., Seifert, N. A., Jäger, W. & Xu, Y. A Direct Link from the Gas to the Condensed Phase: A Rotational Spectroscopic Study of 2,2,2-Trifluoroethanol Trimers. *Angew. Chemie Int. Ed.* **56**, 6289–6293 (2017).

10. Oswald, S. *et al.* The Chiral Trimer and a Metastable Chiral Dimer of Achiral Hexafluoroisopropanol: A Multi- Messenger Study. *Angew. Chemie Int. Ed.* **58**, 5080–5084 (2019).

11. Ghosh, S., Bhattacharyya, S. & Wategaonkar, S. Dissociation Energies of Sulfur-Centered Hydrogen-Bonded Complexes. *J. Phys. Chem. A* **119**, 10863–10870 (2015).

12. Bhattacharyya, S. & Wategaonkar, S. ZEKE Photoelectron Spectroscopy of p -Fluorophenol···H 2 S/H 2 O Complexes and Dissociation Energy Measurement Using the Birge–Sponer Extrapolation Method. *J. Phys. Chem. A* **118**, 9386–9396 (2014).

13. Scheiner, S. *Hydrogen Bonding. A Theoretical Perspective*. (Oxford University Press, 1997).

14. Jeziorski, B., Moszynski, R. & Szalewicz, K. Perturbation Theory Approach to Intermolecular Potential Energy Surfaces of van der Waals Complexes. *Chem. Rev.* **94**, 1887–1930 (1994).

15. Biswal, H. S. Hydrogen Bonding Involving Sulfur: New Insights from Ab Initio Calculations and Gas Phase Laser Spectroscopy. in *Noncovalent Forces* (ed. Scheiner, S.) (Springer Int. Pub., 2015).

16. Biswal, H. S., Bhattacharyya, S., Bhattacherjee, A. & Wategaonkar, S. Nature and strength of sulfur-centred hydrogen bonds: laser spectroscopic investigations in the gas phase and quantum-chemical calculations. *Int. Rev. Phys. Chem.* **34**, 99–160 (2015).

17. Goebel, J. R., Ault, B. S. & Del Bene, J. E. Matrix Isolation and ab Initio Study of 1:1 Hydrogen-Bonded Complexes of H 2 O 2 with Phosphorus and Sulfur Bases. *J. Phys. Chem. A* **105**, 11365–11370 (2001).

18. Wierzejewska, M. Infrared matrix isolation studies of complexes formed between dimethylsulfide, dimethyldisulfide and nitrous acid. *J. Mol. Struct.* **520**, 199–214 (2000).

19. Wang, D., Chopra, P., Wategaonkar, S. & Fujii, A. Electronic and Infrared Spectroscopy of Benzene-(H 2 S) n (n = 1 and 2): The Prototype of the SH-π Interaction. *J. Phys. Chem. A* **123**, 7255–7260

(2019).

20. Wategaonkar, S. & Bhattacherjee, A. N–H···S Interaction Continues To Be an Enigma: Experimental and Computational Investigations of Hydrogen-Bonded Complexes of Benzimidazole with Thioethers. *J. Phys. Chem. A* **122**, 4313–4321 (2018).

21. Dyke, T. R., Mack, K. M. & Muenter, J. S. The structure of water dimer from molecular beam electric resonance spectroscopy. *J. Chem. Phys.* **66**, 498–510 (1977).

22. Das, A. *et al.* The H2S Dimer is Hydrogen- Bonded: Direct Confirmation from Microwave Spectroscopy. *Angew. Chemie Int. Ed.* **57**, 15199–15203 (2018).

23. Gou, Q. *et al.* Interactions between alkanes and aromatic molecules: a rotational study of pyridine–methane. *Phys. Chem. Chem. Phys.* **16**, 13041–13046 (2014).

24. Laplaza, R. *et al.* NCIPLOT and the analysis of noncovalent interactions using the reduced density gradient. *WIREs Comput. Mol. Sci.* **11**, (2021).

25. Lane, J. R., Contreras-García, J., Piquemal, J.-P., Miller, B. J. & Kjaergaard, H. G. Are Bond Critical Points Really Critical for Hydrogen Bonding? *J. Chem. Theory Comput.* **9**, 3263–3266 (2013).

26. Caminati, W. & Grabow, J.-U. Advancements in Microwave Spectroscopy. in *Frontiers and Advancements in Microwave Spectroscopy* (ed. Laane, J.) 569–598 (Elsevier, 2018).

27. Juanes, M., Saragi, R. T., Caminati, W. & Lesarri, A. The Hydrogen Bond and Beyond: Perspectives for Rotational Investigations of Non-Covalent Interactions. *Chem. - A Eur. J.* **25**, (2019).

28. Raghavachari, K. Perspective on 'Density functional thermochemistry. III. The role of exact exchange'. *Theor. Chem. Accounts Theory, Comput. Model. (Theoretica Chim. Acta)* **103**, 361–363 (2000).

29. Yu, H. S., He, X. & Truhlar, D. G. MN15-L: A New Local Exchange-Correlation Functional for Kohn–Sham Density Functional Theory with Broad Accuracy for Atoms, Molecules, and Solids. *J. Chem. Theory Comput.* **12**, 1280–1293 (2016).

30. Weigend, F. & Ahlrichs, R. Balanced basis sets of split valence, triple zeta valence and quadruple zeta valence quality for H to Rn: Design and assessment of accuracy. *Phys. Chem. Chem. Phys.* **7**, 3297 (2005).

31. Grimme, S., Ehrlich, S. & Goerigk, L. Effect of the damping function in dispersion corrected density functional theory. *J. Comput. Chem.* **32**, 1456–1465 (2011).

32. Johnson, E. R. & Becke, A. D. A post-Hartree-Fock model of intermolecular interactions: Inclusion of higher-order corrections. *J. Chem. Phys.* **124**, 174104 (2006).

33. Gilli, G. & Gilli, P. *The Nature of the Hydrogen Bond*. (2009).

34. Pérez, C. *et al.* Isomerism of the Aniline Trimer. *Angew. Chemie Int. Ed.* **57**, 15112–15116 (2018).

35. Goerigk, L. *et al.* A look at the density functional theory zoo with the advanced GMTKN55 database for general main group thermochemistry, kinetics and noncovalent interactions. *Phys. Chem. Chem. Phys.* **19**, 32184–32215 (2017).

Chapter VI

DIMERIZATION OF FURFURYL AND THENYL COMPOUNDS:

(Furfuryl Alcohol)$_2$* and (Thenyl Alcohol)$_2$*

Adapted from:

(*): M. Juanes, R. T. Saragi, C. Pérez, R. Pinacho, M. Jaraíz and A. Lesarri, *Symmetry*, **2021**, *submitted.*

(The Electronic Supporting Information – ESI, can be found in the document: thesis-ESI.pdf)

I. Introduction

The data presented in Chapter IV and Chapter V of this thesis is based on the study of the monohydrates of furfuryl mercaptan, furfuryl alcohol, thenyl mercaptan and thenyl alcohol molecules (FM ··· H_2O, FA ··· H_2O, TM ··· H_2O and TA ··· H_2O). In order to continue the same line of research and with the aim to conclude the study and comparison of the structural influence of the Oxygen or the Sulfur over similar five membered ring complexes, here we present a further analysis of the homodimers of two of those molecules previously studied: Furfuryl-Alcohol$_2$ (FA_2) and Thenyl-Alcohol$_2$ (TA_2), generated in the jet.

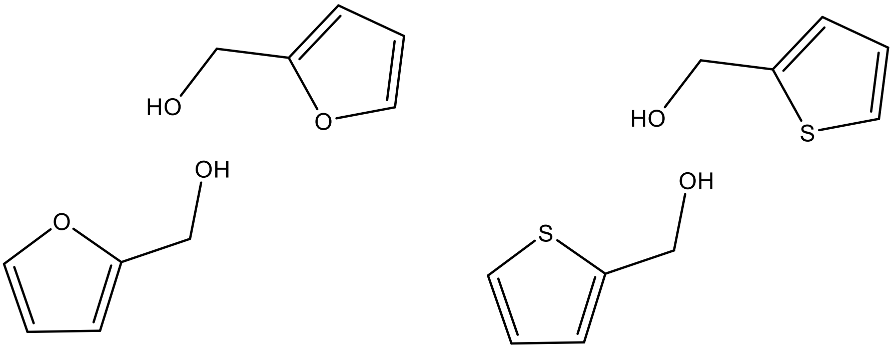

Figure 1. Molecular formulas of the homodimers analysed in this chapter, (Furfuryl alcohol)$_2$ on the left and (thenyl alcohol)$_2$ on the right.

Chirality recognition, defined as the noncovalent chemical interactions by which a chiral molecule (receptor/host) recognizes a specific stereoisomer (substrate/guest), remains at the core of the physical mechanisms supporting life and supramolecular Chemistry. Most of the experimental information on molecular recognition originates from condensed phases.[1,2] Alternatively, gas-phase experiments offer high-resolution,[3,4] cancelation of matrix effects,[5] direct comparison with single-molecule quantum mechanical calculations[6,7] and accurate description of noncovalent forces, necessary for future extrapolation from the molecular scale to the meso- and nano-phases.[8,9] Gas-phase studies mimic molecular interactions with mass-selected intermolecular complexes designed for specific noncovalent host–guest interactions, typically hydrogen bonds[10] and other weak bridging interactions, like those involving s-/p-holes, p clouds and others.[11,12]

In this context, the recognition between molecules with transient chirality offers particular interest, as it converts indistinguishable enantiomeric monomer species into resolvable diastereomeric dimers,[13–15] quenching the stereomutation barriers and revealing the magnitude of the weak multi-contact interactions associated to the asymmetric force balance in the homo and heterochiral species.[3,4] Transient chirality originates from low stereomutation barriers, like the weak torsional barriers[16] where axial enantiomers tunnel between two mirror-image conformations. This phenomenon is designated as atropisomerism[17,18] for larger torsional barriers. Most of gas-phase experiments on transient chirality synchronization used rotational or vibrational spectroscopy, but mostly restricted to alcohols (ethanol,[19–21] 2-propanol,[22] 2-

butanol[23], glicidol[24], cyclohexanol,[25] cyclohexylmethanol,[26] benzyl alcohol[26,27]) and fluoroalcohols (2-fluoroethanol[28], trifluoroethanol[29,30], hexafluoroisopropanol[31]), because of the relatively strong (and IR-intense) O-H···O hydrogen bond. A few ethers[16,32,33] and thiol homodimers[34,35] have also been studied recently. The torsional barriers in alcohols are all quite low (3.35 kJ mol^{-1} in benzyl alcohol,[36] 4.51 kJ mol^{-1} in cyclohexanol[37]), with associated interconversion half-lifetimes in the ns range. Additional experiments with molecules of larger torsional barriers could eventually freeze the two enantiomers within near-isolated potential wells, illustrating the evolution from transient to conventional (kinetically inert) permanent stereocenters. The investigation of stereochemical lability for different stereomutation regimes thus adds molecular information on chiral recognition not restricted to conventional tetrahedral stereogenic centers. Atropisomerism has also been recently recognized as an influential factor for biological compounds and drug development.[38,39]

We report here a rotational investigation on chiral recognition and dimerization of the molecules of furfuryl alcohol and thenyl alcohol (Figure1) using broadband (chirped-pulsed) microwave spectroscopy.[40] Both molecules offer competing binding sites for dimerization and hydrogen bonding, including the hydroxymethyl sidechain, an aromatic five-membered π system and sulfur or oxygen ring heteroatoms. The molecules adopt two preferent mirror gauche orientations of the sidechain, which conceivably would require moderate torsional barriers for interconversion by a ca.n180° rotation of the aromatic ring. The larger barriers respect to the alcohol torsion, despite still categorized as rapidly equilibrating mixtures (Class I: < 80 kJ mol^{-1}) by LaPlante,[41] make these systems interesting to examine the preferences for homo- or heterochiral aggregation and to evaluate their energetic difference, or chirodiastaltic energy.[42–44] At the same time, the comparison between the noncovalent interactions from the sulfur and oxygen atoms in the furfuryl and thenyl groups will add empirical information on sulfur-centered hydrogen bonds, scarcely investigated.[45] This investigation is part of an on-going research on sulfur compounds and was possible only after examining the rotational spectrum of the monomers and their monohydrated species.[46,47]

II. Furfuryl alcohol and Thenyl alcohol homodimers

1. Experimental set up:

As in previous studies carried out in Chapters IV and V, the samples, furfuryl alcohol (FA) and thenyl alcohol (TA), were obtained commercially and used without further purification. Both FA and TA molecules were measured again with some experimental conditions modifications (specially the heating temperatures of the molecules). In both cases we significantly increase the temperature compared with previous experiments (85°C and 75°C respectively) observing the emergence of new groups of spectral lines compared with those of previous experiments. The expanding jet was probed with a broadband chirped-pulsed Fourier transform microwave (CP-FTMW) spectrometer[48–50] defined in Chapter I working in the 2-8GHz frequency region.

	(Furfuryl Alcohol)$_2$	(Thenyl Alcohol)$_2$
Carrier Gas	Ne	Ne
Nozzle Ø (mm)	0.8	0.8
Sample T^a	85°C	75°C
Carrier Gas Pressure	2.5 bar	2.5 bar

2. Computational methods

The experiment was supplemented with several theoretical calculations. A first conformational search used molecular mechanics (MMFF[51]) to generate a dataset of initial structures. In a later stage Grimme's conformer–rotamer ensemble sampling tool (CREST[52]) was used to search for additional structures. All starting geometries were reoptimized using density-functional theory °°(DFT) and ab initio methods. Following different tests, we are reporting exclusively the results with the B3LYP hybrid and B2PLYP[53] double-hybrid methods and D3 empirical dispersion terms (Becke-Johnson damping function),[54] which appeared more satisfactory. A polarized triple-zeta Ahlrichs' basis set def2-TZVP[55] was used in all cases and were implemented in Gaussian 16[56] and ORCA.[57] The vibrational frequency calculations used the harmonic approximation at the same level of theory. Basis set superposition errors (BSSE) in the complexation energies used the counterpoise approximation.[58] The energy decomposition used symmetry adapted perturbation theory (SAPT[59]), implemented in PSI4.[60] Finally, the analysis of non-covalent interactions used a reduced gradient of the electronic density, included in NCIPlot.[61]

3. Conformational landscape

The monomers of furfuryl alcohol and thenyl alcohol have been discussed separately in Chapters IV and V. Comparing both, we can observe how they display a two-dimensional

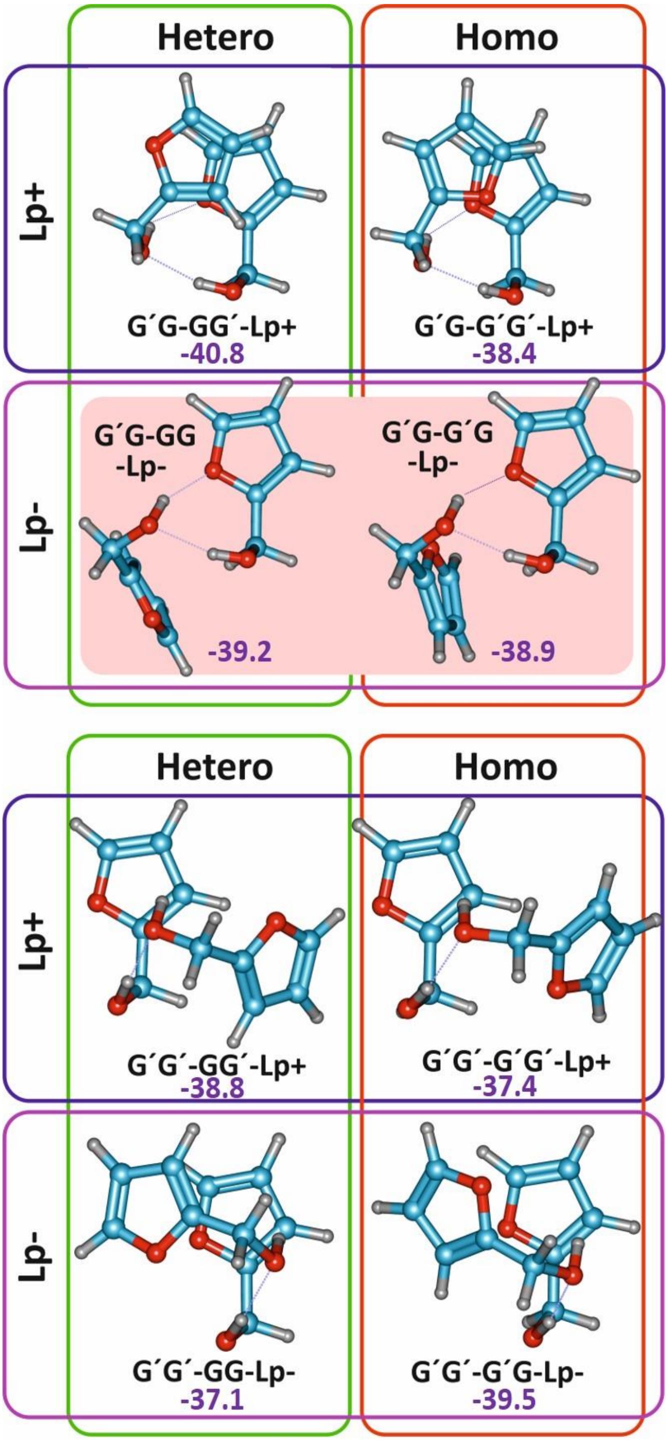
Hetero
Homo
Lp+
Lp-
G´G-GG´-Lp+
-40.8
G´G-G´G´-Lp+
-38.4
G´G-GG
-Lp-
-39.2
G´G-G´G
-Lp-
-38.9
Hetero
Homo
Lp+
Lp-
G´G´-GG´-Lp+
-38.8
G´G´-G´G´-Lp+
-37.4
G´G´-GG-Lp-
-37.1
G´G´-G´G-Lp-
-39.5

Figure 2. Conformational search for the furfuryl alcohol dimer (complexation energies in purple, B2PLYP/def2-TZVP).

potential energy surface characterized by two dihedrals defining the elevation and position of the alcohol group (τ_1(OCα-C2O/S) and τ_2(HO-CαC2)).[46,47] The two molecules share a synclinal (*gauche*) orientation of the hydroxymethyl sidechain ($\tau_1 \sim \pm 60$-$70°$, denoted G or G´ attending to the torsion sign), but differ in the orientation of the terminal alcohol hydrogen atom. In furfuryl alcohol the terminal hydrogen points to the ring and suggest an intramolecular O-H···O hydrogen bond ($\tau_2 \sim \mp 58°$), or GG´ conformation (index notation $\tau_1\tau_2$). Reflection through the ring plane produces the enantiomeric G´G conformation. Conversely, thenyl alcohol orients the hydroxyl group to the adjacent carbon-carbon bond in the π ring system to establish a O-H···π interaction ($\tau_2 \sim \pm 50°$), resulting in the GG conformation or its G´G´ enantiomer.

The presence of enantiomeric pairs in the monomers anticipates the plausible formation of homochiral (i.e., GG´-GG´ in furfuryl alcohol, proton donor denoted first) or heterochiral dimers (i.e., GG´-G´G) for each molecule. For each case two enantiomers with identical scalar properties would be expected for conventional stereocenters (i.e., GG´-GG´=G´G-G´G and GG´-G´G=G´G-GG´). However, we soon noticed in the conformational search that the torsional adaptability of the sidechain occasionally renders additional stereoisomers for the dimers. In particular, monomers with anticlinal (A) orientations of the side chain were predicted at low energies, competing with the synclinal isomers. Moreover, the presence of two diastereotopic acceptor lone pairs (Lp+/-, according to the dihedral LpO-CαC2) and the multiple possibilities for interaction between the polar alcohol groups and the two ring molecules further complicate the conformational space and suggest a shallow potential energy surface.

For the furfuryl alcohol dimer the B3LYP-D3(BJ) method was sufficient to characterize the main structural features and the approximate conformational order. The initial MM conformational screening produced 60 isomers within an energy window of ca. 25 kJ mol^{-1}, later updated with CREST. Additional chemical and symmetry arguments were used to include additional isomers which were not recovered in the automated search, which were later reoptimized with DFT. The eight most representative isomers are collected in Figure 2 and Tables 1 and S5-S6 (ESI), limited to relative energies below ca. 4 kJ mol^{-1}. Because of the close relative energies, the global minimum could not be univocally specified, but the most stable structures exhibit hinged geometries which swing the two rings around a primary O-H···O hydrogen bond axis. The alcohol group in the proton acceptor then establishes a second cooperative O-H···O$_r$ hydrogen bond to the ring oxygen (O$_r$), closing a seven membered-ring. Additional C(sp^3)-H···π interactions finally determine the tilting between the two rings. Since both homo/heterochiral and Lp+/- geometries are possible, the four isomers of Figure 2 may be conceived, with the two monomers respecting the preferred synclinal (G) sidechain.

A second structural family in Figure 2 present also a hinged O-H···O hydrogen bond, complemented with a second O-H···π hydrogen bond to the opposite ring. These interactions may be supplemented by weak C(sp^2)-H···π contacts between the two rings and similarly offer four alternative homo-/heterochiral and Lp+/Lp- geometries. Other structures sharing the O-H···O hydrogen bond and a different anticlinal sidechain in the proton donor are illustrated in Figure S3 (ESI). Interestingly, no stacking or symmetric structures were observed for low-lying isomers. The first (C_i) symmetric structure in Figure S4 (ESI) has an electronic energy of ca. 9 kJ mol^{-1}. Once the conformation preferences were stablished, additional B2PLYP-D3(BJ) reoptimizations were completed for the low-lying isomers in Table S6 (ESI)

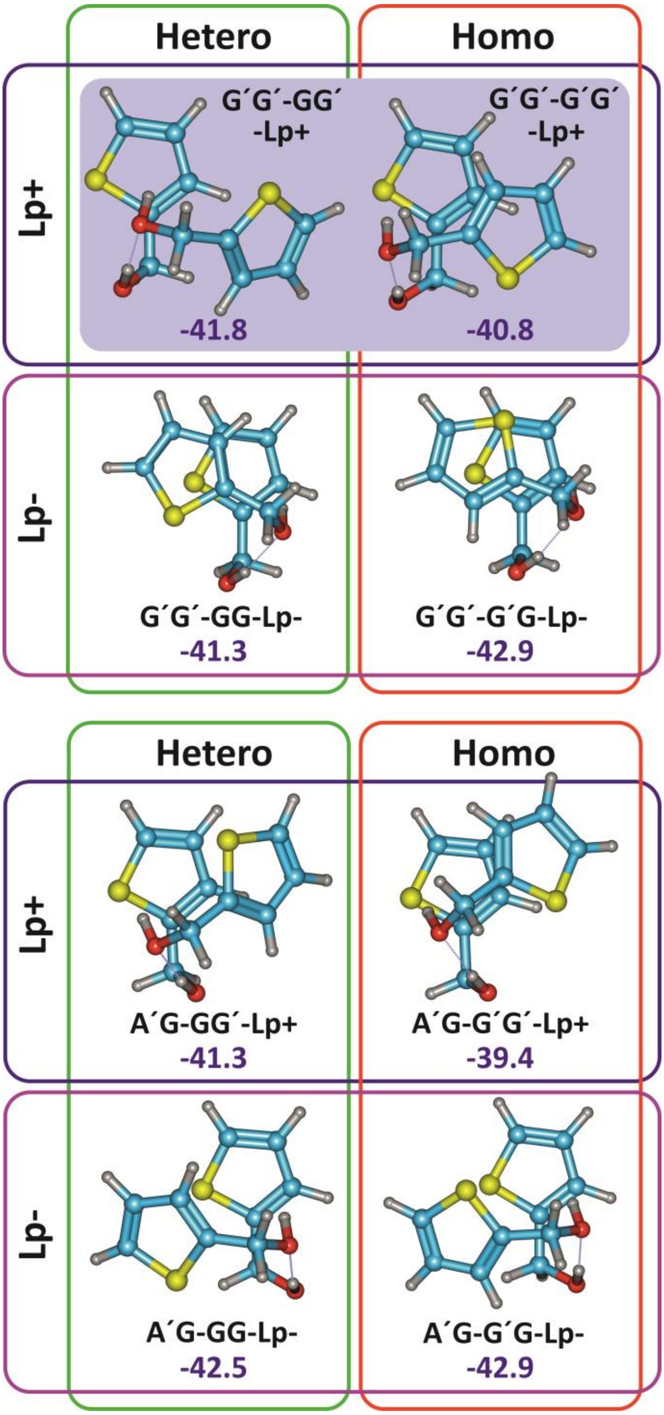
Hetero
Homo
Lp+
G´G´-GG´
-Lp+
-41.8
G´G´-G´G´
-Lp+
-40.8
Lp-
G´G´-GG-Lp-
-41.3
G´G´-G´G-Lp-
-42.9
Hetero
Homo
Lp+
A´G-GG´-Lp+
-41.3
A´G-G´G´-Lp+
-39.4
Lp-
A´G-GG-Lp-
-42.5
A´G-G´G-Lp-
-42.9

Figure 3. Conformational search for the thenyl alcohol dimer (complexation energies in purple, B2PLYP/def2-TZVP).

Table 1. Experimental rotational parameters of the dimer of furfuryl alcohol

	EXPERIMENTAL		THEORY	
	Homociral G´G-G´G-Lp-	Heterochiral G´G-GG-Lp-	G´G-G´G-Lp-	G´G-GG-Lp-
A / MHz[a]	1054.71641(47) [e]	1096.59893(71)	1055.02	1096.27
B / MHz	436.11244(22)	414.49672(44)	443.70	421.88
C / MHz	419.35674(23)	400.89791(55)	427.77	409.86
D_J / kHz	0.2218(14)	0.1640(33)	0.198	0.159
D_{JK} / kHz	-0.7835(41)	-0.6516(78)	-0.676	-0.667
D_K / kHz	1.586(10)	1.749(26)	1.461	1.692
d_1 / kHz	0.03884(46)	0.0162(13)	-0.029	0.018
d_2 / kHz	[0.] [e]	-0.00155(25)	0.002	-0.002
$\lvert\mu_a\rvert$ / D	++	-	0.9	0.1
$\lvert\mu_b\rvert$ / D	+++	-	2.6	0.3
$\lvert\mu_c\rvert$ / D	++	++	1.3	3.8
N[b]	202	87		
σ / kHz	12.6	13.1		
ΔE / kJ mol^{-1}[c]			0.7	2.2
ΔG / kJ mol^{-1}			0.1	2.1
E_C / kJ mol^{-1}			-38.9	-39.2

[a]Rotational constants (A, B, C), Watson's S-reduction centrifugal distortion constants (D_J, D_{JK}, D_K, d_1, d_2) and electric dipole moments (μ_α, α = a, b, c). [b]Number of measured transitions (N) and standard deviation of the fit (s). [c]Relative energies corrected with the zero-point energy (ZPE), Gibbs energy (ΔG, 298K, 1 atm) and complexation energy (including BSSE corrections) using B2PLYP-D3(BJ) and the basis set def2-TZVP. [d]Standard errors in parentheses in units of the last digit. [e]Values in square brackets were fixed to zero.

Table 2. Experimental rotational parameters of the dimer of thenyl alcohol

	EXPERIMENTAL		THEORY	
	Homociral G´G-G´G-Lp-	Heterochiral G´G-GG-Lp-	G´G´-G´G´-Lp+	G´G´-GG´-Lp+
A / MHz[a]	813.40958(30)	824.07911(75)	829.55	859.03
B / MHz	394.62969(16)	382.68442(25)	393.18	358.74
C / MHz	354.53843(17)	348.11932(24)	357.42	329.32
D_J / kHz	0.16796(66)	0.1066(11)	0.241	0.517
D_{JK} / kHz	-0.4034(19)	-0.1297(46)	-0.712	1.312
D_K / kHz	0.5508(32)	0.272(34)	0.912	-1.612
d_1 / kHz	-0.00001353(29)	-0.00658(77)	-0.045	-0.128
d_2 / kHz	[0.]	[0].	-0.003	-0.005
$\lvert\mu_a\rvert$ / D	++	++	2.1	2.1
$\lvert\mu_b\rvert$ / D	+++	++	3.7	2.6
$\lvert\mu_c\rvert$ / D			0.1	0.4
N	266	138		
σ / kHz	12.5	10.3		
ΔE / kJ mol^{-1}			0.4	1.6
ΔG / kJ mol^{-1}			1.1	0.0
E_C / kJ mol^{-1}			-40.8	-41.8

[a]Parameter definition as in Table 1.

For the thenyl alcohol dimer the initial MM conformational search produced 64 isomers within 25 kJ mol^{-1}, later reinvestigated with CREST. However, DFT reoptimization was more difficult and a proper geometry convergence depended on the computational method, as discussed below. Three main structural patterns were detected for the thenyl compound, characterized by the absence of any O-H···S hydrogen bond involving the alcohol and the ring heteroatom. For this reason, the counterparts of the four most stable species of (furfuryl alcohol)$_2$ were not found here. On the other hand, the preferred thenyl dimers in Figure 3 and Tables 2 and S7-S8 (ESI), showed resemblance with the second family of furfuryl dimers, presenting hinged tilted geometries based in the primary O-H···O hydrogen bond axis, together with secondary O-H···π alcohol interactions to the π ring. This motif offers four homo/heterochiral and Lp+/- variations, with the two monomers in the preferred synclinal (G) sidechain. Additional geometries in which the donor hydrogen bond adopts an anticlinal orientation on complexation were also predicted, for which other four (homo/heterochiral and Lp+/-) geometries in Figure 3 are possible. Alternative parallel-displaced stacking geometries were predicted at relatively small energies (~3.5 kJ mol^{-1}), in which the two homo/heterochiral rings align the C2-Cα bonds (Figure S5, ESI), either with synclinal-synclinal or synclinal-anticlinal orientations. The only low-energy symmetric dimer presented a C_2 point group (Figure S6, ESI) and electronic energies of ca. 4 kJ mol^{-1}.

4. Rotational Spectrum

The jet-cooled microwave spectra of furfuryl alcohol and thenyl alcohol and selected rotational transitions are illustrated in Figures 4 and 5. The identification of the monomers and the monohydrated dimers was straightforward in both molecules, as they were previously reported.[46,47] The search for the dimers started from the predictions in Tables S5-S8 (ESI) and proceeded iteratively. For the furfuryl alcohol dimer two different asymmetric rotor spectra were assigned. A first more intense spectrum displayed all three selections rules, composed of *R*- ($J+1 \leftarrow J$) and Q ($J \leftarrow J$) branch transitions (intensities $\mu_b > \mu_a \sim \mu_c$). The large number of (over two hundred) transitions permitted the determination of all rotational constants and quartic centrifugal distortion parameters, using a conventional semi-rigid rotor Watson's (S-reduced) Hamiltonian.[62] Later, a second isomer with only μ_c-selection rules made of (over eighty) *R*- and Q-branch transitions was measured and analysed with the same Hamiltonian. For thenyl alcohol we also identified the spectra of two semi-rigid asymmetric rotors, corresponding to two distinct isomers. As in furfuryl alcohol the largest spectral dataset (273 transitions) was dominated by μ_b *R*- and Q-branch transitions ($\mu_b > \mu_a \sim \mu_c$). The second isomer (138 transitions) presented a majority of ^aR- and ^bR-transitions ($\mu_a \sim \mu_b$). The final spectroscopic parameters of the dimers of furfuryl alcohol and thenyl alcohol are shown in Tables 1 and 2, respectively, while the measured rotational transitions are collected in Tables S9-S12 (ESI).

Characteristically, the two isomers of each dimer showed very similar rotational constants (i.e, a difference below 12 MHz for thenyl alcohol or 42 MHz for furfuryl alcohol). This fact suggested close molecular geometries for the two species of each dimer, probably sharing the most important structural characteristics. A comparison of the rotational parameters with the computations then assured the conformational assignment. For the furfuryl alcohol dimers two homo and heterochiral isomers in Figure 2 were readily assigned to the experimental rotational constants, differing only in the chirality of the proton acceptor (G´G-GG-Lp- and G´G-G´G-Lp-). In both cases the agreement between predictions and experiment was very satisfactory

(<2.2 %). However, for the thenyl alcohol dimer the situation was more difficult. Initially, only a single heterochiral isomer (G´G´-GG´-Lp+) could be assigned to the experiment, but the second experimental partner could not be matched with any of the B3LYP-D3(BJ) predictions.

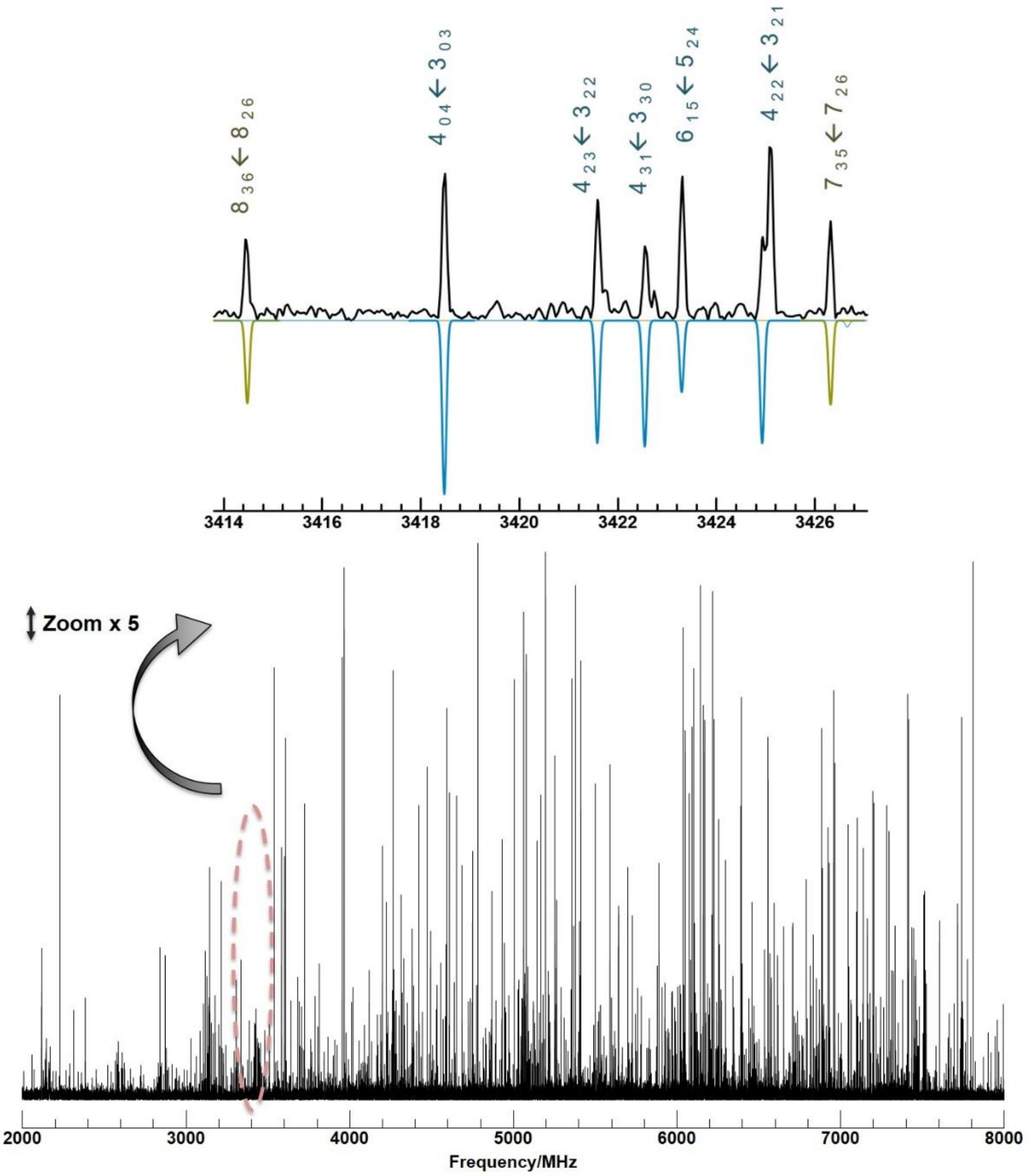

Figure 4. At the bottom, Microwave spectrum of the dimer furfuryl alcohol at 85°C in the 2-8 GHz region. At the top of the image, illustrative rotational transitions of the (furfuryl alcohol)$_2$ isomer G'G-GG-Lp- (marked in blue) and isomer G'G-G'G-Lp- (marked in green). *NOTE: *in the lower part of the figure, the lines corresponding to the rotational transitions of the monomer have been subtracted from the spectrum.* *

This fact motivated new computations with MN-15L, B2PLYP and MP2, which converged to other structural minima, all close to the homochiral form. Based on this fact, the second experimental isomer was finally assigned to the homochiral counterpart G´G´-G´G´-Lp+. The relative deviation of the B2PLYP predictions remained below 2.0% for the heterochiral dimer but was worse for the homochiral form (<6.3%). No other species of reasonable intensity could be found in the spectrum.

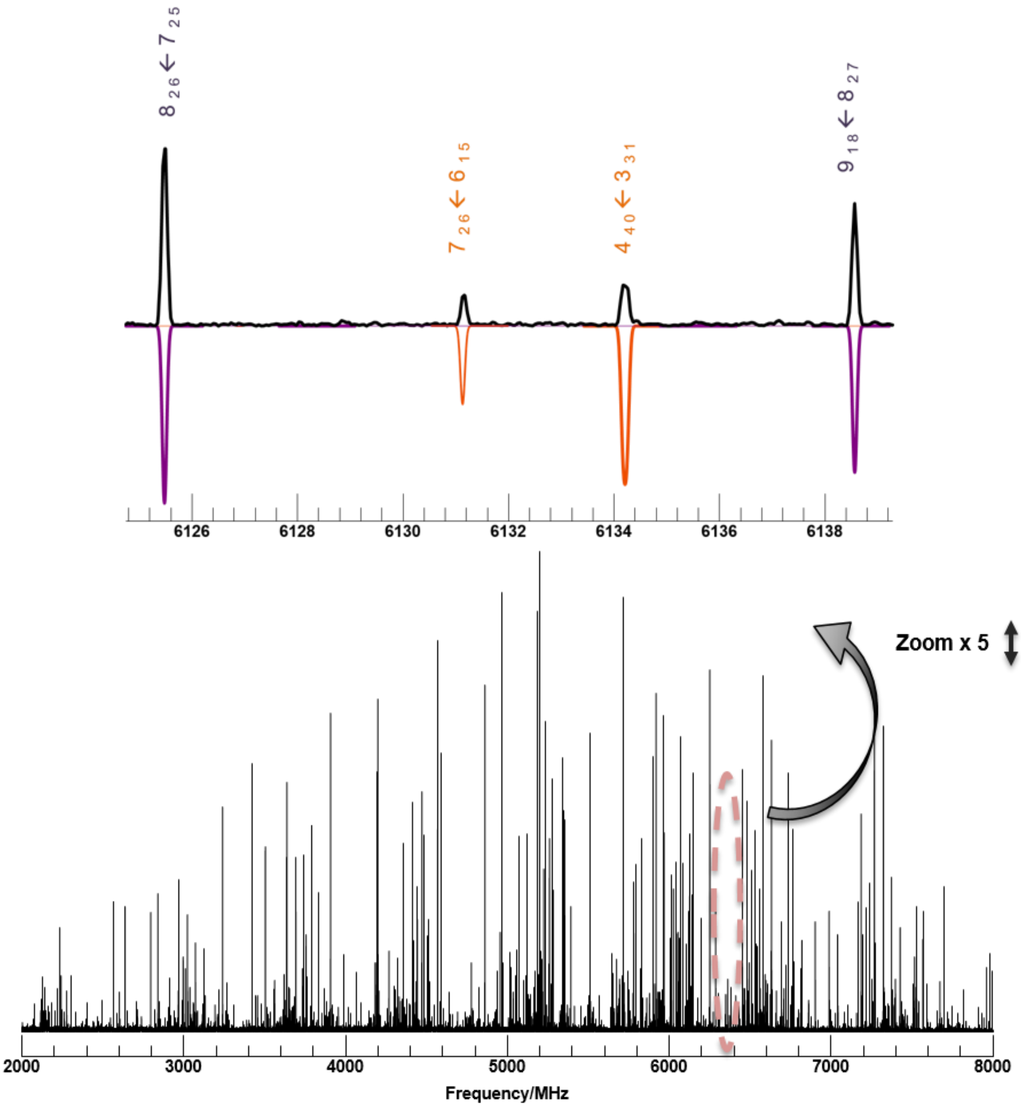

Figure 4. At the bottom, Microwave spectrum of the dimer thenyl alcohol at 75°C in the 2-8 GHz region. At the top of the image, illustrative rotational transitions of the (thenyl alcohol)$_2$ isomer G'G'-GG'-Lp+ (marked in purple) and isomer G'G'-G’G'-Lp+ (marked in orange). *NOTE: *in the lower part of the figure, the lines corresponding to the rotational transitions of the monomer have been subtracted from the spectrum.* *

5. Non-covalent interactions

The non-covalent interactions stabilizing the two alcohol dimers were analysed structurally, energetically and using the electronic density topology. The leading interaction for the dimer structures (collected in Tables S13-S16, (ESI) is the shorter and relatively linear O-H···O hydrogen bond, slightly larger in the heterochiral dimer (B2PLYP: *r*(O-H···O)=1.982 Å, ∠(O-H···O)= 158.6°) than in the homochiral form (B2PLYP: *r*(O-H···O)=1.938 Å, ∠(O-H···O)= 161.8°). This interaction bears similarities with the water monohydrates (B2PLYP: *r*(O-H···O)=1.921 Å, ∠(O-H···O)= 160.3° in the furfuryl monohydrate).[46,47] A second cooperative O-H···O_r hydrogen bond to the ring oxygen closes a cyclic structure, also observed in the monohydrates. This hydrogen bond shows larger contacts for the homochiral (B2PLYP: *r*(O-H···O_r)= 2.015 Å, ∠(O-H···O_r)= 148.8°) and similar values for the heterochiral isomer (B2PLYP: *r*(O-H···O_r)= 1.974 Å, ∠(O-H···O_r)= 156.0°). In the thenyl dimers the primary O-H···O hydrogen bond is also locking the two alcohol groups, now slightly shorter in the heterochiral (B2PLYP: *r*(O-H···O_r)= 1.919 Å, ∠(O-H···O_r)= 166.4°) than in the homochiral form (B2PLYP: *r*(O-H···O_r)= 1.991 Å, ∠(O-H···O_r)= 163.5°). This interaction again parallels the observation in the thenyl monohydrate (B2PLYP: *r*(O-H···O_r)= 1.965 Å, ∠(O-H···O_r)= 159.6°), where, characteristically, the secondary hydrogen bond targets the p system.

The predictions for the complexation energies of the alcohol dimers are quite similar, with slightly larger values for the thenyl alcohol dimer (B2PLYP-D3(BJ): -41.8 and 40.8 kJ mol^{-1}) compared to the furfuryl aggregate (-38.9 and -39.2 kJ mol^{-1}). These calculations would emphasize the leading stabilizer role of the primary O-H···O hydrogen bond, but they contrast with the stability of the monohydrates, where the furfuryl compound has larger complexation energies. The B3LYP-D3(BJ) complexation energies are generally 3-5 kJ mol^{-1} larger than the B2PLYP-D3(BJ) values.

Table 3. Results from a (second-order intramonomer / third-order intermonomer) Symmetry-Adapted Perturbation Theory (SAPT2+(3)/aug-cc-pVDZ) binding energy decomposition of (furfuryl alcohol)$_2$, (thenyl alcohol)$_2$ and related dimers, comparing the magnitude of the electrostatic and dispersion contributions (all values in kJ mol^{-1}) See Tables 1-2 for a comparison of complexation energies using DFT.

	$\Delta E_{Electrostatic}$	$\Delta E_{Induction}$	$\Delta E_{Dispersion}$	ΔE_{Exch}	ΔE_{Total}
FA···H_2O – GG´-W_{da}[a]	-57.2 [57.5%] [h]	-20.3 [20.4%]	-22.1[22.2%]	70.5	-29.0
TA···H_2O – GG-Wa[b]	-49.2 [55.5%]	-17.0 [19.2%]	-22.4 [25.3%]	61.7	-26.8
$(FA)_2$ G´G-G´G- Lp-[c]	-61.7 [49.7%]	-21.5 [17.3%]	-41.0 [33.0%]	85.7	-38.5
$(FA)_2$ G´G-GG- Lp-[c]	-60.3 [49.1%]	-21.7 [17.7%]	-40.8 [33.2%]	83.9	-39.0
$(TA)_2$ G´G´-G´G´- Lp+[c]	-51.4 [43.9%]	-16.3 [13.9%]	-49.4 [42.2%]	76.9	-40.3
$(TA)_2$ G´G´-GG´- Lp+[c]	-57.9 [46.9%]	-18.8[15.2%]	-46.8 [37.9%]	83.0	-40.4
(Cyclohexanol)$_2$[d]	-46.5 [51.8%]	-16.6 [18.5%]	-26.6 [29.7%]	60.5	-29.2
(Phenol)$_2$ [e]	-41.8 [48.3%]	-28.8 [18.4%]	-15.9 [33.3%]	58.9	-27.6
(Thiophenol)$_2$ [f]	-26.0 [29.4%]	-8.5 [9.6%]	-53.8 [60.9%]	61.3	-30.0
$(H_2O)_2$	-35.7 [63.5%]	-9.5 [19.8%]	-11.1 [16.8%]	37.7	-18.6
$(H_2S)_2$[g]	-12.1 [49.0%]	-7.8 [19.3%]	-4.7 [31.7%]	19.2	-5.4

[a] Ref.46. [b] Ref.47. [c] This work. [d] Ref.37. [e] Ref. *Phys. Chem. Chem. Phys.*, **2013**,15, 11468-11477. [f] Ref.35. [g] Ref. 34. [h] Percentage of the total attractive interactions for each molecule.

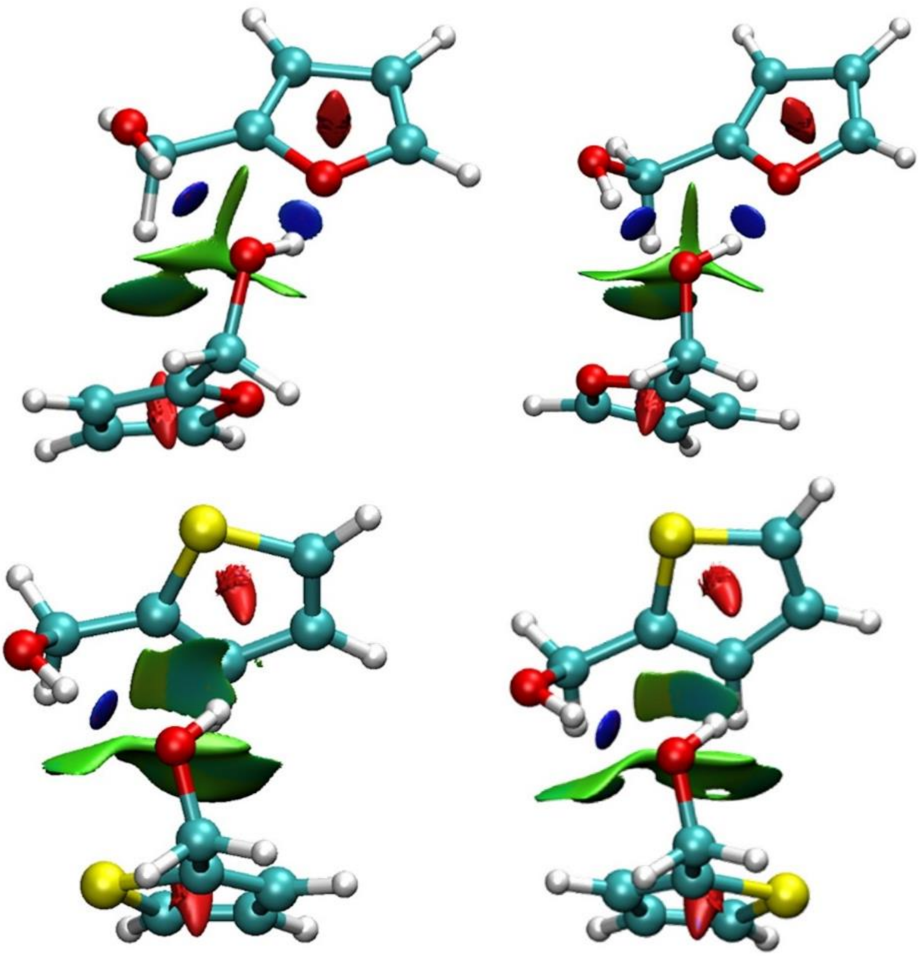

Figure 5. NCIPlot for the homodimers of furfuryl alcohol dimer G'G-G'G- Lp- and furfuryl alcohol dimer G´G-GG- Lp- (upper row), compared to theny alcohol dimer G'G'-G'G'- Lp-+ and theny alcohol dimer G'G'-GG'- Lp-+ (lower row), mapping noncovalent interactions. In this color scale blue shades indicate attractive interactions (associated to bond critical points), green colors indicate weak interactions and red represents repulsive interactions (like the ring critical points).

The participation of electrostatic and dispersion forces in the dimer stability has been estimated using energy decomposition with symmetry-adapted perturbation theory at the SAPT(2+3)/cc-pVTZ level. The calculations in Table 3 and Figure 5, suggest a dominant electrostatic character for the two alcohols, i.e., 49-50% and 44-47% of the total attractive energy, respectively, for the furfuryl and thenyl dimers, slightly smaller than in the monohydrates (56-57%). At the same time, the dimers show a considerable increase of the dispersion contributions, associated to the two aromatic rings (33% and 38-42% for the furfuryl and thenyl dimers, respectively vs. 22-25% in the monohydrates). Calculations on related alcohols[25,27] and thiols,[36] like the water and hydrogen sulfide dimers,[35,66] together with the dispersive pyridine-methane dimer[67] are included for comparison.

The presence of non-covalent interactions has been modelled using NCIPlot electronic density mapping.[64] This method calculates a reduced electronic density gradient $s\left(=\frac{1}{1(3\pi^2)^{1/3}}\frac{|\nabla\rho|}{\rho^{4/3}}\right)$ versus the signed electronic density $(\mathrm{sign}\,(\lambda_2)\,\rho)$ using the second eigenvalue (λ_2) of the electron density Hessian (Figure S3, ESI). Non-covalent interactions are then associated to bond critical points. The spatial plots in Figure 6 compare the four observed dimers, revealing interaction patterns well expected in terms of chemical arguments, in particular the (blue) regions associated to hydrogen bonds and other weakly attractive (green) around the two rings.

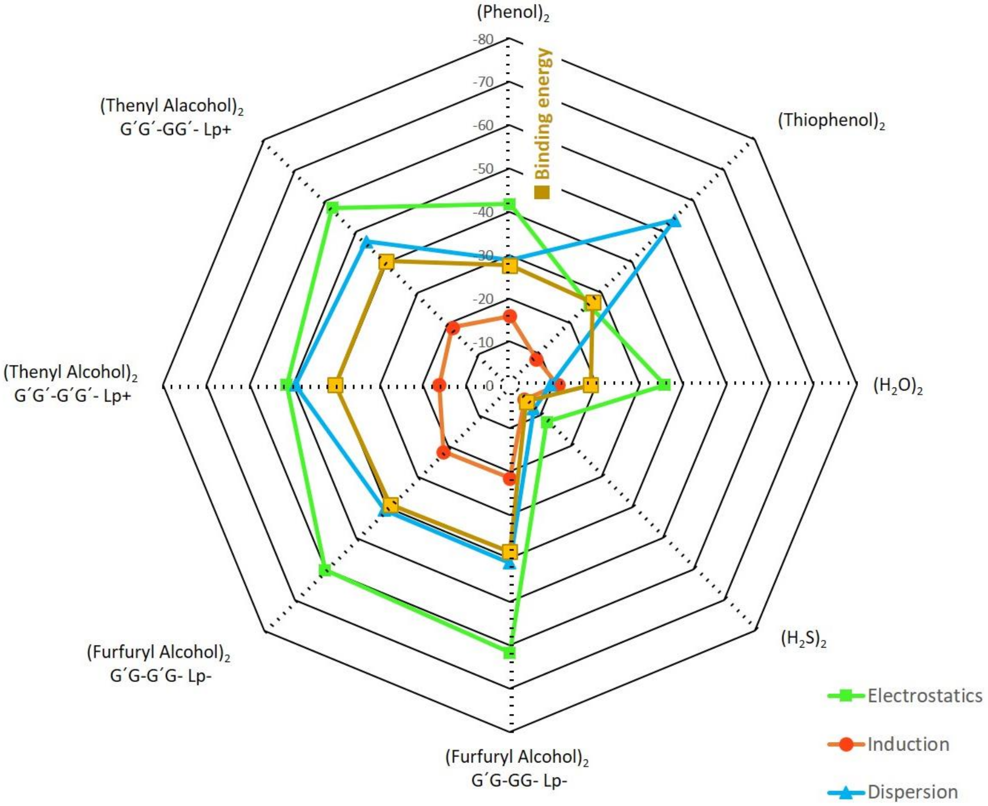

Figure 5. A radar chart showing the SAPT2+(3) binding energy decomposition (kJ mol^{-1}) for the furfuryl and thenyl dimers and comparison with the dimers of phenol, thiophenol, water and hydrogen sulfide reported in Table 3.

6. Conclusion

The conformational landscape and structural properties of the dimers of furfuryl alcohol and thenyl alcohol have been investigated by a combination of jet-cooled (chirped-pulsed) broadband rotational spectroscopy, molecular orbital calculations, binding energy decomposition and electronic density topological analysis. The two alcohol dimers show a combination of conformational issues, particularly the presence of torsional enantiomers, but also the competition of different hydrogen bonds, ring interactions and structural distortions on dimerization. Homochiral and heterochiral structures have been observed experimentally for the two alcohols, which represent a rare occasion where different torsional isomers have been observed independently by spectroscopic means. The close relative energies, even predicted at B2PLYP-D3(BJ) level, were inconclusive on the identification of the global minima, and relied on the experimental findings. The two alcohol dimers were predicted with opposing stereochemical preferences (homochiral for the furfuryl alcohol dimer, heterochiral for the thenyl alcohol dimer) but the small chirodiastaltic energies of 1-2 kJ mol^{-1} prevent any generalization on the dimerization properties and aggregation preferences. Considering the small interconversion barriers between the torsional isomers new experiments can be designed to explore the transition between torsional labile compounds and permanent stereocenters on molecular aggregation.

This study also provides an accurate description of the intermolecular forces in play in the dimerization process, characterized by a cooperative behaviour of two hydrogen bonds. Furthermore, the comparison between the furfuryl and thenyl compounds explores the different role of the hydrogen bond involving sulfur, which in the thenyl compounds have less priority that the interaction to the p ring system. The molecular description of the two alcohol dimers, while structurally similar to the monohydrates, offers a completely different combination of dispersion effects, calling for adequate dispersion-corrected quantum mechanical models. In this sense we have found interesting issues associated to the structural convergence in the two DFT methods used, emphasizing the importance of the calculation grid, convergence thresholds and other numerical problems. Finally, the role of gas-phase intermolecular clusters as interaction models for molecular aggregation should be stressed, outlining the important collaboration beteeen rotationally resolved experiments and DFT and ab initio methods.

Chapter VI. References:

1. Ariga, K., Ito, H., Hill, J. P. & Tsukube, H. Molecular recognition: From solution science to nano/materials technology. *Chem. Soc. Rev.* **41**, 5800–5835 (2012).

2. Persch, E., Dumele, O. & Diederich, F. Molecular recognition in chemical and biological systems. *Angew. Chemie - Int. Ed.* **54**, 3290–3327 (2015).

3. Zehnacker, A. *Chiral Recognition in the Gas Phase*. (CRC Press, 2010).

4. Zehnacker, A. & Suhm, M. A. Chirality Recognition between Neutral Molecules in the Gas Phase. *Angew. Chemie Int. Ed.* **47**, 6970–6992 (2008).

5. Schermann, J.-P. *Spectroscopy and Modeling of Biomolecular Building Blocks*. (Elsevier, 2008). doi:10.1016/B978-0-444-52708-0.X5001-1.

6. Hobza, P. & Muller-Dethlefs, K. *Non-Covalent Interactions*. (Royal Society of Chemistry, 2009). doi:10.1039/9781847559906.

7. *Noncovalent Forces*. vol. 19 (Springer International Publishing, 2015).

8. Liu, M., Zhang, L. & Wang, T. Supramolecular chirality in self-Assembled systems. *Chem. Rev.* **115**, 7304–7397 (2015).

9. Brandt, J. R., Salerno, F. & Fuchter, M. J. The added value of small-molecule chirality in technological applications. *Nat. Rev. Chem.* **1**, (2017).

10. Gilli, G. & Gilli, P. *The Nature of the Hydrogen Bond*. (Oxford University Press, 2009). doi:10.1093/acprof:oso/9780199558964.001.0001.

11. Alkorta, I., Elguero, J. & Frontera, A. Not only hydrogen bonds: Other noncovalent interactions. *Crystals* **10**, (2020).

12. Juanes, M., Saragi, R. T., Caminati, W. & Lesarri, A. The Hydrogen Bond and Beyond: Perspectives for Rotational Investigations of Non-Covalent Interactions. *Chem. - A Eur. J.* **25**, 11402–11411 (2019).

13. Pierini, M. *et al.* Gas-Phase Enantiodifferentiation of Chiral Molecules: Chiral Recognition of 1-Phenyl-1-propanol/2-Butanol Clusters by Resonance Enhanced Multiphoton Ionization Spectroscopy. *Angew. Chemie - Int. Ed.* **36**, 1729–1731 (1997).

14. Le Barbu, K., Brenner, V., Millié, P., Lahmani, F. & Zehnacker-Rentien, A. An Experimental and Theoretical Study of Jet-Cooled Complexes of Chiral Molecules: The Role of Dispersive Forces in Chiral Discrimination. *J. Phys. Chem. A* **102**, 128–137 (1998).

15. Borho, N., Häber, T. & Suhm, M. A. Chiral self-recognition in the gas phase: the case of glycidol dimers. *Phys. Chem. Chem. Phys.* **3**, 1945–1948 (2001).

16. Seifert, N. A. *et al.* Chiral recognition and atropisomerism in the sevoflurane dimer. *Phys. Chem. Chem. Phys.* **17**, 18282–18287 (2015).

17. Oki, M. Recent Advances in Atropisomerism. in *Topics in Stereochemistry, vol. 14* (ed. Allinger, Norman L.;Eliel, Ernest L.;Wilen, S. H.) 1–82 (John Wiley & Sons, Inc, 1983).

18. Ottaviani, P., Maris, A. & Caminati, W. Atropisomerism in bisphenols: Free jet absorption millimeter wave study of 2,2′-biphenol. *J. Mol. Struct.* **695–696**, 353–356 (2004).

19. Hearn, J. P. I., Cobley, R. V. & Howard, B. J. High-resolution spectroscopy of induced chiral dimers: A study of the dimers of ethanol by Fourier transform microwave spectroscopy. *J. Chem. Phys.* **123**, 1–

7 (2005).

20. Wassermann, T. N. & Suhm, M. A. Ethanol Monomers and Dimers Revisited: A Raman Study of Conformational Preferences and Argon Nanocoating Effects. *J. Phys. Chem. A* **114**, 8223–8233 (2010).

21. Loru, D., Peña, I. & Sanz, M. E. Ethanol dimer: Observation of three new conformers by broadband rotational spectroscopy. *J. Mol. Spectrosc.* **335**, 93–101 (2017).

22. Snow, M. S., Howard, B. J., Evangelisti, L. & Caminati, W. From Transient to Induced Permanent Chirality in 2-Propanol upon Dimerization: A Rotational Study. *J. Phys. Chem. A* **115**, 47–51 (2011).

23. King, A. K. & Howard, B. J. A microwave study of the hetero-chiral dimer of butan-2-ol. *Chem. Phys. Lett.* **348**, 343–349 (2001).

24. Maris, A., Giuliano, B. M., Bonazzi, D. & Caminati, W. Molecular recognition of chiral conformers: A rotational study of the dimers of glycidol. *J. Am. Chem. Soc.* **130**, 13860–13861 (2008).

25. Juanes, M. *et al.* The Six Isomers of the Cyclohexanol Dimer: A Delicate Test for Dispersion Models. *Angew. Chemie Int. Ed.* **59**, anie.202005063 (2020).

26. Altnöder, J., Oswald, S. & Suhm, M. A. Phenyl- vs cyclohexyl-substitution in methanol: Implications for the OH conformation and for dispersion-affected aggregation from vibrational spectra in supersonic jets. *J. Phys. Chem. A* **118**, 3266–3279 (2014).

27. Medel, R. & Suhm, M. A. Understanding benzyl alcohol aggregation by chiral modification: The pairing step. *Phys. Chem. Chem. Phys.* **22**, 25538–25551 (2020).

28. Liu, X., Borho, N. & Xu, Y. Molecular self-recognition: Rotational spectra of the dimeric 2-fluoroethanol conformers. *Chem. - A Eur. J.* **15**, 270–277 (2009).

29. Thomas, J. & Xu, Y. Chirality synchronization in trifluoroethanol dimer revisited: The missing heterochiral dimer. *J. Phys. Chem. Lett.* **5**, 1850–1855 (2014).

30. Scharge, T., Häber, T. & Suhm, M. A. Quantitative chirality synchronization in trifluoroethanol dimers. *Phys. Chem. Chem. Phys.* **8**, 4664–4667 (2006).

31. Oswald, S. *et al.* The Chiral Trimer and a Metastable Chiral Dimer of Achiral Hexafluoroisopropanol: A Multi-Messenger Study. *Angew. Chemie Int. Ed.* **58**, 5080–5084 (2019).

32. Su, Z., Borho, N. & Xu, Y. Chiral self-recognition: Direct spectroscopic detection of the homochiral and heterochiral dimers of propylene oxide in the gas phase. *J. Am. Chem. Soc.* **128**, 17126–17131 (2006).

33. Domingos, S. R., Pérez, C., Kreienborg, N. M., Merten, C. & Schnell, M. Dynamic chiral self-recognition in aromatic dimers of styrene oxide revealed by rotational spectroscopy. *Commun. Chem.* **4**, 1–11 (2021).

34. Das, A. *et al.* The H2S Dimer is Hydrogen-Bonded: Direct Confirmation from Microwave Spectroscopy. *Angew. Chemie Int. Ed.* **57**, 15199–15203 (2018).

35. Saragi, R. T. *et al.* Switching Hydrogen Bonding to π-Stacking: The Thiophenol Dimer and Trimer. *J. Phys. Chem. Lett.* **12**, 1367–1373 (2021).

36. Utzat, K. A., Bohn, R. K., Montgomery, J. A., Michels, H. H. & Caminati, W. Rotational spectrum, tunneling motions, and potential barriers of benzyl alcohol. *J. Phys. Chem. A* **114**, 6913–6916 (2010).

37. Juanes, M. *et al.* Internal dynamics of cyclohexanol and the cyclohexanol-water adduct. *Phys. Chem. Chem. Phys.* **21**, 3676–3682 (2019).

38. Maryanoff, B. E. & Greco, M. N. *1.7 Stereochemical Lability in Drug Molecules: Cases Where Chirality May Not Be Critical for Drug Development. Comprehensive Chirality* vol. 1 (Elsevier Ltd., 2012).

39. Toenjes, S. T. & Gustafson, J. L. Atropisomerism in medicinal chemistry: Challenges and opportunities. *Future Med. Chem.* **10**, 409–422 (2018).

40. Park, G. B. & Field, R. W. Perspective: The first ten years of broadband chirped pulse Fourier transform microwave spectroscopy. *J. Chem. Phys.* **144**, 1–10 (2016).

41. Laplante, S. R. *et al.* Assessing atropisomer axial chirality in drug discovery and development. *J. Med. Chem.* **54**, 7005–7022 (2011).

42. Craig, D. P. & Mellor, D. P. Discriminating interactions between chiral molecules. in *Bonding Structure. Topics in Current Chemistry, 63* 1–48 (Springer-Verlag, 1976). doi:10.1007/BFb0046191.

43. Portmann, S., Inauen, A., Lüthi, H. P. & Leutwyler, S. Chiral discrimination in hydrogen-bonded complexes. *J. Chem. Phys.* **113**, 9577–9585 (2000).

44. Alkorta, I. & Elguero, J. Discrimination of hydrogen-bonded complexes with axial chirality. *J. Chem. Phys.* **117**, 6463–6468 (2002).

45. Biswal, H. S., Bhattacharyya, S., Bhattacherjee, A. & Wategaonkar, S. Nature and strength of sulfur-centred hydrogen bonds: laser spectroscopic investigations in the gas phase and quantum-chemical calculations. *Int. Rev. Phys. Chem.* **34**, 99–160 (2015).

46. Juanes, M. *et al.* Sulfur Hydrogen Bonding in Isolated Monohydrates: Furfuryl Mercaptan versus Furfuryl Alcohol. *Chem. - A Eur. J.* **24**, 6564–6571 (2018).

47. Juanes, M., Saragi, R. T., Pinacho, R., Rubio, J. E. & Lesarri, A. Sulfur hydrogen bonding and internal dynamics in the monohydrates of thenyl mercaptan and thenyl alcohol. *Phys. Chem. Chem. Phys.* **22**, 12412–12421 (2020).

48. Shipman, S. T. & Pate, B. H. New Techniques in Microwave Spectroscopy. in *Handbook of High-resolution Spectroscopy* (eds. Quack, M. & Merk, F.) 801–827 (John Wiley & Sons, Ltd., 2011).

49. Grabow, J.-U. *Fourier Transform Microwave Spectroscopy Measurement and Instrumentation. Handbook of High-resolution Spectroscopy* (2011). doi:10.1002/9780470749593.hrs037.

50. Caminati, W. & Grabow, J.-U. Advancements in Microwave Spectroscopy. in *Frontiers and Advances in Molecular Spectroscopy* (ed. Laane, J.) 569–598 (Elsevier Inc., 2018). doi:10.1016/B978-0-12-811220-5.00018-6.

51. Halgren, T. A. MMFF VI. MMFF94s option for energy minimization studies. *J. Comput. Chem.* **20**, 720–729 (1999).

52. Pracht, P., Bohle, F. & Grimme, S. Automated exploration of the low-energy chemical space with fast quantum chemical methods. *Phys. Chem. Chem. Phys.* **22**, 7169–7192 (2020).

53. Grimme, S. Semiempirical hybrid density functional with perturbative second-order correlation. *J. Chem. Phys.* **124**, 034108 (2006).

54. Grimme, S., Ehrlich, S. & Goerigk, L. Effect of the damping function in dispersion corrected density functional theory. *J. Comput. Chem.* **32**, 1456–1465 (2011).

55. Weigend, F. & Ahlrichs, R. Balanced basis sets of split valence, triple zeta valence and quadruple zeta valence quality for H to Rn: Design and assessment of accuracy. *Phys. Chem. Chem. Phys.* **7**, 3297 (2005).

56. Frisch, M. J. *et al.* Gaussian 16, rev. C.01. (2016).

57. Neese, F. Software update: the ORCA program system, version 4.0. *WIREs Comput. Mol. Sci.* **8**,

(2018).

58. Boys, S. F. & Bernardi, F. The calculation of small molecular interactions by the differences of separate total energies. Some procedures with reduced errors. *Mol. Phys.* **19**, 553–566 (1970).

59. Jeziorski, B., Moszynski, R. & Szalewicz, K. Perturbation Theory Approach to Intermolecular Potential Energy Surfaces of van der Waals Complexes. *Chem. Rev.* **94**, 1887–1930 (1994).

60. Parrish, R. M. *et al.* Psi4 1.1: An Open-Source Electronic Structure Program Emphasizing Automation, Advanced Libraries, and Interoperability. *J. Chem. Theory Comput.* **13**, 3185–3197 (2017).

61. Contreras-García, J. *et al.* NCIPLOT: A Program for Plotting Noncovalent Interaction Regions. *J. Chem. Theory Comput.* **7**, 625–632 (2011).

62. Watson, J. K. G. Aspects of Quartic and Sextic Centrifugal Effects on Rotational Energy Levels. in *Vibrational Spectra and Structure, vol. 6* (ed. Durig, J. R.) 1–89 (Elsevier B.V., 1977).

Chapter VII

COMPLEMENTARY STUDIES

I. Complementary Studies

During the course of this Thesis and as part of my Doctoral training, I have also participated in other experimental investigations on rotational spectroscopy not directly connected to the study of non-covalent interactions in intermolecular complexes. These investigations include, in particular, the result of international collaborations of our group and the work carried out in two foreing laboratories:

- Institut fur Physikalische Chemie, Universität Hannover
- I Physikalisches Institut, Universität Kohln

In this section I collect the published studies on these topics, including:

a) Cyclohexyl compounds:

Fluorocyclohexane; Ethynylcyclohexane (**Section 1** and **2** of this Chapter)

- Spectroscopic and theoretical molecular orbital calculations.
- Conformational comparison due to ring inversion.
- Semi-experimental (SE) mixed-estimation structural method as a benchmark for computational calculations.

b) Aliphatic dithiol compounds:

1,2-Butanedithiol; 2,3-Butanedithiol (**Section 3** and **4** of this Chapter)

- Intramolecular S-H ··· S hydrogen bonding observation.
- Homochiral and heterochiral conformational stability.
- Complementary measurments on the cm- and mm-wave regions.

c) Tetracyclic compounds:

trans- and cis- Matrine (**Section 5** of this Chapter)

- Conformational stability of saturated tetracycles.
- Torsional motions in six-membered rings

d) NCI review and its perspective for rotational spectroscopy (**Section 6** of this Chapter)

The abstracts of these publication follow.

1. Equilibrium structures of fluorocyclohexane

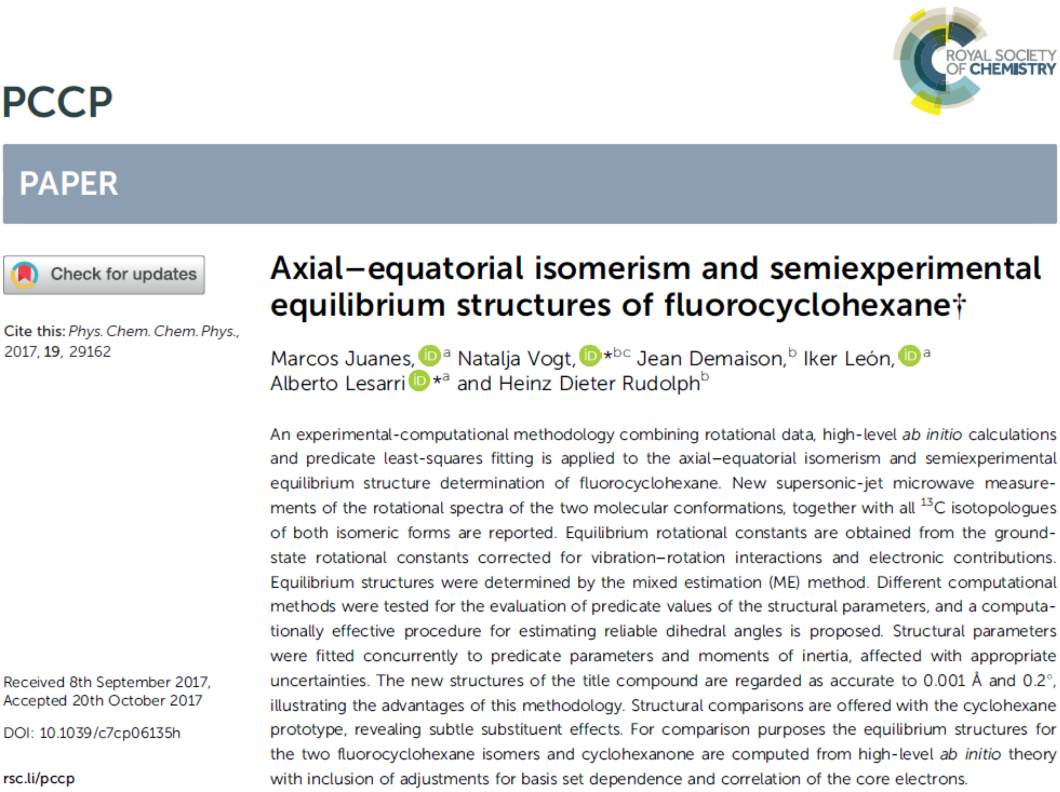

PCCP

ROYAL SOCIETY OF CHEMISTRY

PAPER

Check for updates

Cite this: *Phys. Chem. Chem. Phys.*, 2017, **19**, 29162

Axial–equatorial isomerism and semiexperimental equilibrium structures of fluorocyclohexane†

Marcos Juanes,[a] Natalja Vogt,*[bc] Jean Demaison,[b] Iker León,[a]
Alberto Lesarri*[a] and Heinz Dieter Rudolph[b]

An experimental-computational methodology combining rotational data, high-level *ab initio* calculations and predicate least-squares fitting is applied to the axial–equatorial isomerism and semiexperimental equilibrium structure determination of fluorocyclohexane. New supersonic-jet microwave measurements of the rotational spectra of the two molecular conformations, together with all ^{13}C isotopologues of both isomeric forms are reported. Equilibrium rotational constants are obtained from the ground-state rotational constants corrected for vibration–rotation interactions and electronic contributions. Equilibrium structures were determined by the mixed estimation (ME) method. Different computational methods were tested for the evaluation of predicate values of the structural parameters, and a computationally effective procedure for estimating reliable dihedral angles is proposed. Structural parameters were fitted concurrently to predicate parameters and moments of inertia, affected with appropriate uncertainties. The new structures of the title compound are regarded as accurate to 0.001 Å and 0.2°, illustrating the advantages of this methodology. Structural comparisons are offered with the cyclohexane prototype, revealing subtle substituent effects. For comparison purposes the equilibrium structures for the two fluorocyclohexane isomers and cyclohexanone are computed from high-level *ab initio* theory with inclusion of adjustments for basis set dependence and correlation of the core electrons.

Received 8th September 2017,
Accepted 20th October 2017

DOI: 10.1039/c7cp06135h

rsc.li/pccp

Phys. Chem. Chem. Phys., 2017,**19**, 29162-29169 (https://doi.org/10.1039/C7CP06135H)

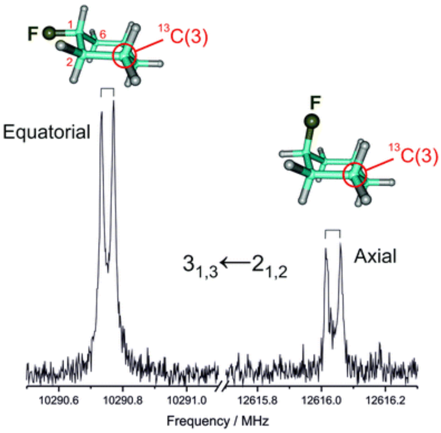

Figure 1. Illustrative rotational transition corresponding to one of the ^{13}C monosubstituted isotopologues of equatorial and axial fluorocyclohexane, measured in natural abundance.

2. Accurate equilibrium structure of the ethynylcyclohexane

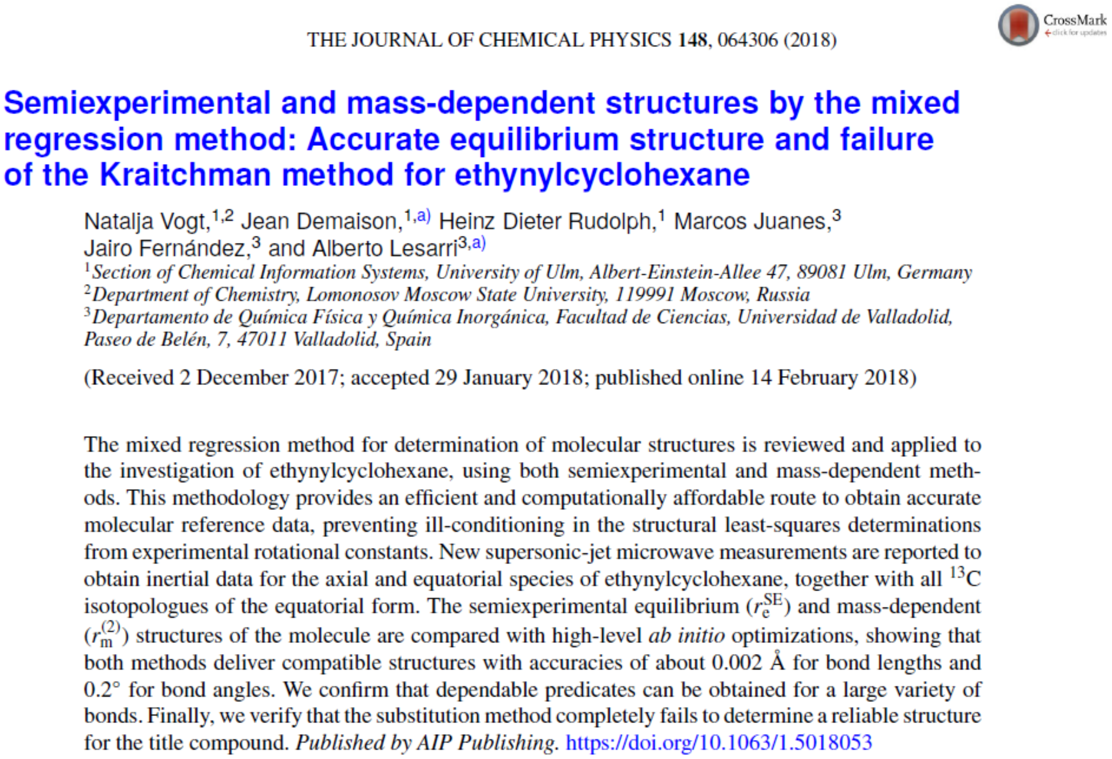

THE JOURNAL OF CHEMICAL PHYSICS **148**, 064306 (2018)

Semiexperimental and mass-dependent structures by the mixed regression method: Accurate equilibrium structure and failure of the Kraitchman method for ethynylcyclohexane

Natalja Vogt,[1,2] Jean Demaison,[1,a)] Heinz Dieter Rudolph,[1] Marcos Juanes,[3]
Jairo Fernández,[3] and Alberto Lesarri[3,a)]
[1] *Section of Chemical Information Systems, University of Ulm, Albert-Einstein-Allee 47, 89081 Ulm, Germany*
[2] *Department of Chemistry, Lomonosov Moscow State University, 119991 Moscow, Russia*
[3] *Departamento de Química Física y Química Inorgánica, Facultad de Ciencias, Universidad de Valladolid, Paseo de Belén, 7, 47011 Valladolid, Spain*

(Received 2 December 2017; accepted 29 January 2018; published online 14 February 2018)

The mixed regression method for determination of molecular structures is reviewed and applied to the investigation of ethynylcyclohexane, using both semiexperimental and mass-dependent methods. This methodology provides an efficient and computationally affordable route to obtain accurate molecular reference data, preventing ill-conditioning in the structural least-squares determinations from experimental rotational constants. New supersonic-jet microwave measurements are reported to obtain inertial data for the axial and equatorial species of ethynylcyclohexane, together with all ^{13}C isotopologues of the equatorial form. The semiexperimental equilibrium (r_e^{SE}) and mass-dependent ($r_m^{(2)}$) structures of the molecule are compared with high-level *ab initio* optimizations, showing that both methods deliver compatible structures with accuracies of about 0.002 Å for bond lengths and 0.2° for bond angles. We confirm that dependable predicates can be obtained for a large variety of bonds. Finally, we verify that the substitution method completely fails to determine a reliable structure for the title compound. *Published by AIP Publishing.* https://doi.org/10.1063/1.5018053

***J. Chem. Phys*, 148,** 064306 (2018) (**https://doi.org/10.1063/1.5018053**)

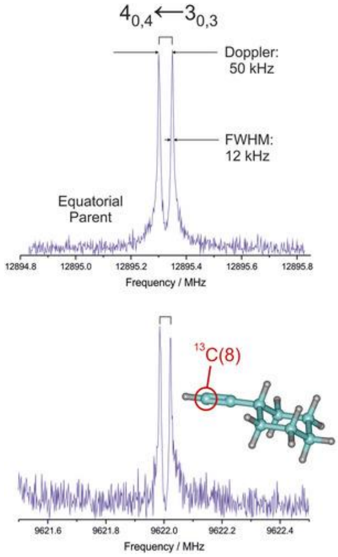

Figure 2. A typical rotational transition for equatorial ethynylcyclohexane (parent and one of the ^{13}C isotopologues in natural abundance.

3. Intramolecular hydrogen bonding in 1,2-butanedithiol

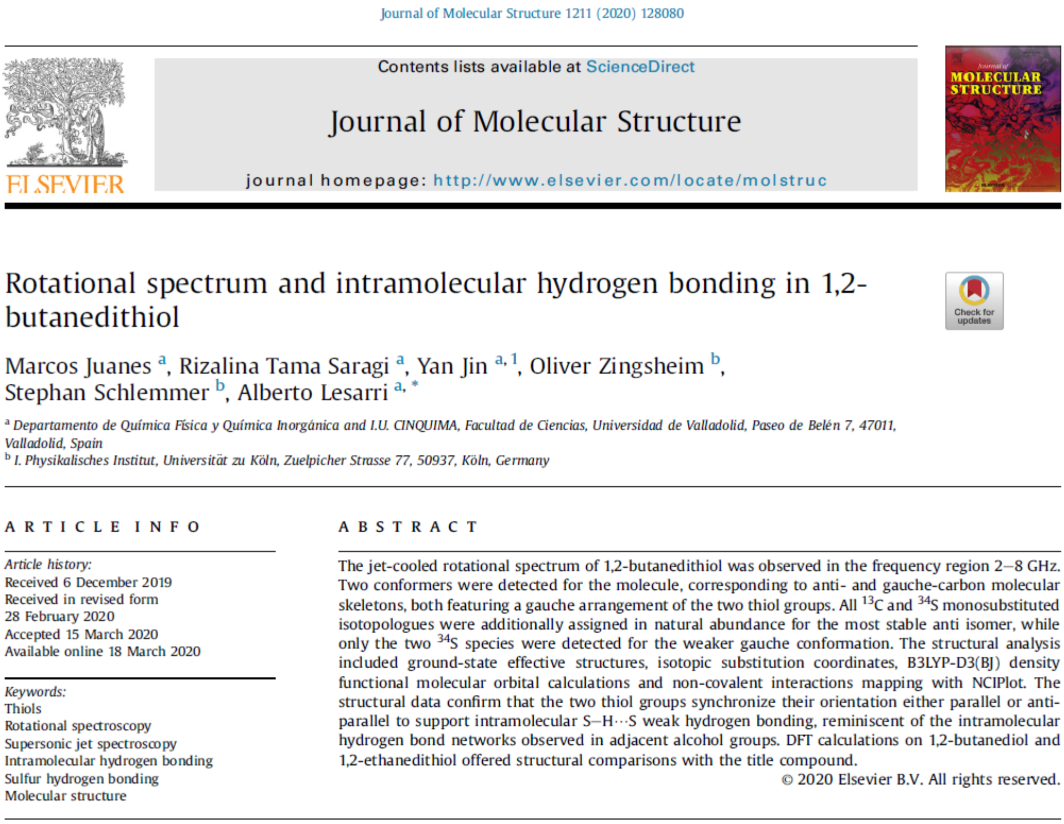

Journal of Molecular Structure 1211 (2020) 128080

Contents lists available at ScienceDirect

Journal of Molecular Structure

journal homepage: http://www.elsevier.com/locate/molstruc

Rotational spectrum and intramolecular hydrogen bonding in 1,2-butanedithiol

Marcos Juanes [a], Rizalina Tama Saragi [a], Yan Jin [a, 1], Oliver Zingsheim [b],
Stephan Schlemmer [b], Alberto Lesarri [a, *]

[a] *Departamento de Química Física y Química Inorgánica and I.U. CINQUIMA, Facultad de Ciencias, Universidad de Valladolid, Paseo de Belén 7, 47011, Valladolid, Spain*
[b] *I. Physikalisches Institut, Universität zu Köln, Zuelpicher Strasse 77, 50937, Köln, Germany*

ARTICLE INFO

Article history:
Received 6 December 2019
Received in revised form
28 February 2020
Accepted 15 March 2020
Available online 18 March 2020

Keywords:
Thiols
Rotational spectroscopy
Supersonic jet spectroscopy
Intramolecular hydrogen bonding
Sulfur hydrogen bonding
Molecular structure

ABSTRACT

The jet-cooled rotational spectrum of 1,2-butanedithiol was observed in the frequency region 2–8 GHz. Two conformers were detected for the molecule, corresponding to anti- and gauche-carbon molecular skeletons, both featuring a gauche arrangement of the two thiol groups. All ^{13}C and ^{34}S monosubstituted isotopologues were additionally assigned in natural abundance for the most stable anti isomer, while only the two ^{34}S species were detected for the weaker gauche conformation. The structural analysis included ground-state effective structures, isotopic substitution coordinates, B3LYP-D3(BJ) density functional molecular orbital calculations and non-covalent interactions mapping with NCIPlot. The structural data confirm that the two thiol groups synchronize their orientation either parallel or anti-parallel to support intramolecular S–H···S weak hydrogen bonding, reminiscent of the intramolecular hydrogen bond networks observed in adjacent alcohol groups. DFT calculations on 1,2-butanediol and 1,2-ethanedithiol offered structural comparisons with the title compound.

© 2020 Elsevier B.V. All rights reserved.

J. Mol. Struct., 1211 (**2020**) 128080 (https://doi.org/10.1016/j.molstruc.2020.128080)

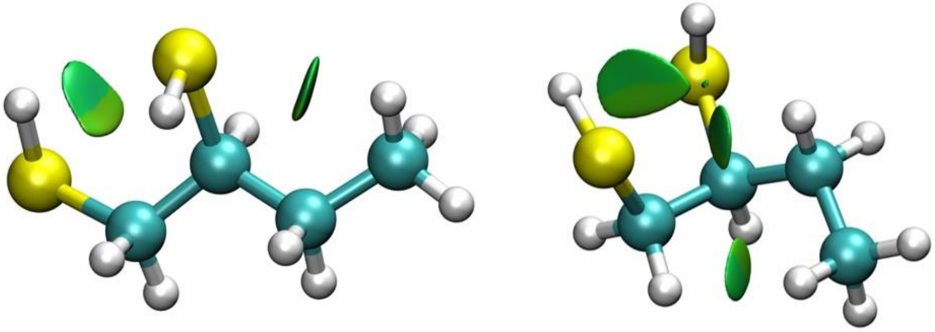

Figure 3. The observed conformers gG'Ag' (left) and g'GG'g' (right) of 1,2-butanedithiol. The molecular conformations include NCIPlot maps of the non-covalent interactions

4. Intramolecular hydrogen bonding in 2,3-butanedithiol

Chirality, Structure and Hydrogen Bonding in Dithiols: Rotational Spectrum of the Chiral and *Meso* 2,3-Butanedithiol

Marcos Juanes,[a] Rizalina Tama Saragi,[a] Oliver Zingsheim,[b] Stephan Schlemmer,[b]
Alberto Lesarri[a]*

[a]Departamento de Química Física y Química Inorgánica, Facultad de Ciencias - I.U. CINQUIMA, Universidad de Valladolid, Paseo de Belén 7, 47011 Valladolid (Spain)

[b]I. Physikalisches Institut, Universität zu Köln, Zuelpicher Strasse 77, 50937 Köln (Germany)

J. Mol. Struct. (**2021**), *Submitted*

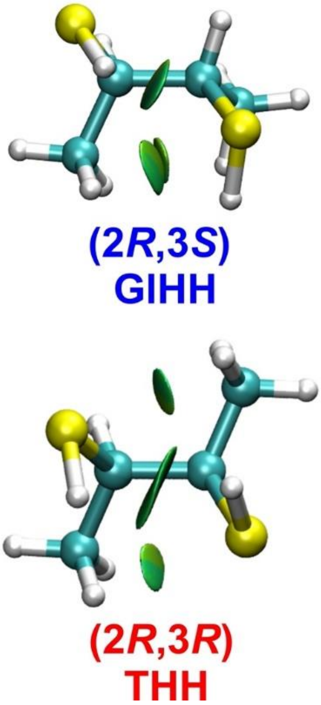

Figure 4. The observed rotamers of the homochiral (2R,3R) and heterochiral (2R,3S) isomers of 2,3-butanedithiol, together with NCIPlot drawings mapping the regions of the non-covalent interactions.

5. Observation of *trans* - Matrine and *cis* - Matrine

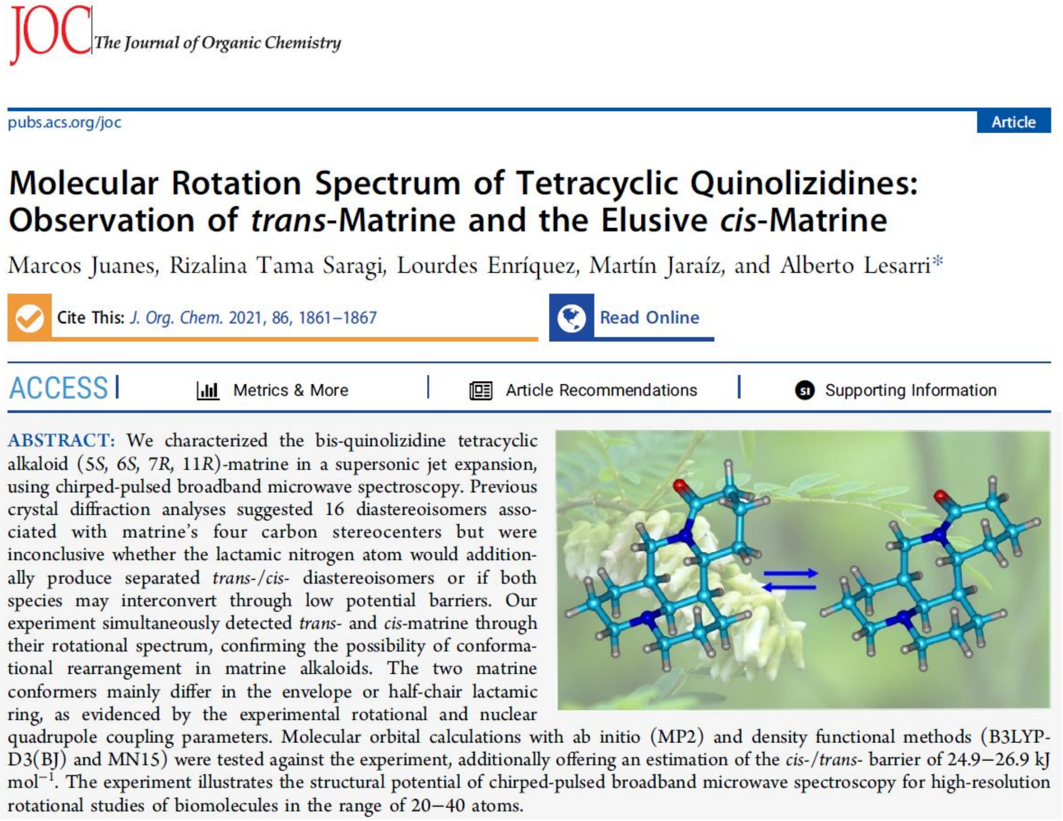

JOC The Journal of Organic Chemistry

pubs.acs.org/joc Article

Molecular Rotation Spectrum of Tetracyclic Quinolizidines: Observation of *trans*-Matrine and the Elusive *cis*-Matrine

Marcos Juanes, Rizalina Tama Saragi, Lourdes Enríquez, Martín Jaraíz, and Alberto Lesarri*

Cite This: *J. Org. Chem.* 2021, 86, 1861−1867 Read Online

ABSTRACT: We characterized the bis-quinolizidine tetracyclic alkaloid (5*S*, 6*S*, 7*R*, 11*R*)-matrine in a supersonic jet expansion, using chirped-pulsed broadband microwave spectroscopy. Previous crystal diffraction analyses suggested 16 diastereoisomers associated with matrine's four carbon stereocenters but were inconclusive whether the lactamic nitrogen atom would additionally produce separated *trans*-/*cis*- diastereoisomers or if both species may interconvert through low potential barriers. Our experiment simultaneously detected *trans*- and *cis*-matrine through their rotational spectrum, confirming the possibility of conformational rearrangement in matrine alkaloids. The two matrine conformers mainly differ in the envelope or half-chair lactamic ring, as evidenced by the experimental rotational and nuclear quadrupole coupling parameters. Molecular orbital calculations with ab initio (MP2) and density functional methods (B3LYP-D3(BJ) and MN15) were tested against the experiment, additionally offering an estimation of the *cis*-/*trans*- barrier of 24.9−26.9 kJ mol^{-1}. The experiment illustrates the structural potential of chirped-pulsed broadband microwave spectroscopy for high-resolution rotational studies of biomolecules in the range of 20−40 atoms.

J. Org. Chem., 2021, **86**, 2, 1861–1867 (https://doi.org/10.1021/acs.joc.0c02689)

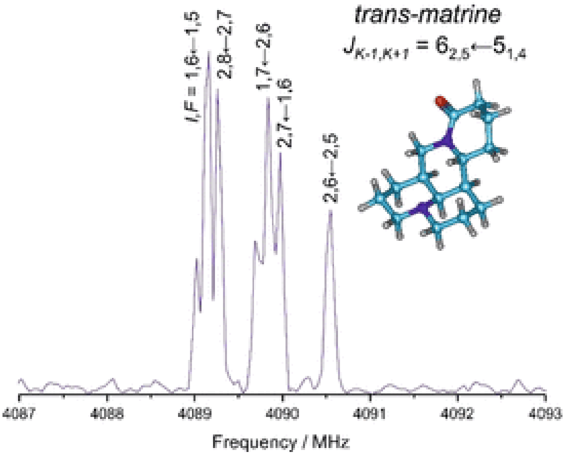

Figure 5. A microwave spectrum section illustrating the nuclear quadrupole coupling hyperfine effects in one of the rotational transitions of the trans- isomer (quantum numbers: J, K_{-1}, K_{+1}, I, F)

6. Perspectives for Rotational Investigations of NCI

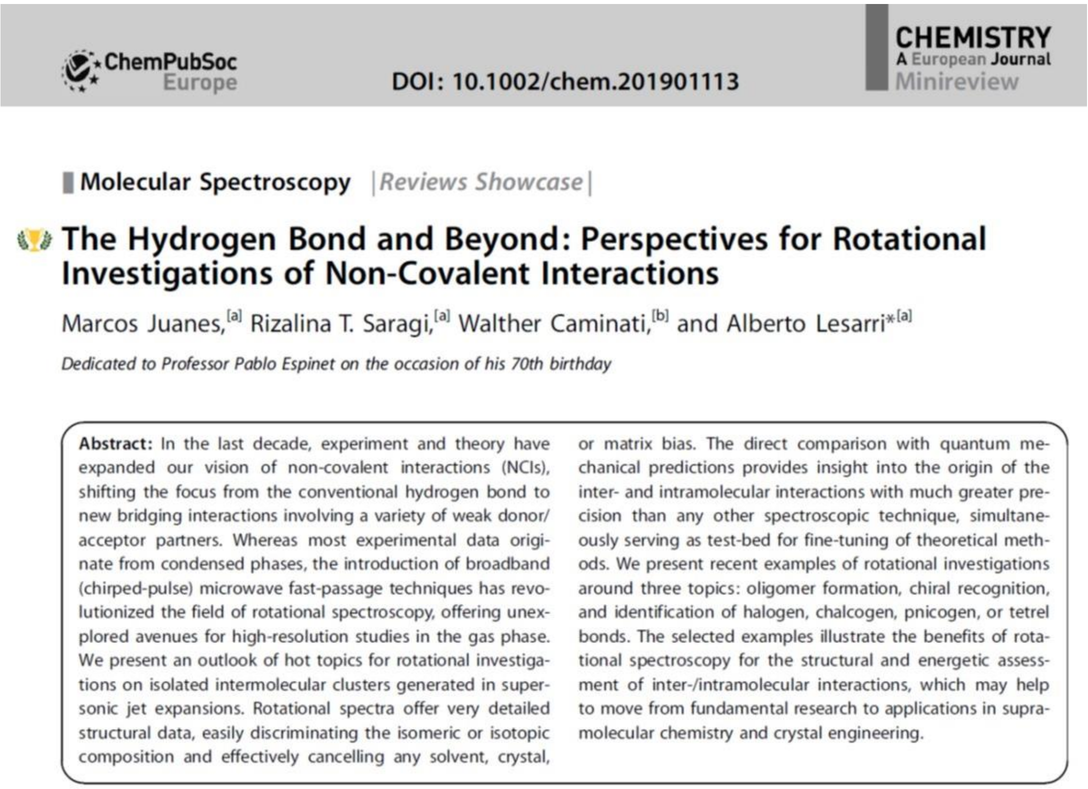

ChemPubSoc Europe
DOI: 10.1002/chem.201901113
CHEMISTRY
A European Journal
Minireview

Molecular Spectroscopy |*Reviews Showcase*|

The Hydrogen Bond and Beyond: Perspectives for Rotational Investigations of Non-Covalent Interactions

Marcos Juanes,[a] Rizalina T. Saragi,[a] Walther Caminati,[b] and Alberto Lesarri*[a]

Dedicated to Professor Pablo Espinet on the occasion of his 70th birthday

Abstract: In the last decade, experiment and theory have expanded our vision of non-covalent interactions (NCIs), shifting the focus from the conventional hydrogen bond to new bridging interactions involving a variety of weak donor/acceptor partners. Whereas most experimental data originate from condensed phases, the introduction of broadband (chirped-pulse) microwave fast-passage techniques has revolutionized the field of rotational spectroscopy, offering unexplored avenues for high-resolution studies in the gas phase. We present an outlook of hot topics for rotational investigations on isolated intermolecular clusters generated in supersonic jet expansions. Rotational spectra offer very detailed structural data, easily discriminating the isomeric or isotopic composition and effectively cancelling any solvent, crystal, or matrix bias. The direct comparison with quantum mechanical predictions provides insight into the origin of the inter- and intramolecular interactions with much greater precision than any other spectroscopic technique, simultaneously serving as test-bed for fine-tuning of theoretical methods. We present recent examples of rotational investigations around three topics: oligomer formation, chiral recognition, and identification of halogen, chalcogen, pnicogen, or tetrel bonds. The selected examples illustrate the benefits of rotational spectroscopy for the structural and energetic assessment of inter-/intramolecular interactions, which may help to move from fundamental research to applications in supramolecular chemistry and crystal engineering.

Chem. Eur. J., 2019, **25**,11402 –11411 (https://doi.org/10.1002/chem.201901113)

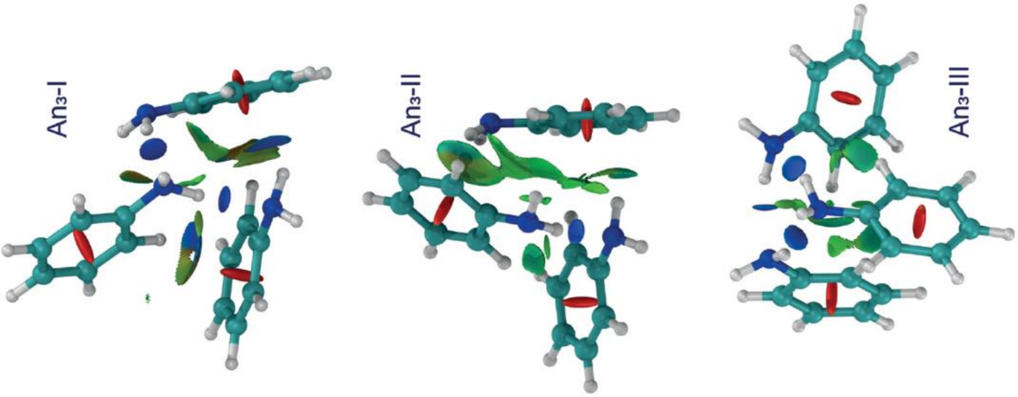

Figure 6. Three isomers of the aniline trimer, with intermolecular interactions mapped with NCI plots.